INTRAOPERATIVE IDENTIFICATION AND DISPLAY OF CORTICAL BRAIN FUNCTION

By

Steven L. Hartmann

Dissertation

Submitted to the Faculty of the

Graduate School of Vanderbilt University

in partial fulfillment of the requirements

for the degree of

DOCTOR OF PHILOSOPHY

in

Biomedical Engineering

May, 2002

Nashville, Tennessee

Approved by:

Professor Robert L. Galloway

Professor Benoit M. Dawant

Professor Peter E. Konrad

Professor J. Michael Fitzpatrick

Professor Michael I. Miga

ACKNOWLEDGEMENTS

This dissertation would not exist without the help of countless others. At the top of the list is my adviser, Dr. Robert L. Galloway, who selflessly shared his knowledge, resources, and time. I will never be able to repay him for everything he has done, but will attempt to be as helpful and patient with others as he has been with me. Dr. Benoit M. Dawant served as the co-chair of this dissertation and contributed greatly to chapters 3 and 4. I am grateful for his personal and professional guidance. Dr. Peter E. Konrad gave much of his limited free time to help support this project. His willingness to help in the operating room was essential, and his guidance and encouragement were greatly appreciated. I sincerely thank Dr. J. Michael Fitzpatrick and Dr. Michael I. Miga for their insightful comments and suggestions that helped to make this a more thorough investigation. It was a privilege to work with and learn from each of my committee members.

The acquisition of clinical data would not have been possible without the support of the Department of Neurological Surgery. In particular, I thank Dr. Robert J. Weil for helping me collect data during neurosurgery. Dr. John Song was extremely helpful coordinating my setup in the operating room and informing me of potential cases. I thank all the residents, nurses, and staff who graciously helped in so many ways.

It has been a pleasure to work with my fellow graduate students in the Snarl lab. Jim Stefansic, Andy Bass, Dave Cash, Tuhin Sinha, Diane Muratore, and Mark Bray have all been gracious with their time and have each contributed to this dissertation.

Finally, I thank my wonderful wife Stacey for her support, guidance, and sacrifice throughout this entire process. This past year we have been blessed by the birth of our daughter Delaney, who continues to inspire me while simultaneously providing a well-needed perspective on life. This dissertation is dedicated to my wife and daughter.

TABLE OF CONTENTS

LIST OF FIGURES

LIST OF TABLES

CHAPTER I

INTRODUCTION

Objective

The incorporation of functional information from the brain into interactive image-guided surgery is both feasible and beneficial. The objective of this work was to develop a system capable of identifying and displaying cortical brain function during neurosurgery.

During a typical image-guided procedure, the neurosurgeon uses anatomical information from tomographic image sets such as magnetic resonance (MR) and computed tomography (CT) to help guide the surgery. These images provide high-level details of the patient's anatomy. The images do not, however, provide the surgeon with information regarding brain function. Identifying functional regions in addition to displaying tomographic images would allow the surgeon to visualize critical areas of the anatomy. This would be beneficial during surgical planning and procedures by identifying eloquent cortical regions (such as speech, sensory, and motor areas) that should be avoided.

In certain neurosurgery procedures, specific functional regions need to be targeted and not avoided. For example, during procedures to control tremor due to Parkinson's disease, an electrical stimulator is implanted in specific regions of the thalamus. Using the proposed system, a database of electrode placement locations from previous patients could be created and used to identify the ideal stimulator location during future procedures. This information could be used in combination with a functional map of the cortex to determine the most appropriate surgical trajectory.

The goal of this research was to design and develop a system for displaying brain function data during interactive image-guided surgery (IIGS). This system is capable of displaying functional data from several different sources, such as that acquired before surgery using functional MRI (fMRI) techniques and that acquired during surgery using a cortical stimulator. In addition, this system is capable of providing a map of functional information from the patient undergoing surgery as well as a probabilistic map of function from a database of previous patients. The functional data is stored in a common coordinate system by mapping the data to corresponding locations on a reference volume. For each surgery, the data from the

reference volume can be mapped to the current patient's image volume. Function information is displayed using a user-selected color index by overlaying the data onto tomographic and rendered images of the anatomy.

Specific Aims

The following four specific aims were necessary to accomplish the objectives of this research:

1) Image Registration and Segmentation: Develop a method for registering inter-patient MR and CT image volumes. This technique was used to accurately map brain function between the database and a specific patient, and to update the database with functional information obtained from each subject. The computed transformation was also used to segment desired anatomic structures, an essential step for creating rendered images. The inter-subject registration process was tested by comparing the location of known structures in a target volume to those obtained by warping a source volume. The registration methods were used to create a population database of brain function. Each database entry contains the image space coordinate and the function type (motor, sensory, or speech), as determined by direct cortical stimulation.

2) Image Display During Surgery: Develop a system capable of displaying the current surgical position on tomographic and rendered images. For displaying rendered images, a method for indicating depth (the distance between the surgical probe and the rendered object) was developed. This image display system is compatible with Vanderbilt's existing image-guided surgery system. The accuracy of the display and identification of surgical position on the rendered images was determined using phantoms.

3) Intraoperative Cortical Region Identification and Display: Design a system to spatially track a cortical stimulator. Tracking the stimulator allows the physical-space location of each stimulation to be determined. This system includes methods for identifying and recording brain function that has been classified according to type and location. The display of functional information was integrated with the image display by overlaying data onto the tomogram and rendered images. Tracking accuracy of the cortical stimulator was determined by comparing its position to that of a tracked surgical probe with known localizing accuracy.

4) Evaluation During Surgery: Investigate the accuracy and evaluate the operation of the image-guided system during human neurosurgical procedures.

CHAPTER II

BACKGROUND AND SIGNIFICANCE

The primary objective of many neurosurgical procedures is to localize and remove a cerebral lesion without causing neurological deficit. The risk involved with these procedures increases when the lesion or the surgical path to the lesion is adjacent to functionally important brain regions, since damage to functional regions is often irreversible [1]. Image-guided technology has increased the accuracy of localizing targets but has not, for the most part, included the identification of functionally important cortical areas. The ability to localize critical cortical regions and their corresponding function would aid in pre-surgical planning by determining the safest and most appropriate trajectory. Intraoperatively, the functional information would complement the anatomical information already utilized during image-guided procedures.

Brain function can be mapped invasively by direct cortical stimulation, non-invasively using transcranial magnetic stimulation (TMS), or non-invasively using different imaging methods such as PET and fMRI. It is not feasible or even possible, however, to create a detailed functional map from each neurosurgery patient. Only a limited area of the brain can be mapped by direct stimulation since the majority of the cortex is inaccessible during surgery and therefore cannot be stimulated. Imaging methods can provide a much greater area of coverage, but require dedicated machines that may not be available and specialized techniques that may not be possible for each patient. Statistical information on brain function and location, obtained from a collection of multiple patients, could be used in particular cases where it is not possible to create a detailed brain map. This type of historical information may also benefit those cases where a cortical function map was available, as an "average" brain map may provide additional information or perspective that cannot be obtained from the particular patient's map alone.

Once a functional brain atlas exists, this information can be displayed along with the corresponding anatomical images during interactive image-guided surgery. The next section of this chapter describes the basic requirements of an image-guided surgery system as well as the specific details of the system developed at Vanderbilt.

In order to create an average brain map, data from each patient must be registered to a standard reference frame. Background information concerning the methods relevant for this type of registration are described later in this chapter.

Interactive Image-Guided Surgery

Medical images are used during interactive image-guided surgery (IIGS) to help guide the surgical procedure. Traditionally, these images have been stacked slice tomograms such as Computed Tomography (CT) and Magnetic Resonance (MR) volumes that are capable of showing high quality details of the human anatomy.

At Vanderbilt University, an image-guided surgery software system called Orion has been developed which is capable of displaying up to four 512 x 512 images. The system has been used to display tomographic image volumes such as CT and MR, and to indicate on these images the current image-space position of a surgical instrument or probe. This system has three key tasks: (1) tracking a surgical probe using a 3-D spatial localizer, (2) computing the transformation that maps the physical-space position of the probe to the image-space position of the image set, and (3) displaying the current position of the probe on the correct tomogram slice using this transformation. These requirements and their implementation are described below.

1) Localization: A spatial localizing system is used to determine the physical-space position of a probe or other surgical instrument. The Orion system is compatible with three different localizing systems: the Optotrak 3020 and Polaris position sensors from Northern Digital, Inc. (Waterloo, Ontario) and the Fastrak system from Polhemus, Inc. (Colchester, VT). The two Northern Digital systems are optical localizers while the Fastrak is a magnetic localizing system. The Optotrak 3020 was used for localization in this study and is shown in Figure 2.1. A typical probe used with this system is cylindrical and contains 24 infrared light emitting diodes (IREDs) around the handle (Figure 2.2). The Optotrak position sensor contains three linear CCDs, each with 1024 elements, and is capable of accurate localization of any IRED in direct line of sight. If three or more of the IREDs can be localized with a high enough degree of certainty, the tip of the probe can be determined since the geometrical arrangement of the IREDs is known. It has been previously shown that the tip of the probe can be localized with an error of approximately 0.8 mm [2].

Figure 2.1: Optotrak 3020 from Northern Digital, Inc.

2) Registration: Registration between physical space and image space can be done in a number of ways, including point-based and surface-based techniques. For this study, a point-based registration method was used that matches the position of extrinsic fiducial markers. Two different types of markers were used in this study – those that are implanted directly into the skull and those that are attached to the surface of the head using an adhesive. The implanted markers are more accurate and therefore the adhesive markers are used only when it is not feasible to attach posts directly to the skull. Both types of markers are perceptible on MR and CT images, and the center of each marker can be identified in image space using either an automatic (implanted markers) or semi-automatic (adhesive markers) method. The image-space position of the implanted fiducial markers have been identified using the technique of Wang *et al* [3]. The implanted imaging markers, caps, and posts can be seen in Figure 2.3. During surgery, the tracked probe is used to identify the physical-space position of the center of the marker. If the corresponding position of three or more fiducials in each space can be identified, then the transformation that maps physical space to image space can be determined using a closed-form solution [4]. Although the registration can be mathematically determined using only three markers, typically at least four markers are used in order to increase the registration accuracy.

Figure 2.2: Surgical probe with IREDs.

3) Display: Tomographic volumes and rendered images can be displayed using the Orion software system. The Orion system consists of a main control program and several modules, which are implemented as independent run-time dynamic link libraries (DLLs). All programs are written in C and compiled for the Windows NT/2000 operating systems. The DLLs are responsible for the various tasks required during IIGS, such as registration and image display. The display of three-dimensional position can be updated at greater than 30 frames per second using the Orion system.

Figure 2.3: Fiducial marker components, showing imaging marker, localizing cap, and screw-in post.

Image Registration and Segmentation

Medical imaging provides a non-invasive method for visualizing internal structures of the human anatomy. Information obtained from medical images can be used in such areas as surgical planning, surgical guidance, radiation therapy, and the diagnosis and treatment of disease. Extracting clinically useful information from the large amount of data present in medical images remains a challenging task. Consider two images of the same object, such as of the human head. If the object has identical orientation and scale within both images, then it is possible to make direct voxel-to-voxel comparisons between the images. For example, a region extracted from one image should exactly correspond to the same region extracted from the other image. If the orientation or scale of the object is not the same in each image, direct voxel-to-voxel comparisons cannot be made. This is usually the case as it is practically impossible to position the object in exactly the same manner for both image sets, especially if the images are acquired on different machines or at different times. In this case, before direct comparisons can be made, the images need to be registered. Registration of two image volumes has been defined as the determination of a one-to-one mapping between the coordinates in one space and those in another, such that points in the two spaces that correspond to the same anatomical point are mapped to each other [3]. Once this mapping has been determined, a structure in one image can be mapped to the corresponding location of the structure in the other image.

Medical image registration has been accomplished using a variety of methods (see [5,6] for good image registration review articles). The majority of the research has been directed towards registration of images of the same subject obtained at different times or with different modalities. Inter-subject registration is also desirable, however, in order to make comparisons across populations. Information from multiple subjects can be stored in a reference volume, called an atlas. An atlas is a standardized representation of a typical image, such as a 3-D image volume of the brain, that can be used as a reference in comparison to other images. Most atlas-based techniques are designed with the objective of inter-subject registration. The underlying assumption is that at a certain level of representation, the topological structure of the brain changes little between subjects. Differences between subjects occur only in the shape of individual structures.

The objective of this type of registration is to obtain the transformation that maps the atlas image to a subject image [7]. This transformation can be used to automatically project data

from the atlas onto the subject. For example, functional brain information collected from previous patients could be mapped to a current patient to provide the surgeon with likely locations of critical cortical areas. This technique can also be used for the segmentation of desired structures. Much research has been done in this area in order to precisely and accurately quantify anatomical structures contained in medical images. A difficult part of this process is isolating the structure of interest from the rest of the image volume. Segmentation is often done manually with visualization software by using a mouse to draw contours on each slice of the image. Segmentation done this way can be very accurate. This is often time consuming, however, and requires that the segmentation be done by someone experienced with the anatomy of the image. Operator fatigue, operator bias, and the inability to reproduce consistent results are all problems with manual segmentation. A method to automatically segment desired structures from medical images would be invaluable. A large number of automatic and semi-automatic segmentation techniques have been proposed. Classification techniques have been used to identify image voxels into gross tissue types such as white matter, gray matter, and cerebral spinal fluid (CSF) (see [8] for a good review of classification techniques). These methods cannot, however, classify voxels according to anatomical structures or function. Using an atlas-based technique, structures of interest can be carefully segmented in the atlas volume, possibly by hand. These structures can be automatically segmented in a different image by first registering this volume with the atlas volume, then using the transformation to map the structures of the atlas to the corresponding locations in the second image. By using an atlas, the process of segmentation becomes a process of registration.

Collins *et al* [9] developed a method for inter-subject registration by aligning brain image volumes with the Talairach stereotaxic atlas space [10]. Talairach space is frequently used since it provides a common anatomical coordinate system for reporting the location of points in the brain. Registration is accomplished by maximizing the cross-correlation between characteristics from each volume, estimated at each voxel position. Two characteristic features were used in this method: image intensity and 3-D gradient magnitude. These features were used to determine a nine parameter (rotation, translation, and scale) transformation that brought the subject volume into correspondence with the atlas. Voxel-to-voxel comparisons can then be made between volumes registered with the atlas. This method is fully automatic.

Andreasen *et al* [11] used a similar method to measure brain structure volumes. Brain image volumes were also transformed into Talairach atlas space in order to make direct voxel comparisons. This was done using a transformation based on eight manually identified control points used by the Talairach atlas (anterior commissure, posterior commissure, and the most anterior, posterior, superior, inferior, left, and right points of the lateral ventricles). This method was designed to measure volumes of large structures (such as whole brain or frontal lobe) in normal subjects. Smaller structures or any structure in a diseased brain cannot be measured accurately. This method also requires initial manual preprocessing of the images in order to extract the brain from the rest of the image.

A nine-parameter transformation was used in these two cases under the assumption that the overall morphology of the human brain is the same between patients. Similar strategies were also used in [12,13].

More recently, a measure of the 2-D joint histogram called mutual information has been proposed independently by Collignon [14,15] and Wells [16]. This measure is robust and permits the automatic computation of the similarity transform. For this work, global transformations (as compared to local transformations) are defined as transformations that can be expressed with a few parameters such as rigid body transformations (three rotation angles and three translation vectors) or similarity transformations (rigid body plus anisotropic scaling). In a large inter-site comparison study involving inter-modality intra-patient registration, voxel-based methods and, in particular, methods using mutual information were shown to be the most robust and accurate techniques for rigid body registration [17]. However, both rigid body and similarity transformations are insufficient to take into account local and subtle anatomical differences that may occur between subjects. Even in the normal population, it has been shown that there can be significant differences in the size, shape, and location of different structures within the brain [18]. In diseased brains, atrophy in certain brain regions makes accurate registration using this type of transformation practically impossible. Thus, brains registered with rigid body or similarity transformations appear to be globally registered but locally the registration remains inaccurate. This problem can be solved by computing local rather than global transformations and a number of methods of varying complexity have been proposed to address this problem.

The idea of using an atlas as an elastic object was originated by Broit [19], who developed a theory for elastically matching a three-dimensional atlas to CT images of the brain.

The matching of two images can be accomplished by using some essential information of both images to determine a mapping that gives the best possible match in terms of a predefined similarity measure. The mapping usually consists of a registration, which is global, and a matching, which can be local or global depending on the information used. This process involves selecting (1) the features to be used in the matching, (2) the constraints in the matching, (3) the matching process, and (4) the similarity used to evaluate the match [20].

All material bodies are to some extent deformable. When the relative positions of particles in a continuous body are altered, as is the case with the elastic matching of the atlas, the body is said to be strained and the change in the relative position of points is a deformation [21]. The deformation may be global or local, large or small, plastic or elastic [20].

Different feature sets have been used for elastic matching. A common method is to use points, contours, or surfaces. An elastic matching algorithm is applied between the corresponding pairs of features (the set of points, contours, or surfaces), and the features in one image are iteratively deformed to match the features in the second image using forces derived from local pattern matches.

Evans *et al* [22] describe an atlas-based warping algorithm that uses the concept of thin-plate splines, described by Goshtasby [23] and Bookstein [24]. This procedure determines the deformation that maps a set of 3-D coordinates onto an equivalent set of corresponding points. In this study, 26 sets of landmarks were manually identified and used for the matching process. The deformation is decomposed into a series of principal warps of decreasing geometric scale. The field is propagated throughout the image using splines in order to determine displacements at regions between landmark points.

Rohr *et al* [25] implemented a similar thin-plate spline technique that was less prone to landmark localization errors. To minimize the localization errors, they used an approximation scheme where the corresponding thin-plate splines result from regularization theory. This generally produces more robust and accurate results, since unlike using a spline interpolation scheme, corresponding landmarks are not forced to exactly match. This reduces the influence of outliers. It is also possible to individually weight the contribution of each landmark based upon their localization certainty.

Moshfeghi *et al* [26] have proposed a method based on the iterative deformation of boundaries. First, two images are globally matched using a principal axis method. Then sets of

contours of significant objects are extracted from slices of the 3-D volumes. This is done by manually drawing approximate contours, which are allowed to deform to match the actual contours using a snakes algorithm proposed by Kass [27]. Snakes are active contour models that can accurately converge on features of an image, such as edges. The contour extraction for an object leads to a stack of 2-D contours, which are used to form a surface model of the object by constructing a mosaic of triangle surface patches. The surface of one image is then warped to match the corresponding surface in the other image using a 3-D extension of the 2-D algorithm proposed by Burr [28]. This algorithm determines a force field that deforms a surface based on local pattern matches with the corresponding surface. For each vertex in the original surface, the nearest triangle surface patch in the corresponding surface is determined. A field of displacement vectors is calculated for each surface, which are combined using interpolation to create a displacement field for the entire image. Trilinear interpolation is used to reformat the original volume, and the steps of contour extraction, surface formation, surface matching, and image resampling are repeated until an error measure reaches a predefined value.

Thompson and Toga [29] developed a surface-based approach for the elastic warping of anatomical images. This method attempts to take into account developmental processes that are responsible for the variations in neuroanatomy between normal individuals. Hybrid surface models known as Chen surfaces (based on superquadrics and spherical harmonics) are fitted through manually identified anatomical landmarks to provide an initial estimate of the surface in each image. These surfaces are then precisely molded to the actual contours using the Euler-Langrange evolution process described in [30]. In this process, a surface relaxes to a minimum energy state in a system of potentials associated with the image space. This is done to extract the surfaces of the cortex and ventricles for each image. Once each surface has been extracted, a deformation field is calculated which warps surfaces into structural correspondence. A separate warp is calculated for each hemisphere since the two hemispheres develop independently. An overall deformation field is determined from the fields used to warp each surface using weighted distortion functions and spherical harmonic interpolation. This total field can be used to register the two brain images.

Sandor *et al* [31] implemented a surface-based technique to automatically find and label the cortical surface in 3-D MR brain images. This method was based on the concept of snakes. An energy function is designed such that its minimum occurs at the desired image features. A

snake initialized near the minimum will converge through an energy minimization process. The 2-D concept of snakes was extended to 3-D deformable spline models by modifying the energy function to ensure that sulci points on the atlas are attracted to sulci points in the subject image. An advantage of this technique is that brain extraction and snake initialization are accomplished automatically using a series of morphological operations. A separate energy minimization process is used to warp the B-spline surfaces of the atlas to corresponding surfaces in the subject image. Anatomical features used in this study were the major sulci of the cerebral cortex. The addition of smaller sulci in the feature matching process may improve the deformation, but this may not be possible for those sulci that vary significantly between the atlas and the subject.

Another class of registration techniques uses the intensity characteristics of each image. This process uses features of the image data to match similar features of a second image, which eliminates the requirement of identifying geometric features such as points, contours, and surfaces. Bajcsy and Kovacic [20] developed a matching technique used to deform an atlas brain onto CT scans of normal subjects. The accuracy of this technique for matching with CT scans was reported by Dann *et al* in [32]. This technique was further implemented to match MR volumes by Gee *et al* [7,33]. Global registration between the atlas and a subject image is accomplished using a principal axes method. The elastic matching process is a multi-resolution version of the technique developed by Broit [19], who was the first to implement an intensity-based deformation algorithm. An atlas is modeled as a rubber sheet and deformed by forces derived from a feature space representation of a subject image. The applied forces tend to bring into correspondence the edges of similar structures in the atlas and the subject image. Matching is accomplished by minimizing a cost function that includes both a deformation constraint and a similarity measure. The deformation of the atlas attempts to model the physical properties of tissue by using the Navier-Stokes equation for fluid body motion and Lame's elasticity constants [21]. Initial preprocessing of the images and manual brain segmentation are required. Deformation is calculated in a coarse to fine manner by matching the outer edge of the brain and the ventricles of the atlas to the subject. Other structures within the brain are deformed as a side effect by propagating the deformation results of the outer edge and ventricle matching. The degree of matching can be controlled in three ways: (1) by adjusting the number of iteration cycles, (2) by adjusting the compliance or elasticity of the atlas, and (3) by the selection of brain structures or features to be matched. The first option is a trade-off between the degree of

convergence, determined by an error measurement, and the amount of time allowed for computation. The second option sets the amount of allowed deformation. A very compliant atlas is not robust to noise and may result in unrealistic deformations. If the compliance of the atlas is small, the registration more approximates a rigid-body transformation. The third option is restricted in that only a limited number of structures can be clearly delineated in multiple image sets, especially in PET images. Computing the elastic match using this technique is computationally intensive, and the manual pre-preparation of images is time consuming.

Davatzikos *et al* [34,35] developed a technique similar to that of Gee *et al*. Both methods compute an elastic warping transformation to spatially normalize two image sets. The major difference is in the way the external deformation forces are calculated. While Gee defines the external forces based on a local optimization, Davatzikos determines the external forces through a correspondence established by a homothetic mapping, which uniformly scales the length of boundaries while providing a length-preserving bending capability. This enables determining a transformation even when there are considerable differences between images. This calculation difference has two important consequences: (1) computational efficiency, which they claim to be one to two orders of magnitude more efficient than the cross-correlation technique of Gee *et al*, and (2) modality independence, since the method uses only boundaries of structures and is therefore independent of image intensity. However, this method still requires manual intervention in identifying approximate initial contours for each structure. After initialization, contours are warped to the desired boundaries using an active contour method similar to that of snakes, differing in how the external forces acting on the contours are specified [36]. As with the Gee method, deformation fields are calculated for a small number of structures, and the rest of the brain is deformed according to a propagation of this deformation field.

The point, contour, and surface methods described above all provide an efficient method for image registration. By extracting certain features, only a small subset of the image is used in the calculations, which reduces the computational requirements of the algorithm. Additionally, these techniques can be used to register multi-modality images. The majority of these methods, however, are not fully automatic and require some level of manual intervention, usually in the initialization or identification of features. This can be time consuming and prone to errors in landmark identification. Additionally, certain landmarks may not appear in all images. The accuracy of surface-based methods depends on the presence of a large set of evenly distributed

corresponding surfaces, which may not be available in all types of image modalities. Also, contours usually must be manually initialized, which can be a tedious process if multiple surfaces are used in the registration, since this often needs to be done at each iteration.

The intensity-based methods of Davatzikos and Gee suffer from a problem inherent in all spline, active contour, or surface based methods: brain deformation is modeled according to that determined for a selection of points, contours, or surfaces. Deformation in the remainder of the volume is obtained by interpolation. Since only a small subset of the image is used to compute the transformation, the matching process is usually fast. However, the total number of solutions is constrained by limiting the number of degrees of freedom. This is acceptable if the goal is segmentation of the feature set, or if there are only minimal changes in structure between the atlas and the subject. These methods fail in cases where an unrepresentative deformation occurs in certain areas of the brain, such as in ventricular enlargement or when a space-occupying lesion is present. Unless the structure of interest is specifically included in the determination of the deformation, propagated deformation fields will not effectively model the actual change in local structures. Matching of the ventricles or the brain surface provides no guarantee that other structures, such as the thalamus or caudate nucleus, will be matched correctly.

An intensity-based deformation approach was developed by Collins *et al* [37] that uses information from the entire image set. This method determines the spatial transformation that best matches corresponding intensity-based features between two MR images. The features used in calculating the transformation are image intensity and image gradient magnitude, which are determined by convolution of the original image data with zero and first order 3-D isotropic Gaussian derivatives. Deformation is calculated by sequentially stepping through the target volume and estimating the local deformation that maximizes a similarity criterion evaluated in the neighborhood region surrounding each voxel. The algorithm is applied iteratively in a multi-scale process so that large objects are aligned first, followed by smaller objects at higher resolution levels. This method produced acceptable registration for deep brain regions such as the basal ganglia, but failed to align cortical structures properly. This algorithm was improved by including a set of cortical constraints in the feature set [38]. Cortical sulci are extracted using an active ribbon method that is similar to the 2-D snakes procedure, and matched to corresponding sulci in a manner similar to the surface matching methods described previously. When sulci information was used in addition to intensity and gradient information, cortical registration was

significantly improved. However, the cortical feature set required manual initialization of the sulci regions. The active ribbon initialization step has since been automated [39].

Gaens *et al* [40] proposed a dynamic non-rigid registration algorithm using mutual information, where image transformations are found by dividing images into regions and translating these regions to increase the local similarity criterion. Initial testing of this algorithm was performed on two sets of 2-D medical images.

Christensen *et al* [41,42] also incorporate information from the entire image volume in order to deform an atlas, or a "deformable textbook" as they define, to another image volume. The textbook can be the entire image volume or a smaller sub-set of the original volume. They assume that large distance, non-linear variations in anatomy exist between the atlas and the subject, a situation where snake and spline methods are ineffective. Their goal is to study the shape of deep brain structures such as the hippocampus. The transformation is required to be homeomorphic (i.e. continuous, 1-to-1, and onto) to ensure the continuity and local structure of the textbook are maintained. In order to account for the large differences between images, the transformation is constrained to be consistent with physical deformations of real materials such as with the viscous fluid model. The deformation of the textbook allows for local changes in anatomy while maintaining topology. This method is automatic and only the volume data is used for calculating the deformation. It was used to segment the hippocampus of 3-D MR image volumes, obtaining good qualitative results in the limited data sets used (2 normal subjects). In this study, after initial global registration of the entire volume, only a smaller sub-region surrounding the hippocampus was used to calculate the fluid transformation.

Bro-Nielsen and Gramkow [43] proposed a fast algorithm for non-rigid fluid registration, similar to the algorithm of Christensen. The difference between these methods is that the fluid computations are implemented with a specially developed convolution filter, which leads to an improvement in speed of at least one order of magnitude.

Wang and Staib [44] used an elastic model approach similar to that of Christensen, except their method incorporated a statistical shape model to constrain solutions to more anatomically consistent deformations. Both intensity information and statistical shape information are used as matching criteria in a Bayesian formulation. Testing of the algorithm has been done on 2-D images only.

Chen *et al* [45] developed a hierarchical deformable matching algorithm that uses a gradient descent method to minimizes the intensity difference between corresponding voxels. This technique was improved by using a statistical atlas for the measurement of the deformation fit [46]. In this method, the posterior probability of the deformation is maximized using statistics (density and geometric variation) gathered from a population.

Thirion [47,48] has implemented an intensity-based deformation technique based on the concept of "demons". This method replaces the complexity of modeling dynamic fluid motion with computational simplicity. The concept of demons originates from Maxwell's demons, which were used in physics to suggest that a semi-permeable membrane could violate the second law of thermodynamics. The idea is to consider the boundaries in one image as semi-permeable membranes. Each membrane consists of "demons" that push contours of a second deformable image toward or away from the membrane, depending on whether points on the deformable contour are classified as "inside" or "outside" particles. The set of demons can include the entire image (one demon per voxel), or be restricted to selected contours. A demon can be defined in many ways; its only requirement is to "push the model outward when [the demon] is outside the model, and inward when [the demon] is inside". Thirion discusses several types of demons, the simplest of which is based on the instantaneous optical flow equation. The advantage of this method is that local deformations do not depend on propagated fields calculated for a few regions in the image. It is also computationally simple, and full 3-D deformations can be performed quickly. It is fully automatic (no initial segmentation or contour identification is required) and is suitable for inter-subject registration. Disadvantages inherent with intensity-based techniques are that direct inter-modal registration is not possible. Intensity variations between images of the same modality can also create distorted deformations.

Identification of Cortical Regions in Medical Images

The cortical surface of the brain is a highly convoluted shell of gray matter. The convolutions allow for increased surface area inside the confined space of the cranium. The elevated convolutions of gray matter are called gyri, which are separated by grooves called sucli or fissures. Fissures are characterized by deep grooves which are consistently present from one brain to the next. Sulci grooves are generally not as deep, and their shape and location are not

reliably consistent across a population. For this discussion, the general term ‘sucli’ will be used to represent both sulci and fissures unless specified otherwise.

In neurosurgery, a cranial target can be accessed by following the grooves of the sulci. Gyri and sulci can be used as anatomical landmarks for defining functional boundaries. These landmarks can also be used as features for image registration algorithms, as described in the previous section. For example, locations of corresponding sulci from separate brain volumes can be used to calculate a transformation that registers the two volumes. Due to the large variability that exists between subjects, a difficult step in this process is identifying the cortical regions in medical images.

Labeling sulci has traditionally been a manual process performed by an expert. This can produce accurate results but can also be a long and tedious process prone to errors such as operator fatigue and bias. An automatic method for sulci identification would obviously be beneficial.

Computerized anatomical atlases, such as the Talairach [10] atlas, have been used to map cortical regions identified on the Talairach brain to the desired brain volume using atlas-based registration techniques. Most of these techniques use linear proportional scaling, which does not account for the large cortical variations between the atlas and desired subject volumes, and therefore are poorly matched at cortical regions.

Numerous techniques for segmenting the cortex, some of which are described in the previous section, have been developed. Segmentation is effective for visualization but not usually for localizing and identifying particular sulci. Segmentation is, however, an important first step in many sucli identification techniques.

Surface extraction techniques are often used to identify the cortical surface, but this surface is usually the envelop of the cortex, which does not distinguish between particular convolutions. Several methods for surface extraction are described in the previous section.

Caunce and Taylor [49] developed a projection method that automatically locates points over the sulcal fissures on the cortical envelop. After a first step of brain segmentation, a closing operator is used to determine the cortical envelop. The intensities along each surface normal are averaged (for a specified depth) and projected onto the envelop. A simple threshold is used to leave a representation of the sulcal fissures on the envelop, which is finally thinned to produce sucli landmark points. The points are assigned to curve segments automatically and registration

between corresponding curves is determined using a variant of the iterative closest point (ICP) algorithm [50].

Ge *et al* [51] developed a cortical surface mapping technique that allows for easy, interactive localization of brain convolutions. This visualization method, a sub-class of volume rendering, creates orthographic projections of an eroded envelop of a brain surface. The brain is first segmented using a 2-D minimization technique to create the envelop. This surface is then eroded a specified distance. Intensities of the eroded envelop are projected orthographically onto several viewing planes. These cortical maps are linked together, which allows a user to interactively localize convolutions. Since the cortical maps are also linked to the original brain volume, the convolutions are simultaneously identified in the image slices. This method can use general types of projections in addition to orthographic and perspective, and is specifically suited for cortex visualization. It was tested on four MR brain volumes (two normal subjects and two patients with Alzheimer's disease).

Rettmann *et al* [52] developed a method that finds the actual cortical regions surrounding the sucli as opposed to extracting the sulcal spaces. This method is automatic with the exception of picking a seed point on the reconstructed cortical surface. The brain of each volume is initially segmented, and sulcal regions are found by generating a depth map on the brain surface. This map is computed by reconstructing two surfaces for each hemisphere – the true cortical surface and an outer "shrink-wrap" surface. Sulcal regions on the true surface are determined by measuring the distance between the cortex and the shrink-wrap surface. Sulcal regions are then extracted using a hierarchical algorithm that alternates between thresholding and region growing operations. Finally, each sulcal region is anatomically assigned to its corresponding sulcus using two features: orientation and center of mass in Talairach space. This technique was applied to three segmented brain volumes.

Lohmann [53] developed an automatic procedure for extracting sulcal and gyral patterns from MR brain images. Highly condensed line representations are found that describe the individual properties of the cortical surface. Separate algorithms are used for extracting line representations of three different kinds of cortical structures: sulcal lines, gyral lines, and fundas lines. Sulcal lines are defined to be line representations of sulci extracted at a certain depth, which is supplied by the user. Likewise, gyral lines are line representations of gyri, also cut at a certain depth. Fundas lines are lines that follow the bottom of a sulcus. Prior to line

identification, MR volumes are segmented to remove non-brain material. Sulcal cuts are found by first segmenting the white matter, which is then closed using a morphological filter. The depth level is determined with respect to this closed white matter image. The cuts are obtained by subtracting the white matter image from the closed image and applying a skeletonization which produces sulcal median surfaces. Gyral and fundus cuts are produced using similar techniques. These algorithms were tested on 60 MR images and verified by visually inspecting the results.

Le Goualher *et al* [54] developed a technique called active ribbons for the 3-D segmentation and representation of cortical folds. Active ribbons are built from active surface, which are similar to the active contour snakes developed by Kass [27]. Active surfaces represent the median surface of a particular sulcus. The active ribbon method uses two stages: a learning stage that determines the shape and topology of the desired object, and a modeling stage which uses the initial shape to create a smooth 3-D model of the object. The learning stage consists of preprocessing steps that define the region of interest where sulci and gyri are located. Once the extracted brain surface is found, sulci are separated from gyri using a curvature analysis method that analyzes the different iso-intensity surfaces of the original MR volume. The sign of the mean curvature determines whether a voxel is labeled as gyrus or sulcus. Outer sulci regions are used to initialize the active ribbon, which then converges towards the interior using forces that minimize internal (regularization) and external (model similarity) energy.

This method for sulci identification is used in SEAL (Surface Extraction and Assisted Labeling), a process for interactively identifying and labeling sulci. A probabilistic atlas of possible labels assists the user in identifying a particular sulci [55].

Several methods for identifying sulci and gyri have been proposed using crest lines. Crest lines are mathematically defined as lines that join points of zero maximal principal curvature. Thirion *et al* [56] developed one method, called the marching lines algorithm, for extracting crest lines from brain images. On the cortical surface crest lines match the anatomically defined pattern of gyri and sulci. Sets of crest line are extracted using low and high values for the sigma of the Gaussian smoothing filter. The two sets of crest lines are then registered. Those crest lines that coincide from each extraction form a single set that are appropriately positioned and smooth. Crest lines associated with sulci and gyri can be distinguished easily by evaluating the sign of the maximum curvature.

Extracted crest lines can be used as feature sets for image registration, as shown by Subsol *et al* [57]. A detailed explanation of crest lines and their applications in medical imaging can be found in [58].

References

[1] GR Cosgrove, BR Buchbinder, and H Jiang, "Functional magnetic resonance imaging for intracranial navigation," *Neurosurgery Clinics Of North America*, vol. 7, no. 2, pp. 313-322, 1996.

[2] RL Galloway, RJ Maciunas, WA Bass, and WJ Carpini, "Optical localization for interactive, image-guided neurosurgery," *SPIE Medical Imaging*, vol. 2164, pp. 137-145, 1994.

[3] MY Wang, CR Maurer, JM Fitzpatrick, and RJ Maciunas, "An automatic technique for finding and localizing externally attached markers in CT and MR volume images of the head," *IEEE Transactions on Biomedical Engineering*, vol. 43, no. 6, pp. 627-637, Jun, 1996.

[4] B Horn, "Closed-form solution of absolute orientation using unit quaternions," *Journal of the Optical Society of America*, vol. 4, pp. 629-642, 1987.

[5] JM Fitzpatrick, DLG Hill, and CR Maurer. Image Registration. In: *Handbook of Medical Imaging, Volume 2: Medical Image Processing and Analysis*, eds. M Sonka and JM Fitzpatrick. Bellingham WA: SPIE Press, 2000. pp. 447-513.

[6] JV Hajnal, DLG Hill, and DJ Hawkes. *Medical Image Registration*, CRC Press: 2001.

[7] JC Gee, M Reivich, and R Bajcsy, "Elastically deforming 3D atlas to match anatomical brain images," *Journal of Computer Assisted Tomography*, vol. 17, no. 2, pp. 225-236, 1993.

[8] JC Bezdek, LO Hall, and LP Clarke, "Review of MR image segmentation techniques using pattern recognition," *Medical Physics*, vol. 20, no. 4, pp. 1033-1048, 1993.

[9] DL Collins, P Neelin, TM Peters, and AC Evans, "Automatic 3D intersubject registration of MR volumetric data in standardized Talairach space," *Journal of Computer Assisted Tomography*, vol. 18, no. 2, pp. 192-205, 1994.

[10] J Talairach and P Tournoux. *Co-planar stereotactic atlas of the human brain*, New York: Thieme Medical, 1988.

[11] NC Andreasen, R Rajarethinam, T Cizadlo, S Arndt, VW Swayze, II, LA Flashman, DS O'Leary, JC Ehrhardt, and WTC Yuh, "Automatic atlas-based volume estimation of human brain regions from MR images," *Journal of Computer Assisted Tomography*, vol. 20, no. 1, pp. 98-106, 1996.

[12] M Kamber, R Shinghal, DL Collins, G Francis, and AC Evans, "Model-based 3D segmentation of multiple sclerosis lesions from magnetic resonance brain images," *IEEE Transactions on Medical Imaging*, vol. 14, no. 3, pp. 442-453, 1994.

[13] H Zachmann, Interpretation of cranial MR images using a digital atlas of the human head. eds. H. H. Lemke, C. C. Rhodes, C. C. Jaffe, and R. Felix. pp. 283-288, 1991. *Proceedings Computer Assisted Radiology*. Springer-Verlag. Berlin.

[14] A Collignon, F Maes, D Delaere, D Vandermeulen, P Suetens, and G Marchal, "Automated multimodality image registration using information theory," *Proceedings of Information Processing in Medical Imaging: IPMI '95*, pp. 263-274, 1995.

[15] F Maes, A Collignon, D Vandermeulen, G Marchal, and P Suetens, "Multimodality image registration by maximization of mutual information," *IEEE Transactions on Medical Imaging*, vol. 16, no. 2, pp. 187-198, 1997.

[16] WM Wells III, P Viola, H Atsumi, S Nakajima, and R Kikinis, "Multi-modal volume registration by maximization of mutual information," *Medical Image Analysis*, vol. 1, pp. 35-51, 1996.

[17] JB West, JM Fitzpatrick, MY Wang, BM Dawant, CR Maurer, RM Kessler, RJ Maciunas, C Barillot, D Lemoine, A Collignon, F Maes, P Suetens, D Vandermeulen, PA vandenElsen, S Napel, TS Sumanaweera, B Harkness, PF Hemler, DLG Hill, DJ Hawkes, C Studholme, JBA Maintz, MA Viergever, G Malandain, X Pennec, ME Noz, GQ Maguire, M Pollack, CA Pelizzari, RA Robb, D Hanson, and RP Woods, "Comparison and evaluation of retrospective intermodality image registration techniques," *Journal of Computer Assisted Tomography*, vol. 21, no. 4, pp. 554-566, 1997.

[18] JA Wada, R Clarke, and A Hamm, "Cerebral hemispheric asymmetry in humans: cortical speech zones in 100 adult and 100 infant brains," *Archives of Neurology*, vol. 32, pp. 239-246, 1975.

[19] C Broit, Optimal registration of deformed images. *Doctoral dissertation*, University of Pennsylvania, 1981.

[20] R Bajcsy and S Kovacic, "Multiresolution elastic matching," *Computer Vision, Graphics, and Image Processing*, vol. 46, pp. 1-21, 1989.

[21] IS Sokolnikoff. *Mathematical theory of elasticity*, New York:1956.

[22] AC Evans, W Dai, DL Collins, P Neelin, and S Marrett, "Warping of a computerized 3-D atlas to match brain image volumes for quantitative neuroanatomical and functional analysis," *SPIE Medical Imaging*, vol. 1445, pp. 236-246, 1991.

[23] A Goshtasby, "Registration of images with geometric distortions," *IEEE Transactions on Geoscience and Remote Sensing*, vol. 26, no. 1, pp. 60-64, 1988.

[24] FL Bookstein, "Principal warps: thin-plate splines and the decomposition of deformations," *IEEE Transactions on Pattern Analysis and Machine Intelligence*, vol. 11, no. 6, pp. 567-585, 1989.

[25] K Rohr, HS Stiehl, R Sprengel, W Beil, TM Buzug, J Weese, and MH Kuhn, "Point-based elastic registration of medical image data using approximating thin-plate splines," *Visualization In Biomedical Computing*, vol. 1131, pp. 297-306, Sep, 1996.

[26] M Moshfeghi, S Ranganath, and K Nawyn, "Three-dimensional elastic matching of volumes," *IEEE Transactions on Image Processing*, vol. 3, no. 2, pp. 128-138, 1994.

[27] M Kass, A Witkin, and D Terzopoulos, "Snakes: active contour models," *International Journal of Computer Vision*, vol. 1, no. 4, pp. 321-331, 1988.

[28] DJ Burr, "Elastic matching of line drawings," *IEEE Transactions on Pattern Analysis and Machine Intelligence*, vol. 3, no. 6, pp. 708-713, 1981.

[29] P Thompson and AW Toga, "A surface-based technique for warping three-dimensional images of the brain," *IEEE Transactions on Medical Imaging*, vol. 15, no. 4, pp. 402-417, 1996.

[30] LD Cohen and I Cohen, "Deformable models for 3-D medical images using finite elements and balloons," *IEEE Computer Society Conference on Computer Vision and Pattern Recognition*, pp. 592-598, 1992.

[31] S Sandor and R Leahy, "Surface-based labeling of cortical anatomy using a deformable atlas," *IEEE Transactions on Medical Imaging*, vol. 16, no. 1, pp. 41-54, Feb, 1997.

[32] R Dann, J Hoford, S Kovacic, M Reivich, and R Bajcsy, "Evaluation of elastic matching system for anatomic (CT, MR) and functional (PET) cerebral images," *Journal of Computer Assisted Tomography*, vol. 13, no. 4, pp. 603-611, 1989.

[33] JC Gee, M Reivich, L Bilaniuk, D Hackney, R Zimmerman, S Kovacic, and R Bajcsy, "Evaluation of multiresolution elastic matching using MRI data," *Proceedings of SPIE: Medical Imaging*, vol. 1445, pp. 226-234, 1991.

[34] C Davatzikos, JL Prince, and RN Bryan, "Image registration based on boundary mapping," *IEEE Transactions on Medical Imaging*, vol. 15, no. 1, pp. 112-115, Feb, 1996.

[35] C Davatzikos, "Spatial Normalization of 3D brain images using deformable models," *Journal of Computer Assisted Tomography*, vol. 20, no. 4, pp. 656-665, 1996.

[36] C Davatzikos and JL Prince, "An active contour model for mapping the cortex," *IEEE Transactions on Medical Imaging* , vol. 14, no. 1, pp. 65-80, Mar, 1995.

[37] DL Collins, CJ Holmes, TM Peters, and AC Evans, "Automatic 3-D model-based neuroanatomical segmentation," *Human Brain Mapping*, vol. 3, no. 3, pp. 190-208, 1995.

[38] DL Collins, G Le Goualher, R Venugopal, A Caramanos, AC Evans, and C Barillot, "Cortical constraints for non-linear cortical registration," *Visualization In Biomedical Computing*, vol. 1131, pp. 307-316, Sep, 1996.

[39] DL Collins, G Le Goualher, and AC Evans, "Non-linear cerebral registration with sulcal constraints," *Medical Image Computing and Computer-Assisted Intervention: MICCAI '98*, vol. 1496, pp. 974-984, Oct, 1998.

[40] T Gaens, F Maes, D Vandermeulen, and P Suetens, "Non-rigid multimodal image registration using mutual information," *Medical Image Computing and Computer-Assisted Intervention: MICCAI '98*, vol. 1496, pp. 1099-1106, Oct 1, 1998.

[41] GE Christensen, RD Rabbit, MI Miller, SC Joshi, U Grenander, TA Coogan, and DC Van Essen, "Topological properties of smooth anatomic maps," *Information Processing In Medical Imaging*, pp. 101-112, 1995.

[42] GE Christensen, SC Joshi, and MI Miller, "Individual anatomical atlases of the head," *Visualization In Biomedical Computing*, vol. 1131, pp. 343-348, Sep, 1996.

[43] M Bro-Nielsen and C Gramkow, "Fast fluid registration of medical images," *Visualization In Biomedical Computing*, vol. 1131, pp. 267-276, Sep, 1995.

[44] YM Wang and LH Staib, "Elastic model based non-rigid registration incorporating statistical shape information," *Medical Image Computing and Computer-Assisted Intervention: MICCAI '98*, vol. 1496, pp. 1162-1173, 1998.

[45] M Chen, T Kanade, D Pomerleau, and HA Rowley, "Anomaly detection through registration," *Pattern Recognition*, vol. 32, no. 1, pp. 113-128, 1999.

[46] M Chen, T Kanade, D Pomerleau, and J Schneider, "3-D deformable registration of medical images using a statistical atlas," *Medical Image Computing and Computer-Assisted Intervention: MICCAI '99*, pp. 621-630, 1999.

[47] J-P Thirion, Fast non-rigid matching of medical images. INRIA technical report, nr. 2547, pp. 1-37, May, 1995.

[48] J-P Thirion, "Image matching as a diffusion process: an analogy with Maxwell's demons," *Medical Image Analysis*, vol. 2, no. 3, pp. 243-260, 1998.

[49] A Caunce and CJ Taylor, "Using local geometry to build 3D sulcal models," *Proceedings of Information Processing in Medical Imaging: IPMI '99*, vol. 1613, pp. 196-209, 1999.

[50] P Besl and N McKay, "A method for the registration of 3-D shapes," *IEEE Transactions on Pattern Analysis and Machine Intelligence*, vol. 14, no. 2, pp. 239-256, Feb, 1992.

[51] YR Ge, JM Fitzpatrick, BM Dawant, J Bao, RM Kessler, and RA Margolin, "Accurate localization of cortical convolutions in MR brain images," *IEEE Transactions on Medical Imaging*, vol. 15, no. 4, pp. 418-428, 1996.

[52] ME Rettmann, C Xu, DL Pham, and JL Prince, "Automated segmentation of sulcal regions," *Medical Image Computing and Computer-Assisted Intervention: MICCAI '99*, pp. 158-165, 1999.

[53] G Lohmann, "Extracting line representations of sulcal and gyral patterns in MR images of the human brain," *IEEE Transactions on Medical Imaging*, vol. 17, no. 6, pp. 1040-1048, Dec, 1998.

[54] G Le Goualher, C Barillot, and Y Bizais, "Modeling cortical sulci with active ribbons," *International Journal Of Pattern Recognition And Artificial Intelligence*, vol. 11, no. 8, pp. 1295-1315, 1997.

[55] G Le Goualher, E Procyk, DL Collins, R Venugopal, C Barillot, and AC Evans, "Automated extraction and variability analysis of sulcal neuroanatomy," *IEEE Transactions on Medical Imaging*, vol. 18, no. 3, pp. 206-217, 1999.

[56] JP Thirion and A Gourdon, "The 3D marching lines algorithm," *Graphical Models and Image Processing*, vol. 58, no. 6, pp. 503-509, 1996.

[57] G Subsol, N Roberts, M Doran, J-P Thirion, and G Whitehouse, "Automatic analysis of cerebral atrophy," *Magnetic Resonance Imaging*, vol. 15, no. 8, pp. 917-927, 1997.

[58] G Subsol. Crest lines for curve-based warping. In: *Brain Warping*, ed. AW Toga. Academic Press, 1998. pp. 241-262.

CHAPTER III

AUTOMATIC 3-D SEGMENTATION OF INTERNAL STRUCTURES OF THE HEAD IN MR IMAGES USING A COMBINATION OF SIMILARITY AND FREE FORM TRANSFORMATIONS

Steven L. Hartmann[1], Mitchell H. Parks[2], Peter R. Martin[2], and Benoît M. Dawant[3]

[1]Department of Biomedical Engineering
[2]Department of Psychology
[3]Department of Electrical and Computer Engineering

Vanderbilt University

Nashville, TN 37235

Portions of this manuscript have been published in:

IEEE Transactions on Medical Imaging,
Vol. 18, No. 10, pp. 917-926, October 1999.

Abstract

Studies aimed at quantifying neuroanatomical differences between populations require the volume measurements of individual brain structures. If the study contains a large number of images, manual segmentation is not practical. This study tests the hypothesis that a fully automatic, atlas-based segmentation method can be used to quantify atrophy indices derived from the brain and cerebellum volumes in normal subjects and chronic alcoholics. This is accomplished by registering an atlas volume with a subject volume, first using a global transformation and then improving the registration using a local transformation. Segmented structures in the atlas volume are then mapped to the corresponding structures in the subject volume using the combined global and local transformations.

This technique has been applied to seven normal and seven alcoholic subjects. Three magnetic resonance volumes were obtained for each subject, and each volume was segmented automatically using the atlas-based method. Accuracy was assessed by manually segmenting regions and measuring the similarity between corresponding regions obtained automatically. Repeatability was determined by comparing volume measurements of segmented structures from each acquisition of the same subject. Results demonstrate that the method is accurate, that the results are repeatable, and that it can provide a method for automatic quantification of brain atrophy, even when the degree of atrophy is large.

Introduction

Medical imaging provides non-invasive methods for visualizing internal structures of the human anatomy. Information obtained from these images can be used in such areas as surgical planning, surgical guidance, radiation therapy, and the diagnosis and treatment of disease. Extracting clinically useful information automatically from these data sets, however, remains a challenging task.

Studies aimed at quantifying neuroanatomical differences between populations require the volume measurements of individual brain structures. If the study contains a large number of images, manual segmentation is not practical. This study tests the hypothesis that a fully automatic, atlas-based segmentation method can be used to quantify atrophy indices derived from the brain and cerebellum volumes in normal subjects and chronic alcoholics.

Atlas-based segmentation methods use a reference volume (the atlas) in which the structures of interest have been carefully segmented, possibly by hand. These structures can be automatically segmented in a second image by first registering this volume with the atlas, then using the transformation to map the structures of the atlas to the corresponding locations in the second image.

Image registration has been studied by many researchers in the medical imaging field (see [1], [2] for good review articles). The majority of the research has been directed toward registration of images of the same subject obtained at different times or with different modalities. In this case, it is often sufficient to determine the registration using a similarity transformation (rotation, translation, and anisotropic scaling). However, when images of different subjects are to be registered, a similarity transformation is unable to account for the anatomical differences that occur between subjects. Even in normal populations, it has been shown that there can be significant differences in the size or shape of various brain structures [3]. Since atlas-based segmentation involves inter-subject registration, registration methods with more degrees of freedom than similarity transformations are necessary.

Figure 3.1 illustrates the complexity of the task. The left panel illustrates one slice in a 3-D volume of a normal subject. The right panel illustrates a slice in approximately the same location in an alcoholic subject volume. The panel in the middle shows the results obtained when registering the alcoholic volume to the normal volume using a similarity transformation. This registration was determined using a mutual information similarity criterion. Brain and cerebellum contours have been drawn on the normal subject volume and echoed on the two other panels. If a similarity transformation was sufficient, these contours should precisely circumscribe the brain and the cerebellum on the middle panel as well. The fact that this does not happen even though the images appear globally registered simply reveals that a transformation involving rotation, translation, and anisotropic scaling is unable to take into account non-linear morphological differences between human brains.

This study tests and evaluates the robustness of an automatic atlas-based segmentation method for the computation of pre-atrophy brain volumes and the post-atrophy brain and cerebellum volumes. This is accomplished by registering an atlas volume with a subject volume, first using a global transformation and then improving the registration using a non-linear local

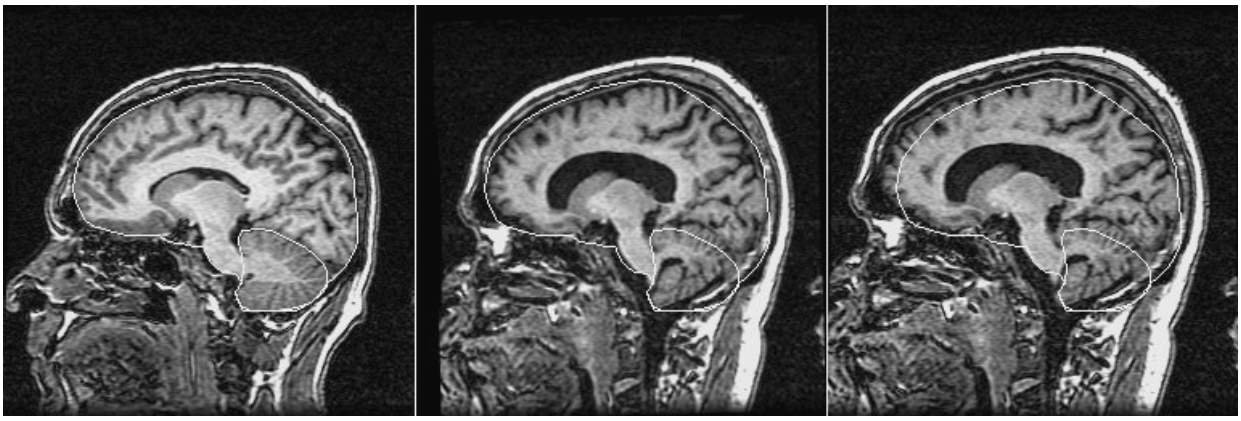

Figure 3.1: Registration results obtained using a similarity transformation. Left: One MR slice from a normal subject volunteer. Right: Corresponding slice from an alcoholic subject. Middle: Corresponding slice of a volume created by registering the alcoholic subject volume to the normal subject volume using a similarity transformation. The brain and cerebellum have been manually segmented on the normal subject volume, and these contours are repeated on the other two volumes.

transformation. Segmented structures in the atlas volume are then mapped to the corresponding structures in the subject volume using the combined global and local transformations.

Methods

A. Data Sets

Seven patients with a history of alcoholism and seven normal subject volunteers were used in this study. Multiple 3-D magnetic resonance (MR) image volumes were obtained of each subject. Normal subjects were scanned three times within a period of three weeks (n=5) or within a period of 5 months (n=2). Alcoholic subjects were admitted to a detoxification program, and the first scan was obtained within 5 days of abstinence. The second scan was obtained within one month, followed by a third scan at approximately 3 months after the first scan. An additional image volume obtained with the same imaging parameters was used as the atlas. All image volumes were acquired with a General Electric 1.5 Tesla Signa MR scanner using a spoiled gradient echo pulse sequence (T1/TR/TE = 400/11/2 msec). Each volume consists of 124 sagittal slices, and each slice has dimensions of 256 x 256 pixels. Voxel dimensions were .94 x .94 x 1.3 mm^3. All image volumes used in this study were acquired at approximately the same time of the day.

B. Image Registration

The registration algorithm used in this study consists of two major steps. First, a seven parameter (three rotation angles, three translation vectors, and one scaling factor) transformation that brings the two volumes into global correspondence is computed. This transformation will be referred to as the global transformation. Next, the volumes are deformed using a highly non-linear transformation to bring these two volumes into local correspondence. This second transformation will be subsequently referred to as the local transformation. Both of these steps are fully automatic. Because the method used in step (2) is also used to compute the transformation in step (1), the local transformation method is described first. All the algorithms used in this study were written in IDL (Interactive Data Language, Research Systems, Inc.) and executed on a Sun Ultra 1 workstation (Sun Microsystems, Mountain View, CA).

1) Local Registration: Thirion [4] presented the problem of image matching in terms of "demons" (by analogy with Maxwell's demons). This is a general framework in which object boundaries in one image are viewed as semi-permeable membranes. The other image, considered as a deformable grid, diffuses through these interfaces driven by the action of effectors (the demons) situated within the membranes. In the particular case of deformations based on voxel-by-voxel intensity similarity the demons paradigm is similar to optical flow methods. Optical flow was developed to estimate small displacements in temporal image sequences (for a more detailed description of optical flow techniques see [5]). The basic tenet of optical flow is that the intensity of a point in an image remains constant under motion. This concept can be used to match the intensity pattern of one image to another. As proposed by Thirion [6] the registration between two images can be determined by computing a displacement vector for each voxel:

$$\vec{v}_{I_2 \to I_1} = \frac{(I_2 - I_1)\vec{\nabla} I_1}{\vec{\nabla} I_1^{\,2} + (I_2 - I_1)^2} \tag{3.1}$$

where $\vec{v}_{I_2 \to I_1}$ is the deformation field that registers image I_2 to image I_1.

Using this approach, global smoothness of the displacement field is not enforced. In order to ensure that like structures of an image are deformed reasonably (i.e. adjacent voxels move in a similar manner), a Gaussian filter is used to smooth the deformation field. The standard deviation of the Gaussian filter can also be used to change the characteristics of the matching

transformation. The larger the standard deviation of the filter, the less elastic the transformation. Large morphological differences and possible topological differences between image volumes could render optical flow methods ineffective. Two mechanisms have been used to make the algorithm more robust to both of these types of differences. First, the algorithm is applied in a hierarchical way. An image pyramid is constructed and the algorithm is applied at the lowest level of resolution. Results obtained at this level are used to initialize the displacement field at the next level and the process is repeated until the highest level of resolution is reached. Second, a mechanism has been implemented that maintains compatibility between the forward and the reverse deformation fields. As proposed in [4,7] this is done by computing the deformation field T_{12} (the deformation field warping image 1 onto image 2) and the deformation field T_{21} (the deformation field warping image 2 onto image 1) and distributing the residual $R = T_{12} \circ T_{21}$ onto these two fields.

Since the deformation algorithm aims at reducing intensity differences between images, it is sensitive to global intensity differences that may occur due to the setting of image acquisition parameters. To reduce these intensity differences, the intensity histogram of each volume was matched to the histogram of a standard volume prior to registration.

Image volumes need not be perfectly aligned in order for this algorithm to work properly. However, if the two volumes are out of position by more than 5 degrees in any direction, the algorithm is unlikely to succeed. Therefore, it is necessary to initially align the volumes using a global transformation.

2) Global registration: Prior to applying the deformation algorithms, the images to be matched are brought into approximate correspondence using a seven degrees of freedom transformation (rotation, translation, and isotropic scaling). Displacement vectors computed as described in the previous section were used to estimate this transformation. First, the deformation field between the two images is computed at the lowest level of resolution. Once this is done, a transformation $T: (x, y, z) \rightarrow (x', y', z')$ which maps any point in one image onto a point in the other image is established. A set of 3-D points p in the first image and the corresponding set of points p' in the other image can thus be determined. For this study, points were randomly selected from the first image from a bounding box surrounding the brain that helped eliminate the background. Background points should not be used since they may contain deformations of random magnitude and direction. Points where the intensity was below a certain

threshold were also eliminated, and new points were picked until a complete set of 20 points was obtained. Using these homologous points the seven degrees of freedom transformation is computed. This is done by first computing a rigid body transformation using the algorithm proposed by Arun *et al* [8] and then determining the isotropic scaling factor.

This process can be repeated until the transformation no longer changes between iterations or until a set number of iterations are completed. For this study, the algorithm was repeated for five iterations.

The original full-resolution image was then reformatted using the accumulated transformation and the local registration algorithm was applied to this new image volume. Typically, the global transformation computed with this approach is not as accurate as one computed with other methods such as mutual information. However, it has the advantage of being fast and is sufficiently accurate to provide a reliable starting point for the local deformation algorithm. This technique produced acceptable results in each registration case used in this study. The entire segmentation process (global and local transformations) was repeated on several subjects. Although the global transformation was usually slightly different between trials, the final segmentation results were identical.

C. Segmentation

Computing the desired indices of atrophy require pre- and post-atrophy brain volumes as well as cerebellum volumes. Pre-atrophy brain volumes are difficult to obtain as historical data that would provide these volumes were not available for each subject. Instead, the intra-dural volume was used as the reference to which brain volumes are compared. The intra-dural volume in the atlas image was determined by careful manual segmentation. The spinal cord was not included in this region, and was eliminated by excluding that which did not fall within a straight line from the pons-medulla junction to the tip of the tonsil of the cerebellum.

Contours were outlined in each slice of the sagittal volume, and a binary mask of the intra-dural volume was created. Six slices of the atlas volume are shown in Figure 3.2, along with the contours used to extract the intradural volume. Notice in the last two panels the method used to eliminate the spinal cord.

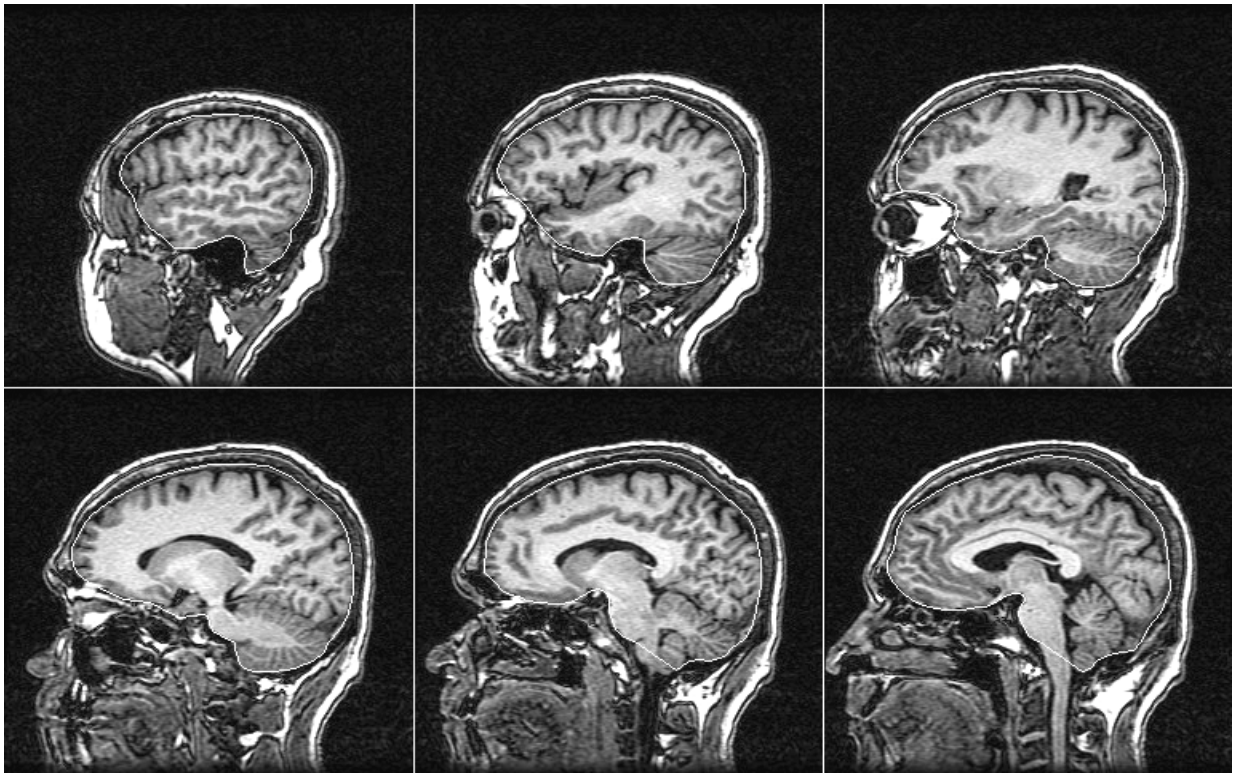

Figure 3.2: Six slice images of the atlas volume showing the location of the manually drawn contours used to segment the brain atlas.

This same method was repeated to obtain a binary volume of the cerebellum (both hemispheres) in the atlas. The region was segmented to include the entire cerebellum region, and individual folia were not followed. Note that the first mask does also include the cerebellum.

In order to segment the intra-dural region and the cerebellum in subject volumes, the atlas was first registered to each volume. The deformation field was then applied to the binary atlas volumes to create intra-dural and cerebellum masks in each individual volume.

D. Volume Measurements

The intra-dural brain volume of each subject is determined by calculating the volume of the mask created by projecting the atlas mask onto each individual image volume. The brain volume (white and gray matter) is obtained by thresholding the intra-dural image to eliminate cerebrospinal fluid (CSF). The threshold value was manually chosen in the atlas volume. In order to compensate for inter-scan intensity variations, an intensity correction algorithm was applied to

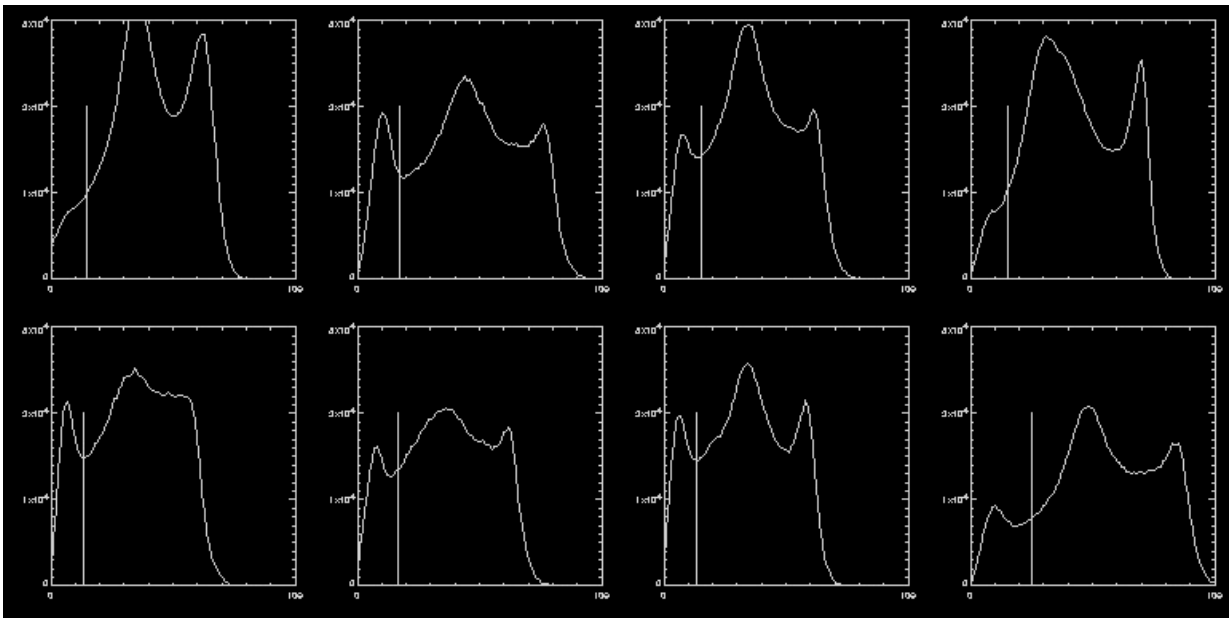

Figure 3.3: Intensity histograms of the segmented brain for the atlas (top left) followed by each of the seven alcoholic subjects used in this study (the third acquisition is shown). The manually identified tissue threshold is shown in the atlas histogram, as well as the thresholds obtained automatically for the alcoholic subjects.

automatically adjust this threshold level to the proper value for each of the subject volumes. This was done by calculating the histogram of the segmented brain of the subject, eliminating a fixed small percentage of the largest values to reduce the sensitivity to noise, and scaling the intensity threshold used in the atlas by the ratio of largest intensity value in the subject volume and the largest intensity value in the atlas volume. This threshold was then applied to the segmented intra-dural images, and a brain volume was determined. The cerebellum volumes were computed in the same manner as the brain volumes, using a separate intensity threshold.

Example histograms and corresponding thresholds are shown in Figure 3.3. The histogram and threshold of the atlas brain are shown in the first panel, followed by the histograms and thresholds of the brain images for each of the seven alcoholic subjects (acquisition 3 is shown). This figure shows the algorithm's ability to automatically determine the intensity value separating CSF from brain tissue.

Results

Figure 3.4 illustrates qualitatively the type of results that were obtained. The top row of this figure shows three slices in one MR volume (a normal volunteer). The bottom row shows the

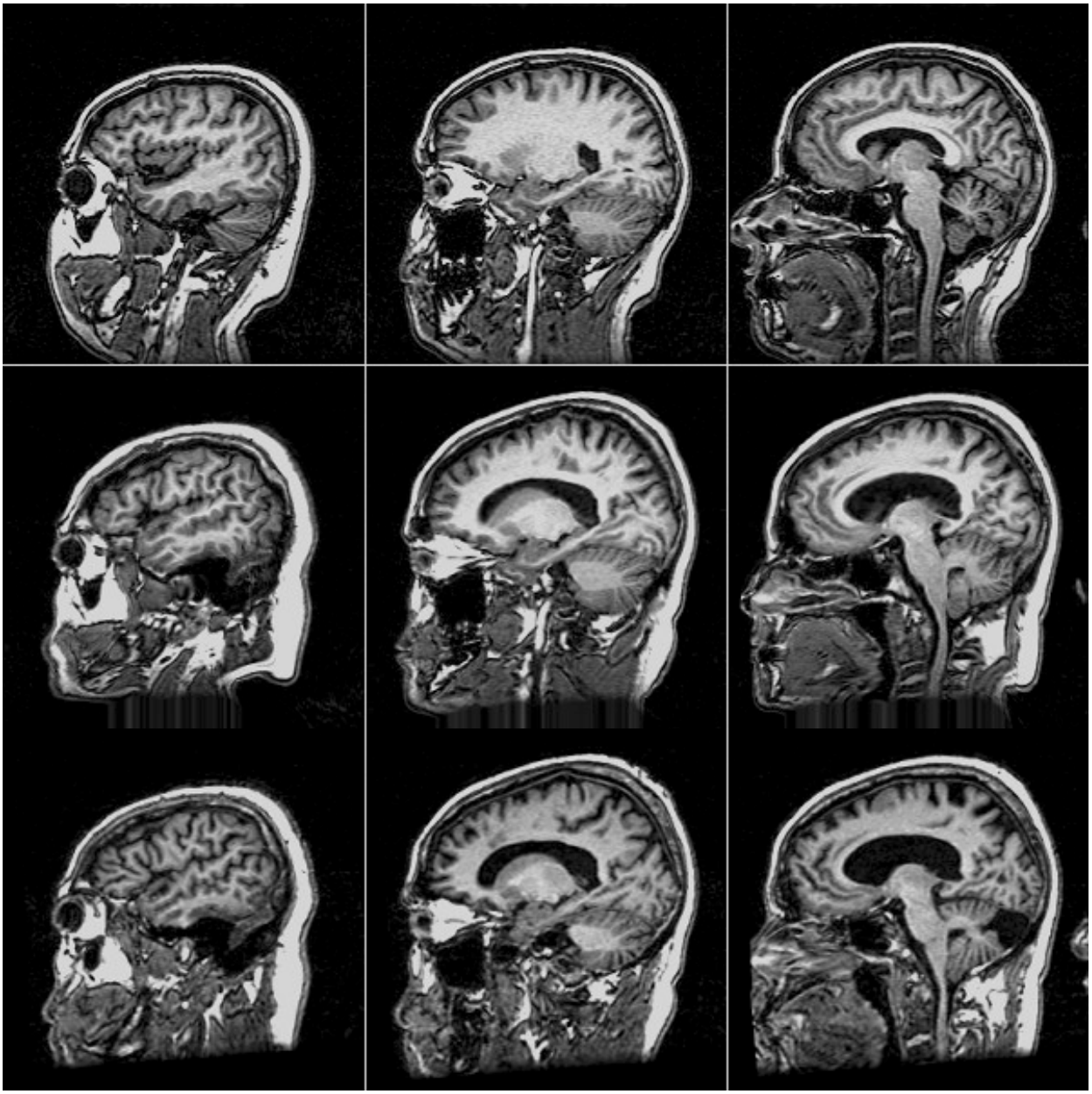

Figure 3.4: Results of the non-rigid registration algorithm. Top row, three slices from a normal subject volunteer, used as the source volume. Bottom row, corresponding slices from an alcoholic subject volunteer, used as the target volume. Middle row, corresponding slices obtained by deforming the source volume to match the target volume.

slices with the same index in another volume (an alcoholic patient). Observe the large amount of atrophy (enlarged sulci and ventricles and atrophied cerebellum) visible in the patient volume. The middle row shows the slices with the same index in the volume obtained by warping the normal brain volume onto the atrophied brain volume. After deformation, the ventricles and sulci

Figure 3.5: Cerebellum segmentation results of one slice for three normal subjects (top row) and three alcoholic subjects (bottom row). The automatically computed contours are shown in white.

in the normal brain volume have been enlarged, the thickness of the corpus callosum has been reduced, and the overall shape of the head has been modified, but the integrity of the cortical structures have been preserved. This figure illustrates the ability of the algorithm to minimize morphological differences while preserving topological differences.

Figure 3.5 shows representative results for the automatic segmentation of the cerebellum. This figure shows one slice in each of three normal volunteer volumes (top row) and three alcoholic subjects (bottom row). The cerebellar contours obtained with the automatic technique are overlaid in white (the third acquisition was used). Observe the ability of the algorithm to produce accurate results even though the shape and orientation of the cerebellum varies greatly from one volume to the other.

Results obtained for each volume included in this study were inspected visually and found to be comparable to those shown in Figures 3.4 and 3.5. Quantitative assessment of

automatic segmentation methods is a difficult and time-consuming task. Yet it is critical to assess the robustness and accuracy of these methods. To evaluate the results quantitatively a distinction is made between repeatability and accuracy. The data set used includes three acquisitions per subjects (both for the normal and the alcoholic volunteers). This permits the evaluation of the consistency and repeatability of the measurements. Changes are not expected in the volume encompassed by the dura in either the normal or the patient population and only minor changes (if any) are expected in the brain and cerebellar volumes for the normal population. Changes related to abstinence may be observed both in the brain and the cerebellum volumes for the patient population. Consistent values for structures that are not expected to change in serial scans of the same subject are thus good indicators of the reliability of the measurements. Accuracy is more difficult to assess because it can only be measured against a gold standard. For this study, accuracy was assessed by comparing the results obtained automatically to results obtained by manual delineation.

A. Repeatability

Figure 3.6 shows the intra-dural volumes obtained for both the normal and the patient population as well as the brain and cerebellum volumes obtained for each acquisition for the normal population. For each subject, this figure shows the volume measurements that have been obtained for the three acquisitions.

These results demonstrate the consistency of the measurements. For the intra-dural volume and the normal population, the average coefficient of variation (COV), defined as the standard deviation divided by the mean, was calculated to be 0.7% with a maximum of 2.3%. This average was obtained by first computing a COV for each subject and then computing a population average. For the patient population these numbers were 1.09% and 1.9%, respectively. For the normal population and the brain volume, the average and maximum COV were 1.11% and 3.5% respectively. For the normal population and the cerebellum volume, these values were 1.9% and 2.8%. The larger values observed for the cerebellum COVs are explained by the fact that the total cerebellar volume is smaller than the total brain volume. Note that the results involving intra-dural measurements evaluate the deformation algorithm alone. Results involving the brain and the cerebellum evaluate the combination of the deformation and the automatic thresholding algorithms.

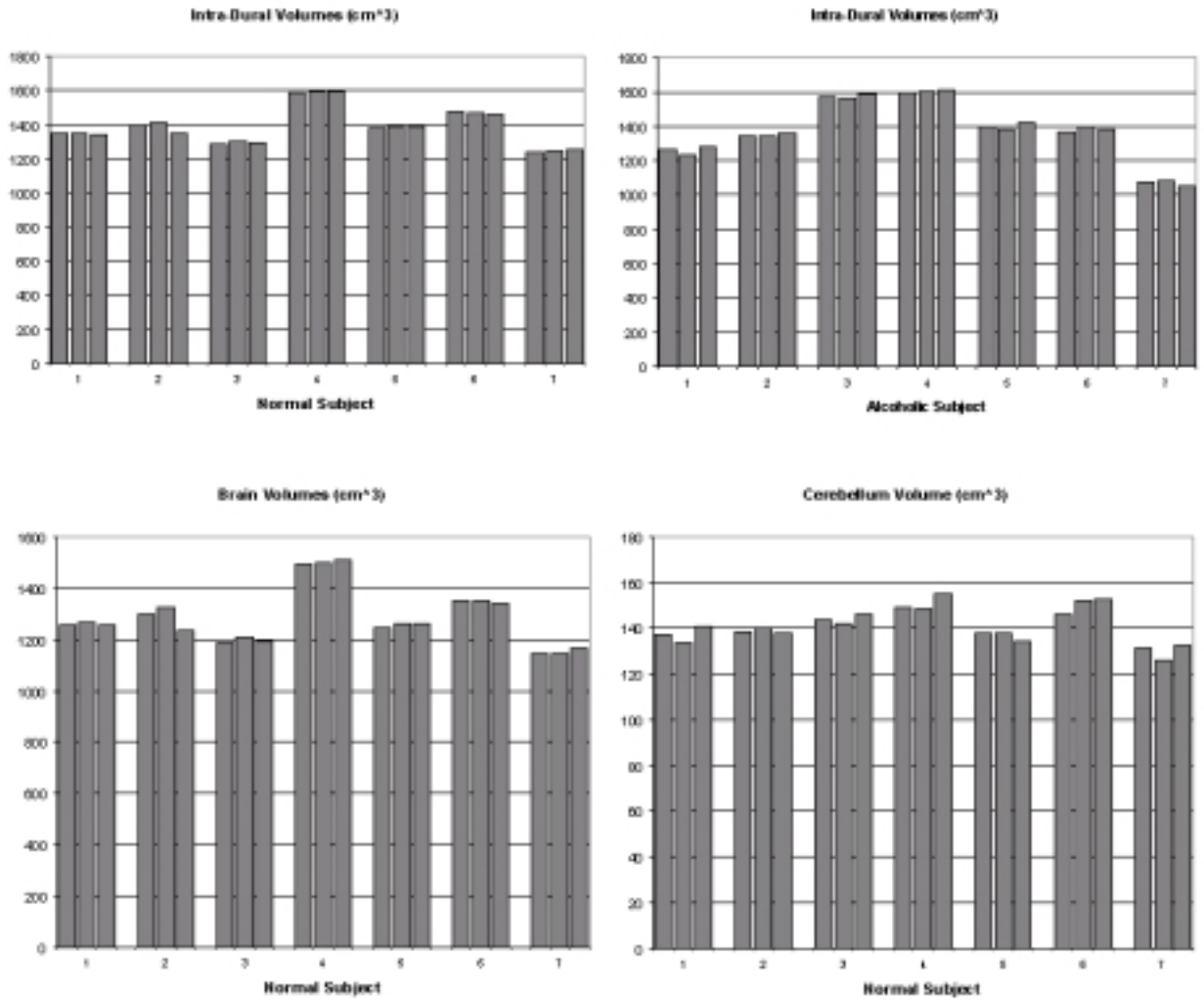

Figure 3.6: Top row, intra-dural volumes obtained for each normal subject (left) and alcoholic subject (right) acquisition used in the study. Bottom row, brain (left) and cerebellum (right) volumes for each normal subject acquisition.

B. Accuracy

Due to the large amount of data included in this study, it was not feasible to manually segment the brain and the cerebellum in each volume (this would have resulted in approximately 10,000 hand-drawn contours). Instead, for each normal and patient volume, four slices were segmented manually (two of the brain and two of the cerebellum). These slices were chosen by first determining the range of slices on which the structures were visible in the image volumes and then randomly selecting two slices per structure within this range. Ranges and selected slices were different for the cerebellum and for the brain. The similarity between contours obtained

Table 3.1: Similarity indices between manually and automatically obtained regions for the normal (top) and alcoholic (bottom) subjects.

	Normal Subjects	
	Dura (n=42)	Cerebellum (n=42)
mean	0.98	0.95
median	0.98	0.96
min	0.96	0.87
max	0.99	0.98

	Alcoholic Subjects	
	Dura (n=42)	Cerebellum (n=42)
mean	0.97	0.94
median	0.97	0.94
min	0.95	0.88
max	0.98	0.98

manually and contours obtained automatically was computed using a similarity index S related to the kappa statistic [9], defined as follows:

$$S = \frac{2N(C1 \cap C2)}{N(C1) + N(C2)} \tag{3.2}$$

where N(C1) equals the number of pixels included in the manual contour and N(C2) equals the number of pixels included in the automatic contour. This index varies between 0 and 1 (1 indicates perfect agreement between two contours while 0 indicates no overlap) and is sensitive to both differences in size and relative position. This strategy resulted in 84 brain and cerebellum contours for the normal population and 84 contours for the alcoholics. Table 3.1 lists the mean, median, minimum, and maximum values for the indices of similarity that were obtained. This table shows that both for the normal and the patient population manual and automatically obtained contours are virtually identical.

C. Comparison of atrophy indices between normal and patient populations

The intra-dural, brain, and cerebellum volumes can be used to compute indices of atrophy. Figure 3.7 shows the intra-dural/brain volume ratios as well as the brain/cerebellum volume ratios for both the normal and the patient population. The first index measures the total

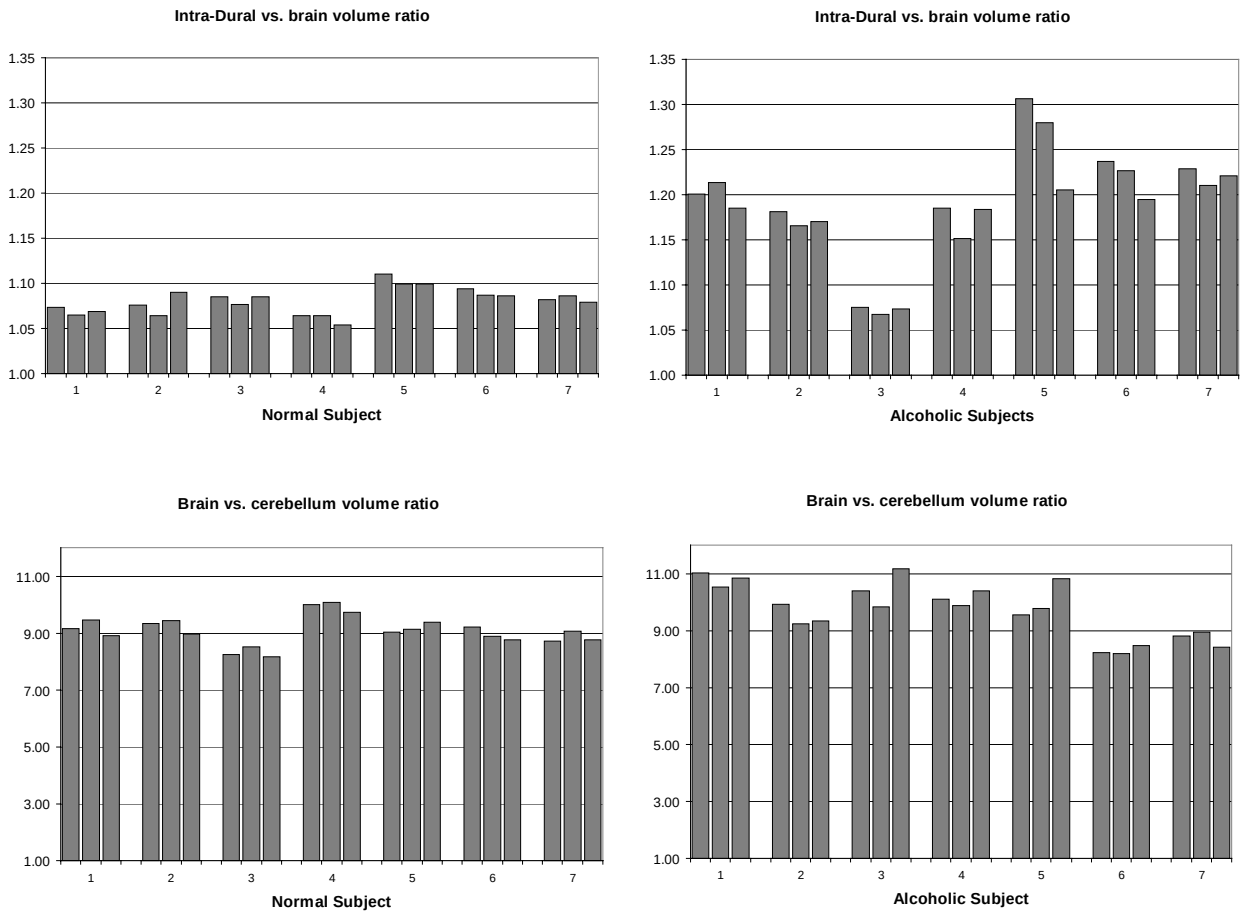

Figure 3.7: Top row, total brain atrophy measured as a ratio between the intra-dural volume and the brain tissue volume for each normal subject (left) and alcoholic subject (right) acquisition used in the study. Bottom row, relative atrophy between the brain and cerebellum as a ratio between the brain volume and the cerebellum volume for each normal subject (left) and alcoholic subject (right) acquisition used in the study.

brain atrophy while the second measures the relative atrophy between the brain and the cerebellum.

This figure reveals a number of trends. First of all, as expected, the intra-dural/brain ratios as well as the brain/cerebellum ratios remain within a narrow range for the normal population (the largest variation was observed for subject 2 - this is also the subject for which we observed the largest variation in brain volume). Second, the intra-dural/brain ratios are much larger for the alcoholics than they are for the normal population; the average ratio went from 1.08 in the normal population to 1.19 in the alcoholic population. This is consistent with global brain atrophy. The clinical significance of these findings is, however, difficult to assess because

the normal and the alcoholic populations were not age-matched. With this data set, it is therefore not possible to separate the effects of age and alcohol on this atrophy index (however, it is interesting to note that patient 3 is the youngest patient included in the study). Third, brain/cerebellum ratios are larger for the patient population, moving from 9.09 for the normal population to 9.70 for the alcoholic population. This indicates a relative rate of atrophy that is faster for the cerebellum than for the entire brain. Several patients did, however, have a brain/cerebellum ratio in the normal range. Finally, a large change in dura/brain volume over time was observed for patients 5 and 6. Visual inspection did not reveal segmentation errors, which suggested a change in brain volume between acquisitions. This was confirmed by registering sequential scans with a rigid body transformation and computing difference images. This is shown in Figure 3.8 for one slice of alcoholic subject 5 (top row) and subject 6 (bottom row). The left panel shows one slice of the first acquisition after it has been registered with the third acquisition (using a rigid-body transformation) and reformatted. The middle panel shows the corresponding slice of the third acquisition, and the right panel shows the difference image (left image subtracted from middle image). The difference images clearly show that volume changes have in fact occurred around the ventricles. The sign of the difference image indicates a reduction in the ventricular volume between the first and the third acquisition. This corresponds to an increase in brain volume, a trend that has been documented in recovering alcoholics [10].

Discussion

This study demonstrates that atlas-based segmentation techniques can be made robust enough to deal with large morphologic differences between brains caused by severe atrophy. To the best of the authors' knowledge, this is the first time that results have been reported on a study involving atlas-based segmentation of brains with pathologies that can alter brain morphology to the extent observed in the data set analyzed in this study. The approach used in this study is fully automatic and only requires a few parameters: the number of levels used in the multi-resolution pyramid, the number of iterations at each level, and the standard deviation of the filter used to smooth the deformation field. Both for the normal and the patient volumes, these parameters were kept constant, indicating the insensitivity of the algorithm to these values.

The intra-dural volumes reported in Figure 3.6 demonstrate the excellent repeatability of the results obtained using the deformation algorithm. Brain and cerebellum volumes vary slightly

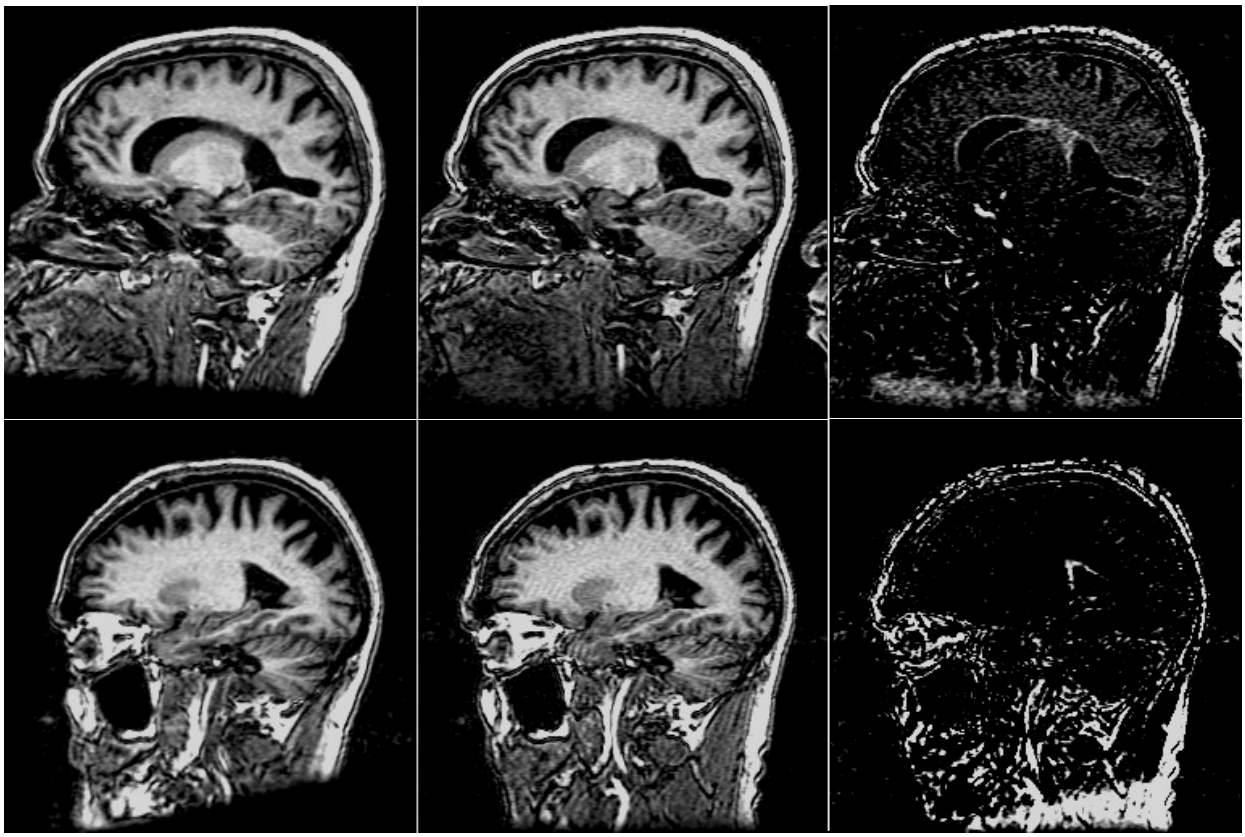

Figure 3.8: Visual confirmation of changes measured between the first and third acquisitions in two different alcoholic subjects (subject 5 shown in the top row, subject 6 in the bottom row). The left panel in each case shows one slice of the first acquisition after it has been registered with the third acquisition (using a rigid-body transformation) and reformatted. The middle panel shows the corresponding slice of the third acquisition. The right panel shows the corresponding slice of the difference volume obtained between the left and middle panels.

more, reflecting the fact that two steps are involved in the process: deformation and thresholding. Slight misplacement of the intensity threshold used to separate the brain from CSF will indeed affect the volume measurements. This is compounded with inaccuracies in the placement of the contour. Nevertheless, the average coefficient of variations remain as low as 1.11% and 2.25% for the whole brain and the cerebellum, respectively. For comparison purposes, the brain volume of one subject was calculated after changing the threshold used for segmentation. Changing the threshold by 5, 10, and 15 intensity values from the computed value led to changes in brain volumes of 3%, 8%, and 14%, respectively. In each case the new volume (after the threshold was applied) was visually assessed. Even though there were visual differences between the volumes, it was difficult to determine which threshold was the most appropriate for eliminating CSF. This

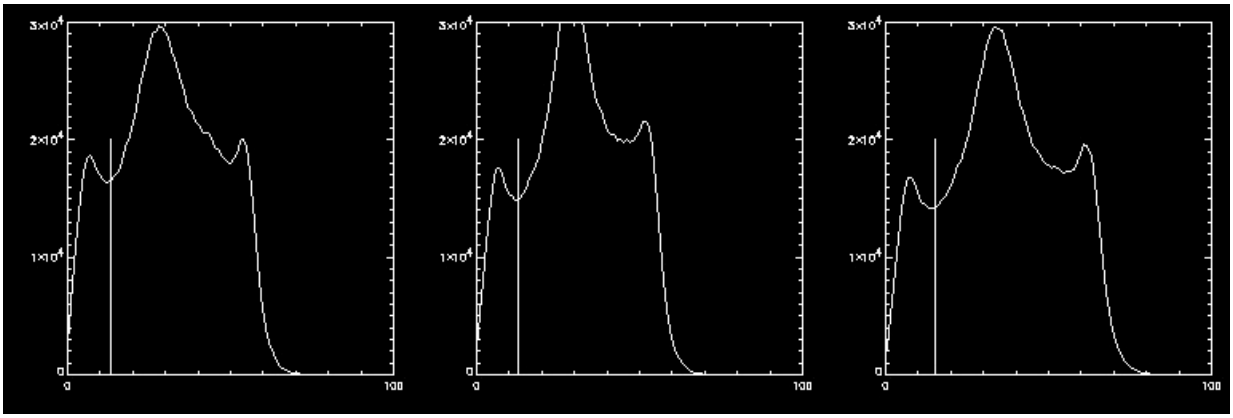

Figure 3.9: Intensity histograms of the segmented brain for each of the three acquisitions of one alcoholic subject (subject 3). The automatically computed threshold used to separate CSF from brain tissue is drawn for each histogram.

indicates the subjectivity involved in the selection of the threshold and confirms the excellent repeatability achieved in this study. Figure 3.9 shows histograms of the segmented brain volumes, and the computed threshold that was used to segment CSF from brain tissue, for all three studies of one alcoholic subject. The histograms in each case have very similar shape, which is to be expected. The automatically computed threshold values were 14, 13, and 16 for each study, and appear to be placed correctly for proper segmentation.

Assessing the accuracy of automatic segmentation is a difficult task, one that can only be done by comparing results to a gold standard. For this study the automatic segmentation results were compared to measurements obtained by manual delineation. Arguably, manually delineated contours are not the ultimate gold standard. But, in this study, the contours were drawn by the same rater on the atlas and on each slice used for the validation purposes. The entire atlas was also delineated twice and similarity indices of 0.98 and 0.96 were observed between these two delineations for the intra-dural and the cerebellar contours, respectively. The average similarity indices observed between manual and automatic delineation on the slices selected for evaluation are therefore comparable to the intra-rater variability observed when delineating the atlas. Thus, results obtained on this data set support the hypothesis that automatic segmentation is as reliable and accurate as manual segmentation.

Acknowledgements

This work was supported in part by NIH grant R01 AA 10583. The authors wish to thank Dr. Jean-Philippe Thirion for discussing details of the “demons” deformation algorithm.

References

[1] CR Maurer and JM Fitzpatrick. A review of medical image registration. In: *Interactive Image-Guided Neurosurgery*, ed. RJ Maciunas. Park Ridge, IL: American Association of Neurological Surgeons, 1993. pp. 17-44.

[2] JBA Maintz and MA Viergever, "A survey of medical image registration," *Medical Image Analysis*, vol. 2, no. 1, pp. 1-36, Apr, 1998.

[3] JA Wada, R Clarke, and A Hamm, "Cerebral hemispheric asymmetry in humans: cortical speech zones in 100 adult and 100 infant brains," *Archives of Neurology*, vol. 32, pp. 239-246, 1975.

[4] J-P Thirion, "Image matching as a diffusion process: an analogy with Maxwell's demons," *Medical Image Analysis*, vol. 2, no. 3, pp. 243-260, 1998.

[5] B Horn and B Schunck, "Determining optical flow," *Artificial Intelligence*, vol. 17, pp. 185-203, 1981.

[6] J-P Thirion, Fast non-rigid matching of medical images. INRIA technical report, nr. 2547, pp. 1-37, May, 1995.

[7] DJ Burr, "A dynamic model for image registration," *Computer Graphics and Image Processing*, vol. 15, pp. 102-112, 1981.

[8] KS Arun, TS Huang, and SD Blostein, "Least-squares fitting of two 3-D point sets," *IEEE Transactions on Pattern Analysis and Machine Intelligence*, vol. 9, no. 5, pp. 698-700, Sep, 1987.

[9] AP Zijdenbos, BM Dawant, and R Margolin, "Morphometric analysis of white matter lesions in MR images: method and validation," *IEEE Transactions on Medical Imaging*, vol. 13, no. 4, pp. 716-724, 1994.

[10] A Pfefferbaum, EV Sullivan, DH Mathalon, PK Shear, MJ Rosenbloom, and KO Lim, "Longitudinal changes in magnetic resonance imaging brain volumes in abstinent and relapsed alcoholics," *Alcoholism: clinical and experimental research*, vol. 19, no. 5, pp. 1177-1191, 1995.

CHAPTER IV

OPTICAL FLOW BASED BRAIN REGISTRATION WITH SULCAL CONSTRAINTS FOR IMPROVED CORTICAL ALIGNMENT

Steven L. Hartmann[1], Robert L. Galloway, Jr.[1], and Benoît M. Dawant[2]

[1]Department of Biomedical Engineering
[2]Department of Electrical and Computer Engineering

Vanderbilt University

Nashville, TN 37235

Portions of this manuscript have been submitted for publication in:

IEEE Transactions on Medical Imaging, January 2002.

Abstract

This study presents a method for accurate inter-subject registration of MR brain volumes using an optical-flow based deformation technique. In order to improve the quality of the registration around cortical regions, the location of brain sulci in the desired area are identified and used to guide and constrain the registration process. This method was used to register 18 MR volumes of the head to a standard reference (atlas) volume. Accuracy was determined by measuring the distance between corresponding contours before and after registration. Comparisons were made to results obtained using a global transformation and results obtained using optical flow without cortical constraints. The addition of cortical constraints consistently improved the overall registration accuracy.

Introduction

During a typical neurosurgical procedure, the primary objective is to localize and remove a cerebral lesion without causing neurological deficit. The risk involved with these procedures increases when the lesion or the surgical path to the lesion is adjacent to functionally important brain regions, since damage to functional regions is often irreversible [1]. Image-guided technology has increased the accuracy of localizing targets but has not, for the most part, included the identification of functionally important areas of the cortex. The ability to identify these critical brain regions would aid in pre-surgical planning by determining the safest and most appropriate trajectory. Intraoperatively, the functional information would complement the anatomical information already available during image-guided procedures.

Functional regions of the cortex can be determined invasively by direct cortical stimulation or non-invasively using different imaging methods such as PET and fMRI. It is not feasible or even possible, however, to create a detailed functional map from each neurosurgery patient. Only a limited area of the brain can be mapped by direct stimulation since the majority of the cortex is inaccessible during surgery. Imaging methods can provide a much greater area of coverage, but require dedicated machines that may not be available and specialized techniques that may not be possible for each patient.

Statistical information on brain function and location, obtained from a collection of multiple patients, could be used in particular cases where it is not possible to create a detailed brain map. This type of historical information may also benefit those cases where a cortical

function map was available, as an "average" brain map may provide additional information or perspective that cannot be obtained from the particular patient's map alone.

An average brain map can be created by registering each patient's tomogram to a standard reference frame. Once this transformation is determined, the location of functional data can be mapped to the same reference space. A number of atlas-based registration techniques have been developed for the purpose of inter-subject registration (see [2] for a detailed review).

Computerized anatomical atlases, such as the Talairach atlas [3], have been used to map cortical regions identified on the Talairach brain to the desired brain volume using atlas-based registration techniques. Most of these techniques use linear proportional scaling, which does not account for the large cortical variations between the atlas and desired subject volumes, and therefore result in poorly matched cortical regions.

The study described in [4] demonstrated that an optical-flow based registration method was capable of accurately matching major brain structures (cerebrum and cerebellum) between magnetic resonance (MR) image volumes of different subjects. For accurately mapping cortical location from an atlas volume to a patient volume, however, this method must be improved. Initial observations of matched cortical structures (using the optical flow deformation algorithm) showed that major cortical gyri were not consistently aligned after registration. This can be seen in Figure 4.1. The panel on the left shows one MR slice from one subject, while the panel on the right shows the same slice of an MR volume from a second subject. The panel in the middle shows the same slice of the volume created by registering the volume on the right with the volume on the left. The registration was computed using the optical flow algorithm described in [4], which is an independent implementation of the technique originally proposed by Thirion [5]. The optical flow algorithm does not use any structural information from features in the image to determine the registration, but instead computes a 3-D deformation field (i.e. a displacement for each voxel in the image) using the intensity characteristics of each image (this technique will be explained in more detail in the next section). Contours were drawn around the cerebrum and cerebellum on the slice in the left panel in Figure 4.1, and these contours were mirrored onto the other two images. If the registration were accurate, these contours would exactly define the same regions in the slice shown in the middle panel, which appears to be the case. Closer analysis, however, shows that several of the cortical gyri have not been registered correctly. The central sulcus has been identified for this slice on the image in the left panel, and the mirrored location

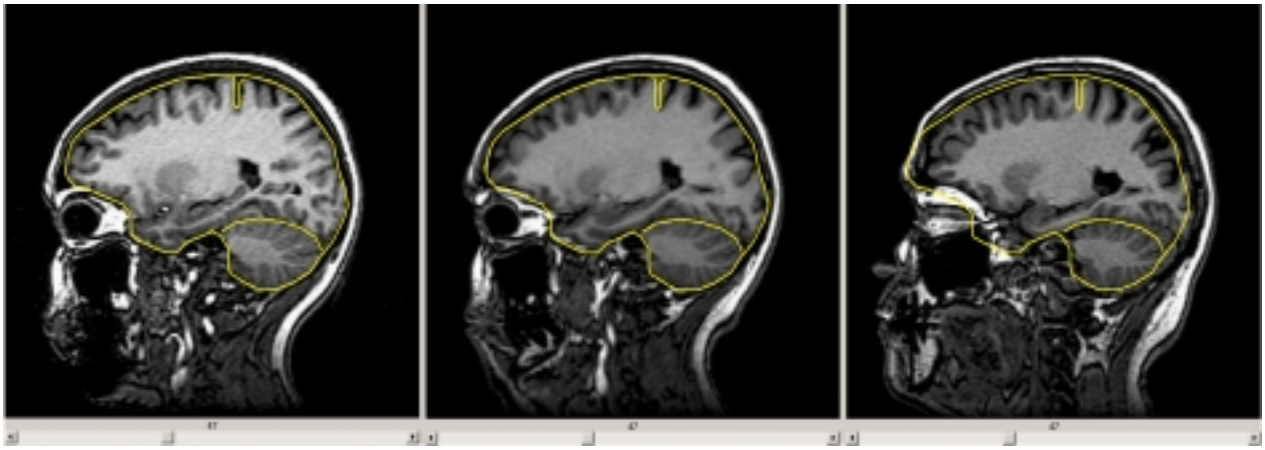

Figure 4.1: Sample registration results using the optical flow algorithm. Each panel shows the same slice index (slice 47) from 3 different MR volumes. The transformation that registers the volume on the right with the volume on the left is used to create the volume shown in the middle panel. Contours have been drawn on the image on the left and mirrored onto the other two images.

of this line on the deformed image clearly show that the registration is not accurate in this region. Since this alignment is critical for matching functional regions of the cortex, several improvements have been made to this inter-subject registration process. The deformation field calculated by the optical flow algorithm can be "constrained" by using the location of the major cortical sulci. This requires a method of identifying the sulci in the tomogram images.

Labeling sulci has traditionally been a manual process performed by an expert. This can produce accurate results but since the sulci typically need to be identified on each slice of the tomogram, it can also be a long and tedious process prone to errors such as operator fatigue and bias. An automatic or semi-automatic method for sulci identification would be beneficial. Several techniques have been introduced for this purpose.

Caunce and Taylor [6] developed a projection method that automatically locates points over the sulcal fissures on the cortical envelop. The points are assigned to curve segments automatically and registration between corresponding curves is determined using a variant of the iterative closest point (ICP) algorithm [7].

Ge *et al* [8] developed a cortical surface mapping technique that allows for interactive localization of brain convolutions. This visualization method, a sub-class of volume rendering, creates orthographic projections of an eroded envelop of a brain surface. These cortical maps are linked together, which allows a user to interactively localize convolutions.

Rettmann *et al* [9] developed a method that finds the actual cortical regions surrounding the sulci as opposed to extracting the sulcal spaces. The brain of each volume is initially segmented, and sulcal regions are found by generating a depth map on the brain surface.

Lohmann [10] developed an automatic procedure for extracting sulcal and gyral patterns from MR brain images. Highly condensed line representations are found that describe the individual properties of the cortical surface. Sulcal cuts are found by first segmenting the white matter, which is then closed using a morphological filter. The depth level is determined with respect to this closed white matter image. The cuts are obtained by subtracting the white matter image from the closed image and applying a skeletonization which produces sulcal median surfaces. Gyral and fundus cuts are produced using similar techniques.

Le Goualher *et al* [11] developed a technique called active ribbons for the 3-D segmentation and representation of cortical folds. Active ribbons are built from active surfaces, which are similar to the active contour snakes developed by Kass [12]. Outer sulci regions are found and used to initialize the active ribbon, which then converges towards the interior using forces that minimize internal (regularization) and external (model similarity) energy. This method for sulci identification is used in SEAL (Surface Extraction and Assisted Labeling), a process for interactively identifying and labeling sulci. A probabilistic atlas of possible labels assists the user in identifying a particular sulci [13].

Several methods for identifying sulci and gyri have been proposed using crest lines. Crest lines are mathematically defined as lines that join points of zero maximal principal curvature. Thirion *et al* [14] developed the marching lines algorithm for extracting crest lines from brain images. On the cortical surface crest lines match the anatomically defined pattern of gyri and sulci. Extracted crest lines can be used as feature sets for image registration, as shown by Subsol *et al* [15]. A detailed explanation of crest lines and their applications in medical imaging can be found in [16].

Additional methods for identifying cortical brain regions have also been developed [17-22]. The goal of most of these methods is to identify and label gyri or sulci regions and use the results for atlas creation or for registration (for detailed examples, see [17, 20]). This requires that a complete set of cortical regions must be acquired. For this study, this was not necessary since the cortical regions are used only to initialize and guide the free-form deformation of the optical flow algorithm. Since only the brain function from major functional regions such as

motor, sensory, and speech will be identified and displayed during surgery, only these cortical areas will be used to constrain the deformation field.

Methods

A. *Data Sets*

Multiple 3-D magnetic resonance image volumes were obtained from six normal subject volunteers. The subjects were scanned three times within a period of three weeks (n=5) or within a period of 5 months (n=1). An additional image volume of a seventh volunteer, obtained with the same imaging parameters, was used as the reference volume. All image volumes were acquired with a General Electric 1.5 Tesla Signa MR scanner using a spoiled gradient echo pulse sequence (T1/TR/TE = 400/11/2 ms). Each volume consists of 124 sagittal slices, and each slice has dimensions of 256 x 256 pixels. Voxel dimensions were .94 x .94 x 1.3 mm^3.

B. *Optical Flow Based Image Registration*

The optical flow registration algorithm used in this study is explained in detail elsewhere [4,23]. The non-linear portion of this algorithm is an independent implementation of the technique proposed by Thirion [5]. In summary, the registration algorithm consists of two major steps. First, a seven-parameters (three rotation angles, three translation vectors, and one scaling factor) transformation that brings the two volumes into global correspondence is computed. Next, the volumes are deformed using a non-rigid transformation to bring these two volumes into local correspondence. Both of these steps are fully automatic, and are described briefly below.

1) Local Registration: Optical flow was developed to estimate small displacements in temporal image sequences (for a more detailed description of optical flow techniques see [24]). The basic assumption of optical flow is that the intensity of a point in an image remains constant under motion. This concept can be used to match the intensity pattern of one image to another. As proposed by Thirion [5] the registration between two images can be determined by computing a displacement vector for each voxel:

$$\vec{v}_{I_2 \to I_1} = \frac{(I_2 - I_1)\vec{\nabla} I_1}{\vec{\nabla} I_1^{\,2} + (I_2 - I_1)^2} \tag{4.1}$$

where $\vec{v}_{I_2 \to I_1}$ is the deformation field that registers image I_2 to image I_1.

The local transformation is computed using an iterative, multi-scale approach. Low-resolution images are created from the original tomograms and these images are matched first. Results obtained at this level are used to initialize the displacement field at the next level and the process is repeated until the highest level of resolution is reached. This algorithm results in a 3-D deformation field (i.e., a displacement vector for every voxel in the volume) that can be used to warp one image onto the other.

Image volumes need not be perfectly aligned in order for this algorithm to work properly. However, if the two volumes are out of position by more than 5° in any direction, the algorithm is unlikely to succeed. Therefore, it is necessary to initially align the volumes using a global transformation.

2) Global Registration: Prior to applying the deformation algorithm, the images to be matched are brought into approximate correspondence using a transformation with seven degrees of freedom (rigid body plus isotropic scaling). Displacement vectors computed as described in the previous section were used to identify a set of points in the first image and a corresponding set of points in the second image. Using these homologous points the transformation is determined by first computing a rigid body transformation using the algorithm proposed by Arun *et al* [25] and then determining an isotropic scaling factor [26].

This global registration method is typically not as accurate as other techniques (such as mutual information), but it has the advantage of being fast and is sufficiently accurate to serve as a reliable starting point for the deformation algorithm.

C. Identification of Brain Sulci

The registration accuracy near the cortical surface can be improved by using the location of desired cortical sulci to constrain the deformation field. This requires the ability to accurately identify the location of the sulci in the tomogram images. For this study, a semi-automatic procedure is used to identify the major cortical sulci on 3-D volume rendered images of the cortical surface instead of on the original tomogram slices.

Before the cortical surface can be rendered accurately, the cerebrum must be segmented from the rest of the tomogram. This was accomplished using an atlas-based segmentation method [4]. The cerebrum of a selected reference volume (the atlas) was accurately segmented by hand,

and a binary mask of this region was created. In order to segment the intra-dural region of the desired subject, the atlas volume was registered with the subject volume using the optical flow technique described in the previous section, and a deformation field was determined. The binary mask of the atlas volume was transformed using this deformation field, which created a second binary mask appropriate for segmenting the subject's brain region.

A set of rendered images of the cortical surface was then created from the segmented MR volume using the volume rendering capabilities of Interactive Data Language (IDL) (Research Systems, Inc.), as described in [27]. The viewing angle of a particular rendering is chosen to show the desired sulcus. For each pixel of a rendered image, a corresponding distance is stored in a separate depth buffer file of the same dimensions as the rendering. This depth value, in millimeters, is the perpendicular distance between the point on the rendered image and the center plane of rotation for the angular view used to create the rendering. This information is used to determine the corresponding 3-D location in the original MR volume for each pixel in the rendered image.

The rendered image set and corresponding depth buffer information are loaded into an image visualization toolkit which was created in IDL. This graphical user interface allows a user to view tomogram and rendered image sets, perform basic image processing functions, and use the mouse to draw contours on top of the images. This interface can be seen in Figure 4.2. The number of display windows and the window size is adjustable – in this case there is one row and two columns of display windows. A tomogram (MR) volume is loaded in the left-hand window, with slice number 30 currently being displayed. A rendered image set is loaded in the right-hand window. Sample contours have been drawn on each image.

The sulci are initially identified by drawing the approximate location of the contour on a rendering of the cortical surface using the graphical user interface shown in Figure 4.2. This contour is then automatically refined by searching for regions of low intensity, features which are characteristic of the sulci in the rendered images. Each pixel that makes up the contour is replaced by the pixel in the surrounding region with the lowest intensity. For this study, the search region was set to a 7x7 pixel area around each contour point. Points outside the rendered image of zero-intensity were not considered in the search. This technique provides a quick and accurate method to identify the major sulci in a rendering of the cortical surface. Stepping through multiple tomogram slices and identifying the sulcus in each is not required. Figure 4.3

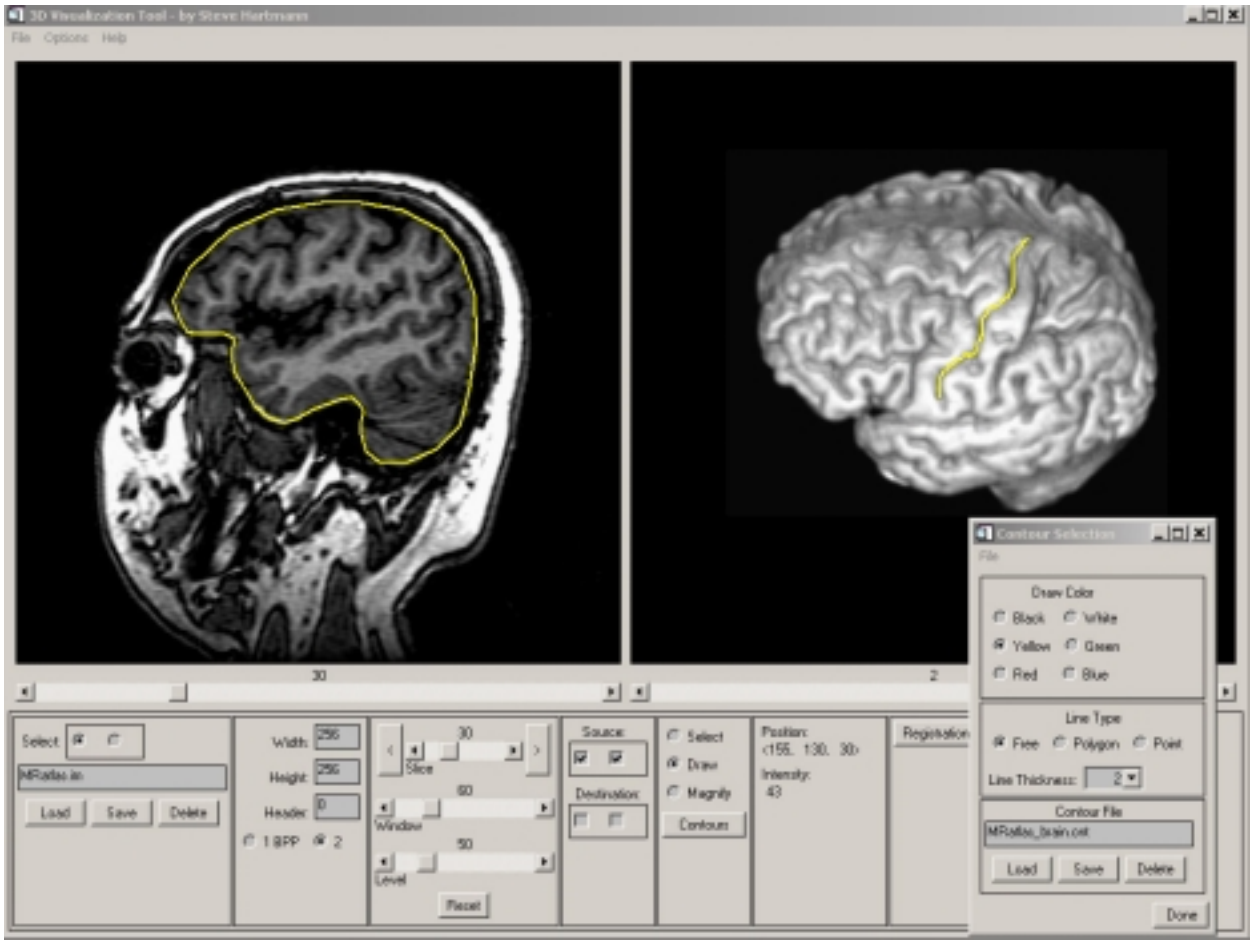

Figure 4.2: The visualization tool used to display and process tomogram and rendered image sets. Example contours have been drawn on each image.

shows an example using this method. The left-hand panel shows a rendering of the cortical surface. A contour has been drawn to approximate the location of the central sulcus (the contour has intentionally been drawn poorly in this case). The right-hand panel shows the same contour after it has been automatically refined. Even poorly approximated initial contours can be automatically adjusted to define cortical sulci using this method. After a contour has been refined, it is possible (and even likely) that adjacent points in the contour will be assigned to a single location. Since these additional points are not needed to define the contour, they are removed from the set.

On occasion, a contour is refined to a less than ideal location. This can happens when a particular point on the contour is moved to a location not on the sulcus. Most frequently this point was the endpoint of the contour near the longitudinal fissure since this is typically a low

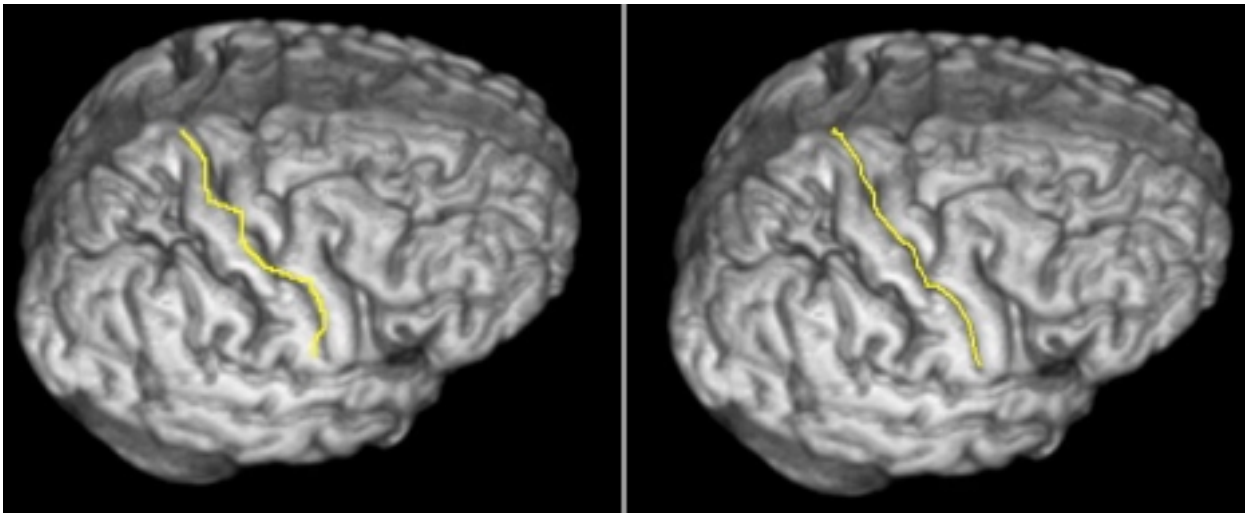

Figure 4.3: Cortical surface renderings showing typical results of the contour refinement procedure. A contour drawn approximately by hand (left panel) has been automatically adjusted to identify the central sulcus (right panel).

intensity region on the rendered image. When this occurs, the user can identify the desired endpoint using the mouse and the poorly defined point is replaced. Occasionally a point in the middle of the contour is moved to nearby sulci area. When this occurs, the contour can be quickly deleted and the process is repeated. This happened twice during the identification of approximately 100 sulci contours.

A complete set of contours for all major sulci can be created for the reference brain. This process only needs to be done once. For each patient only the desired sulci are identified, and only this information is used to constrain the registration.

D. Constrained Optical Flow

For this study each of the MR volumes from all six subjects were registered to the reference (atlas) volume. A set of corresponding sulci contours were created for each of the images in order to constrain the deformation field calculated by the optical flow algorithm. The objective of this study was to improve the registration alignment of the motor cortex. Therefore, the central sulcus of both hemispheres was identified and used for constraining the registration.

The set of points that make up each sulcal contour on the rendered images are first converted to their corresponding 3-D positions in the original MR volume. This is done by using the geometry information used to create the rendered image along with the depth buffer file that

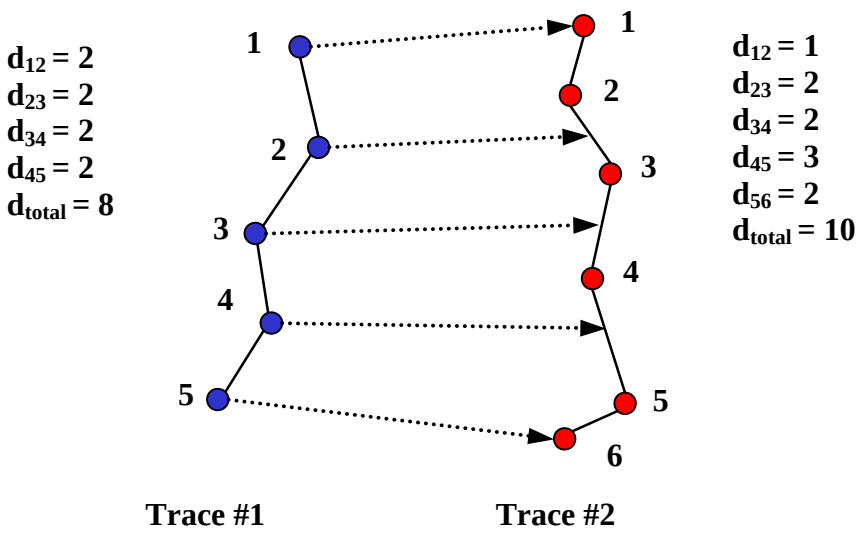

Figure 4.4: Point correspondence between two sulcal representations. Points from the contour on the left are matched to their appropriate position on the contour on the right so that corresponding points are at the same fractional distance along the contour.

was created at the time of the rendering. After this conversion, each sulcus is represented by a set of 3-D image-space points. The number of points in a set may be different for each sulcus.

Only a portion of the points that make up each contour were used as landmarks for constraining the deformation. For this study, 15 landmarks per contour were used, which represented about 10-25% of the total contour points. The points that make up the contours of one image (the subject image) were sampled evenly to create a set of 15 landmark points. The corresponding landmarks in the other image (the reference image) were determined by interpolation so that each landmark was the same distance (as a fraction of the overall contour length) from the start of its respective contour. This concept for establishing point correspondence is shown in Figure 4.4. The contour on the left is made up of five points while the contour on the right is made up of six points. For each point of contour #1 the corresponding location on contour #2 is determined using the total length of each contour. For example, point #2 of the first contour is at a location that is 2 distance units from the start of the contour, which represents 25% of the total contour length (2 out of 8 total distance units). The corresponding point on the second contour is chosen so that it will also be 25% of the total contour length (in this case 2.5 out of 10 total distance units). Interpolation between points 2 and 3 on the second

contour is required to determine this location. The corresponding location on contour #2 for each point on contour #1 is shown in the figure by arrows.

The landmark information is used during each iteration of the optical flow registration to help determine the overall transformation. During a typical iteration, the deformation field is updated using Equation 4.1. At regions surrounding the landmarks, this field is adjusted in order to help guide the deformation towards the corresponding landmark location in the other image. Note that the deformation field at these locations is not simply set to exactly enforce correspondence between the landmarks, as this would result is unrealistic deformations, especially early in the registration process. Instead, the deformation field surrounding each landmark is set to a combination of that computed using optical flow alone and that necessary to match the landmarks. This strategy helps reduce the error due to any inaccuracies in identifying the sulci. A constraint factor (α) is adjusted to control the combination of each of these factors. If this is set to $\alpha = 0.0$, the landmark information is not used and the deformation is due to optical flow only. If set to $\alpha = 1.0$, the landmarks are forced to match and the deformation computed by optical flow is not used in this region. For this study a factor of $\alpha = 0.5$ was used, which equally weighted the combination of the two factors. Before the two factors were combined, the contribution from the landmark location was multiplied by a Gaussian window.

The size of the constrained region surrounding each landmarks was set depending on the current resolution level of the multi-scale process. It varied from a 5x5x3 region for the lowest resolution images (32x32x15) to a 9x9x5 region for the original highest resolution images (256x256x124). A flowchart of this concept is shown in Figure 4.5. A 2-D grid of displacement vectors is shown for a particular region surrounding one landmark used for constraining the optical flow deformation field. The deformation field due to optical flow is shown in the top grid while the translation vectors needed to match the corresponding landmarks is shown in the bottom grid. In this case the displacement needed to match the corresponding landmarks is towards the bottom of the grid, and the size of the constrained region is 7x7 pixels. With the constraint factor set to $\alpha = 0.5$, applying constraints to this region results in the total deformation being pushed toward the bottom of the grid (when compared to optical flow alone), as shown in the grid on the right-hand side of the figure.

A flowchart describing the overall registration process is shown in Figure 4.6. The entire process is automatic except for the identification of cortical sulci on the rendered images of the

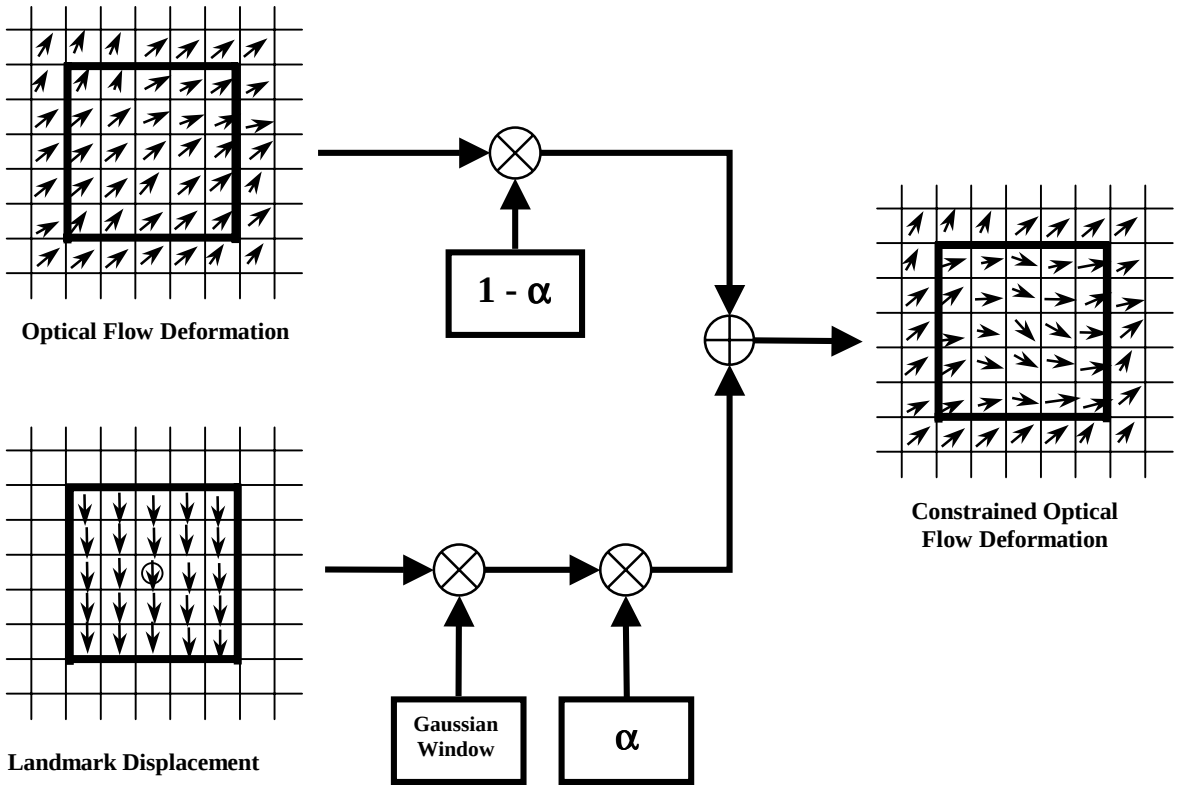

Figure 4.5: Flowchart describing the combination of the optical flow field (top grid) with the translation needed to match corresponding landmarks (bottom grid). The landmark is located at the center of the grid. The constraint is applied using a 5x5 region surrounding the landmark.

patient's cortex. Note that the brain segmentation and sulci identification for the atlas volume is also a manual process but this only needs to be done once. All steps in the registration process can be executed using the graphical user interface shown in Figure 4.2.

Results

Each of the 18 MR volumes was registered with the atlas volume using three different methods: global (7-parameter) transformation only, optical flow transformation, optical flow transformation with sulcal constraints. The global registration results are used to initialize the optical flow transformation in both the unconstrained and constrained cases. All parameters required by the optical flow program such as number of iterations and resolution levels were kept constant for every registration. The registration results were analyzed in three separate ways. First, the transformed images were visually inspected to qualitatively evaluate the accuracy of the registration. Second, contours representing the central sulcus and the motor cortex were used

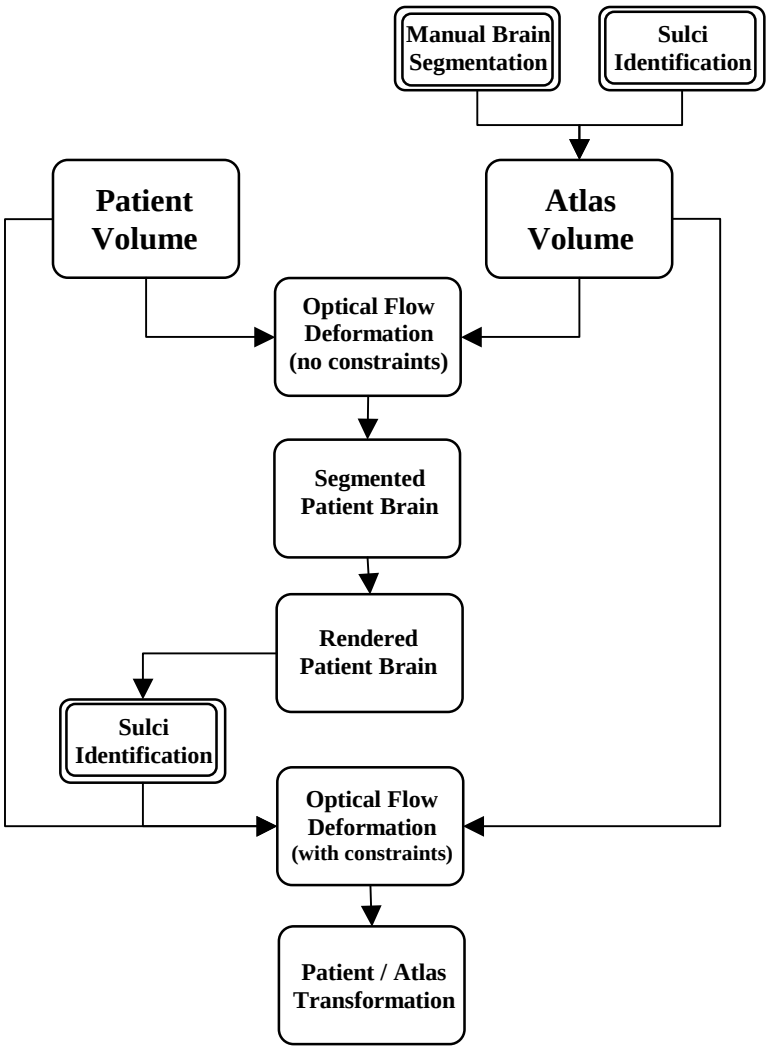

Figure 4.6: Flowchart of the overall registration process. Tasks denoted by a double line require manual interaction. All other tasks are completely automatic. Note that the brain segmentation and sulci identification of the atlas volume only need to be done once.

to quantitatively assess the accuracy of each registration method. Finally, areas of the cortex approximately corresponding to the facial motor region were identified on each subject and mapped onto the reference brain in order to simulate the creation of a functional brain atlas.

A. Visual analysis of the registration methods

The registration between the subject and the atlas was evaluated visually for each of the 18 subject volumes used in this study. Registration results from two subject volumes are shown in Figures 4.7 and 4.8. The 3-D transformation that registered the atlas volume with the subject volume was determined for each of the three registration methods. The atlas volume was

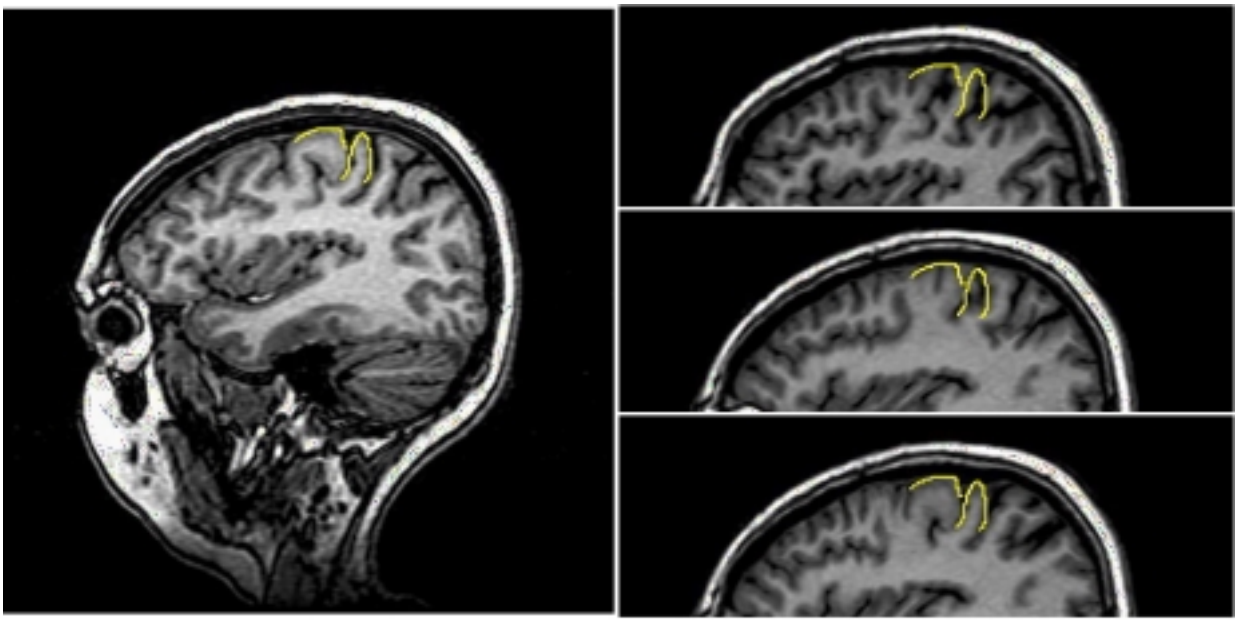

Figure 4.7: Registration results for each of the three different methods. A single image slice from one of the 18 subject volumes is shown in the left-hand panel. In the right-hand panel, enlarged cortical regions are shown after the atlas volume has been reformatted using one of three transformations: global (top), optical flow (middle), and constrained optical flow (bottom). Contours have been drawn on the image on the left and mirrored onto the other three images.

reformatted using each transformation. A single slice from each 3-D subject volume is shown on the left-hand side of Figures 4.7 and 4.8. The three images on the right-hand side of each figure show a portion of the same slice of the atlas volume after it has been reformatted using each of the three different registration methods. The results after global transformation (top), optical flow deformation (middle), and optical flow deformation with sulcal constraints (bottom) are shown. Contours have been drawn near the central sulcus on the original subject volume, and these contours have been mirrored onto each of the registered atlas images. For both subjects, the cortex is obviously not registered correctly in the central sulcus region using global or unconstrained optical flow transformations. This same cortical region, however, appears to be properly aligned when cortical constraints are used in the registration process.

Registration results from a third subject are shown in Figure 4.9. For this example, the brain regions of the original subject and reformatted atlas volumes were segmented and volume renderings of the cortical surface were created. Renderings for both the left (top row) and right (bottom row) hemispheres are shown. The original subject brain is shown in the left-hand panels, the registered atlas volume after optical flow deformation is shown in the middle panels, and the

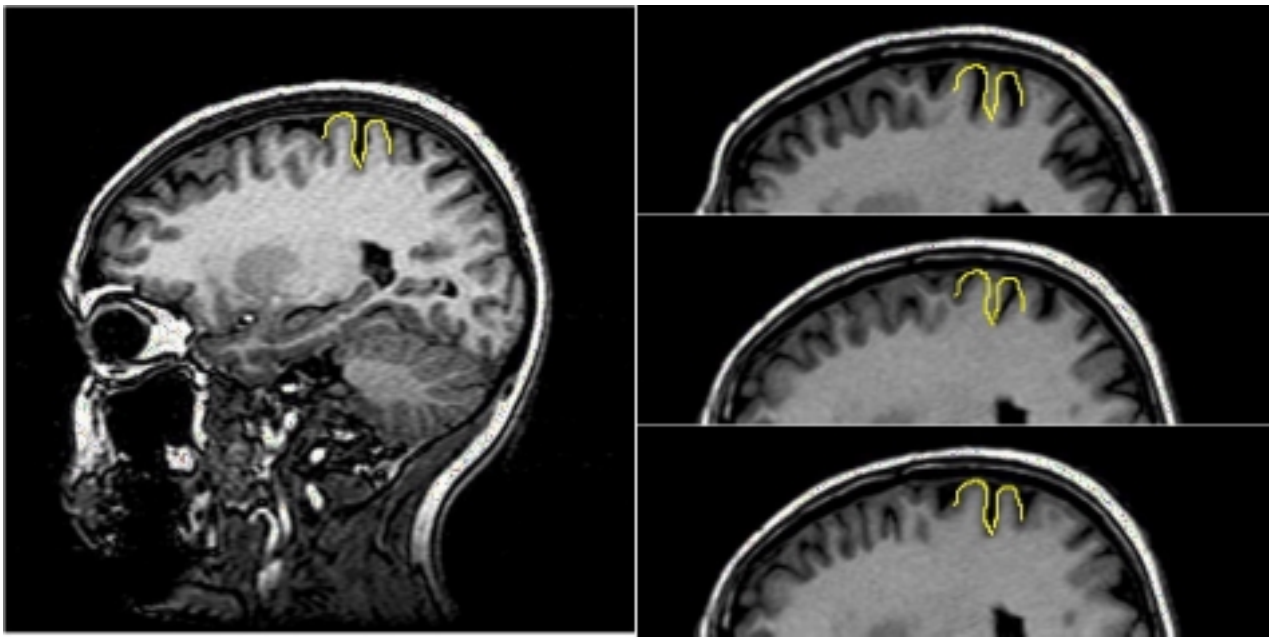

Figure 4.8: A second example from a different subject, similar to Figure 4.7.

registered atlas volume using cortical constraints is shown in the right-hand panels. Contours have been drawn on the original subject brain to depict the central sulcus. These contours have been mirrored onto the registered atlas results. If the registration were perfect, these contours would exactly identify the central sulcus on the reformatted atlas volume. In this case it is apparent that the optical flow algorithm alone fails to properly register the cortical regions surrounding the central sulcus. Particularly in the right hemisphere (bottom row of the figure) the algorithm appeared to match the central sulcus of the subject volume with the pre-central sulcus (the sulcus immediately in front of the central sulcus) of the atlas volume. The addition of sulcal constraints to the registration process prevented this matching error from occurring, as can be seen in the bottom right-hand panel.

B. Quantitative analysis of the registration methods

The three registration methods were evaluated quantitatively by computing the distance between corresponding contours before and after registration. The central sulcus was identified on both hemispheres for the atlas volume and each of the 18 subject volumes used in this study, as described in the previous section. The subset of points from each contour that was used to constrain the optical flow deformation were not used for evaluation. The remaining points on

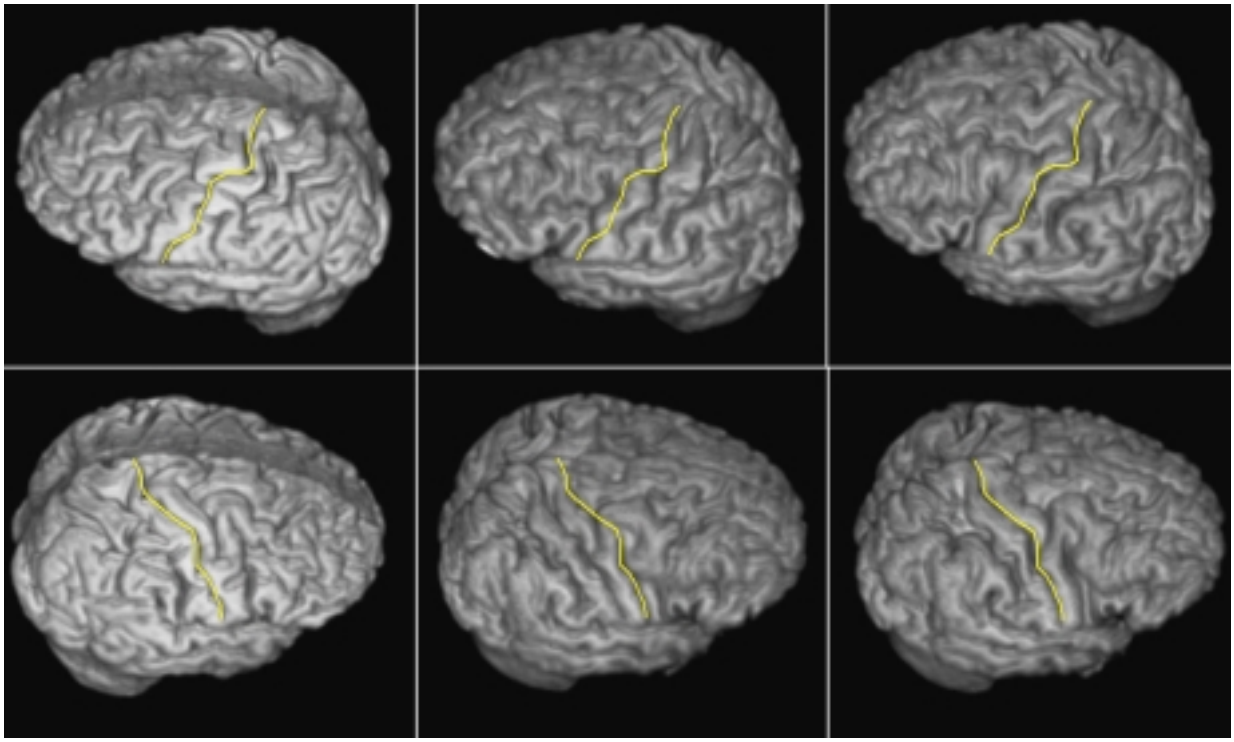

Figure 4.9: Cortical surface renderings showing the registration results for one subject. The original subject rendering is shown in the left-hand panels. The reformatted atlas is shown after optical flow deformation (middle panel) and after constrained optical flow deformation (right panel). The left hemisphere is shown in the top row, the right hemisphere in the bottom row. Contours have been drawn on the images on the left and mirrored onto the other images.

each contour were converted from their rendered image locations to 3-D image-space coordinates using the method described previously.

The distance between two contours was determined by finding, for each 3-D point on a contour from the subject volume, the closest point on the corresponding contour from the atlas volume. Points on one contour were not enforced to match a specific point on the other contour since it is unlikely that this requirement exists between brains of two different subjects. The distance between two contours is represented by the root-mean-square (rms) of the difference between all corresponding points.

Results for aligning the central sulcus using each of the three registration methods are shown in Figure 4.10. Each case represents the rms error (in pixels) for all 36 contours (2 contours for each of the 18 subjects) after the set of points have been transformed using the appropriate transformation. The contour error before registration is also shown for reference. As mentioned previously, this error is a 3-D error using the image-space coordinates of each point

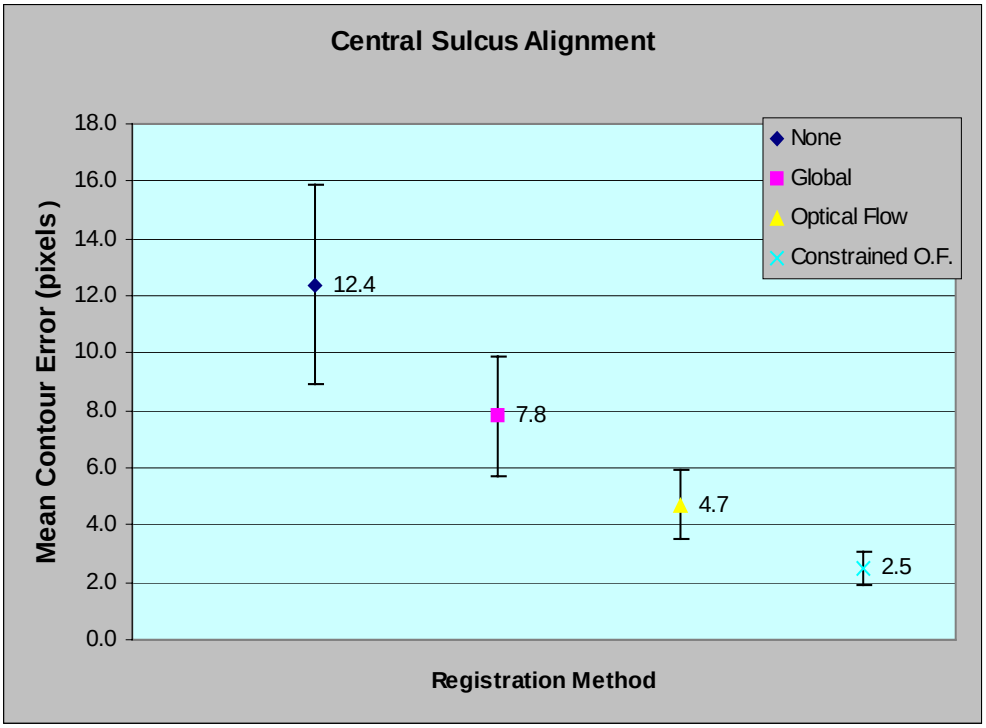

Figure 4.10: Contour error for the central sulcus for the following registration methods (from left to right on the graph): none, global, optical flow, constrained optical flow. Each data point is the average (rms) error for the 36 central sulcus contours (one per hemisphere for all 18 subjects). The error bars show the standard deviation in each case.

and not the 2-D location of the point on the rendered image. The error bars indicate the standard deviation in each case. The addition of cortical constraints to the optical flow algorithm improved the registration in this area by 47%.

The alignment of the central sulcus can be seen visually in Figure 4.11. In this example, contours from each subject are mapped to their corresponding location in the atlas volume. To do this, each point of the contour is first converted to its 3-D image-space location. These image-space coordinates are then mapped to the atlas coordinate system using the appropriate transformation. Finally, the 3-D image space coordinates are projected onto the volume renderings of the atlas brain and contours are drawn for each set of points. The 18 mapped contours are shown for both the right (left-hand side of the figure) and left (right-hand side of the figure) hemispheres. The top panel of the figure shows the case before registration. The next three panels show the contour locations after being mapped using global, unconstrained optical flow, and constrained optical flow transformations, respectively.

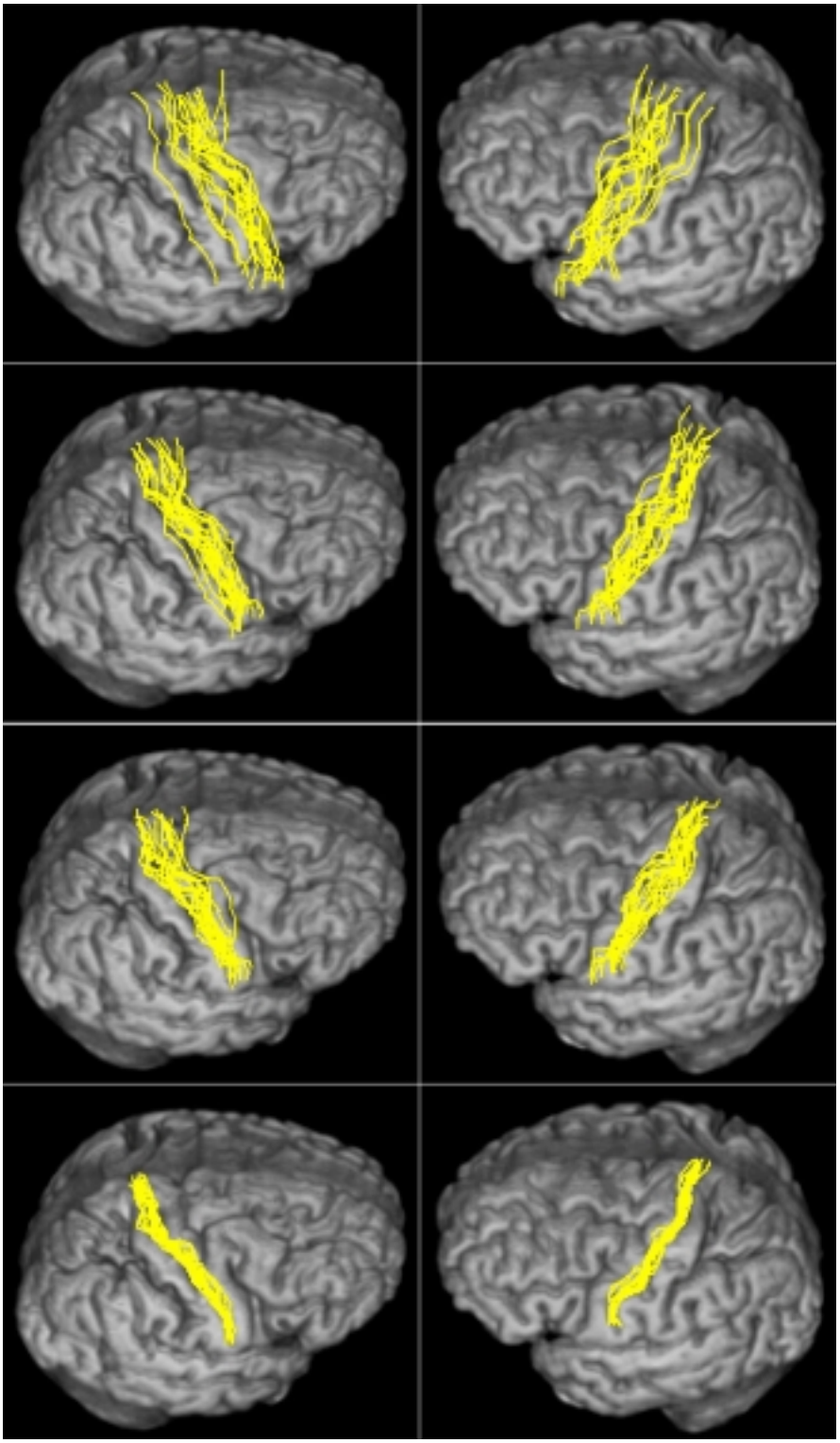

Figure 4.11: The location on rendered images of the atlas brain (both hemispheres) of contours representing the central sulcus for each of the 18 subjects. Each contour has been transformed using the following registration method: none (top row), global (second row), optical flow (third row), and constrained optical flow (bottom row).

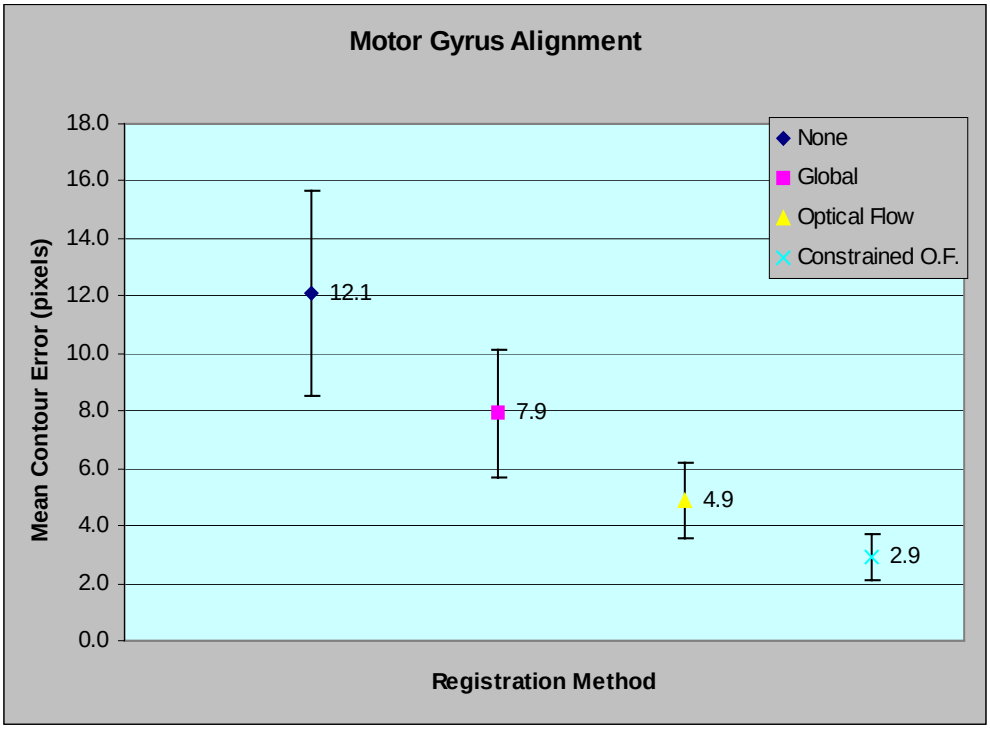

Figure 4.12: Contour error for the motor gyrus, similar to Figure 4.10.

Since the goal of this study is to map the location of brain function onto a common reference frame, it is more important to properly align the cortical gyri than the cortical sulci. To test the ability of the registration techniques described in this study to align cortical gyri, an additional set of contours were used. The motor gyrus was identified by a single contour (one for each hemisphere) using the same visualization tool used to identify the central sulcus. The motor gyrus is the area of the brain directly forward of the central sulcus. Using this gyrus also tests the ability to properly match areas not directly used in the constraining process. The rms error between corresponding contours was calculated using the same methods used for calculating the central sulcus error. These results are shown in Figure 4.12 for each registration method. As was done for the central sulcus, each contour was mapped into the atlas coordinate system using each registration method. In this example, the constraints improved the registration by 41%, when compared to using optical flow alone. The projections of these contours onto rendered images of the atlas brain are shown in Figure 4.13. As in Figure 4.11, the top panel of the figure shows the case before registration. The next three panels show the contour locations after being mapped using global, unconstrained optical flow, and constrained optical flow transformations, respectively.

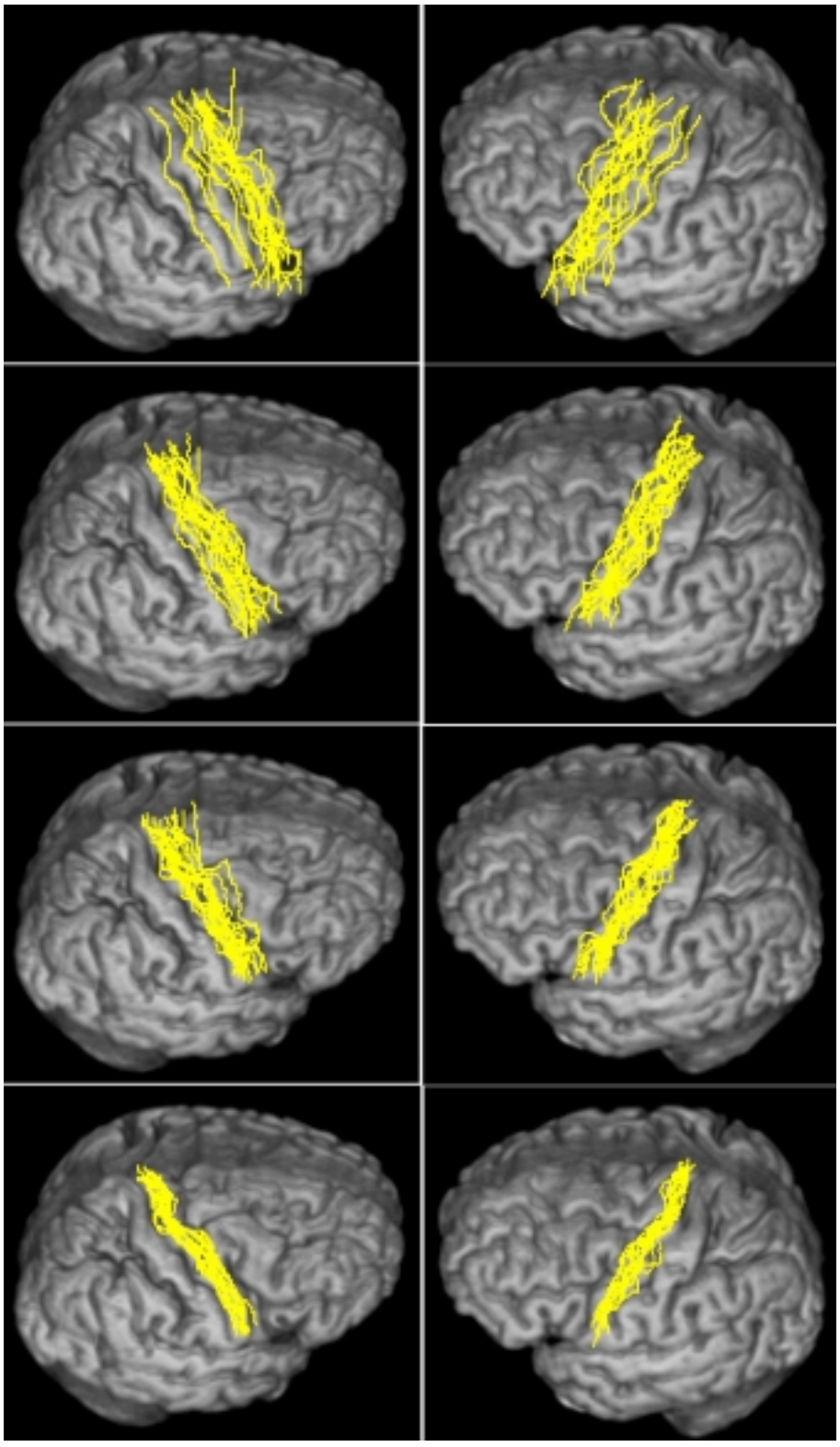

Figure 4.13: The location on rendered images of the atlas brain of contours representing the motor sulcus for each of the 18 subjects, similar to Figure 4.11.

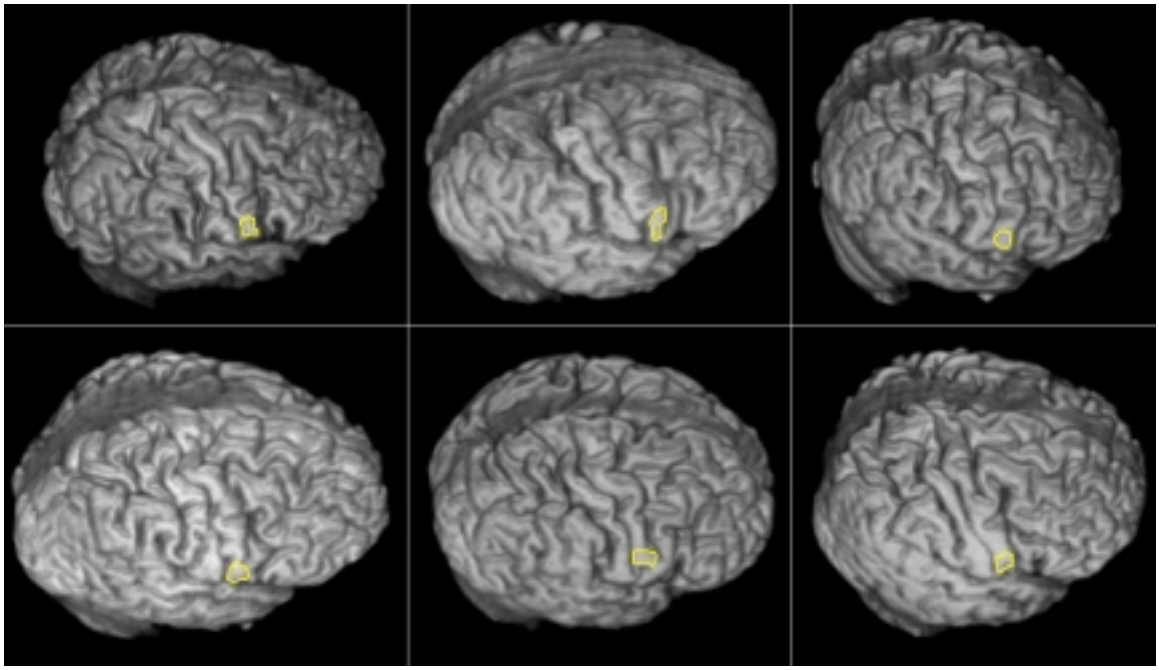

Figure 4.14: Outlined region of interest on the motor cortex for six of the 18 volumes used in this study. This region approximately corresponds to the facial motor cortex.

The results shown in Figures 4.10 and 4.12 are dependant on the constraint factor used to weight the contribution from the sulci locations on the total deformation field. This factor was set to $\alpha = 0.5$ for this study. Higher values would improve the results, but at the potential expense of reduced registration accuracy in other locations.

C. Simulated creation of a functional brain atlas

In order to create a functional brain atlas, the location of certain functional regions will be mapped to the corresponding location on the atlas volume. To simulate this, a small region of the motor cortex was identified in the right hemisphere of each of the 18 subject volumes. Figure 4.14 shows the outline of this region on rendered images of one study for all six subjects. Similar regions were identified on each of the remaining volumes. This region approximately corresponds to the facial motor cortex. For each pixel within the region on the rendered image, a corresponding 3-D image-space position was determined so that all points on the surface of the cortex in this region were identified. All of these points were transformed to their corresponding location in the atlas volume, and then projected to the appropriate position on rendered images of the atlas brain. These results are shown in Figure 4.15. The rendered image of the right

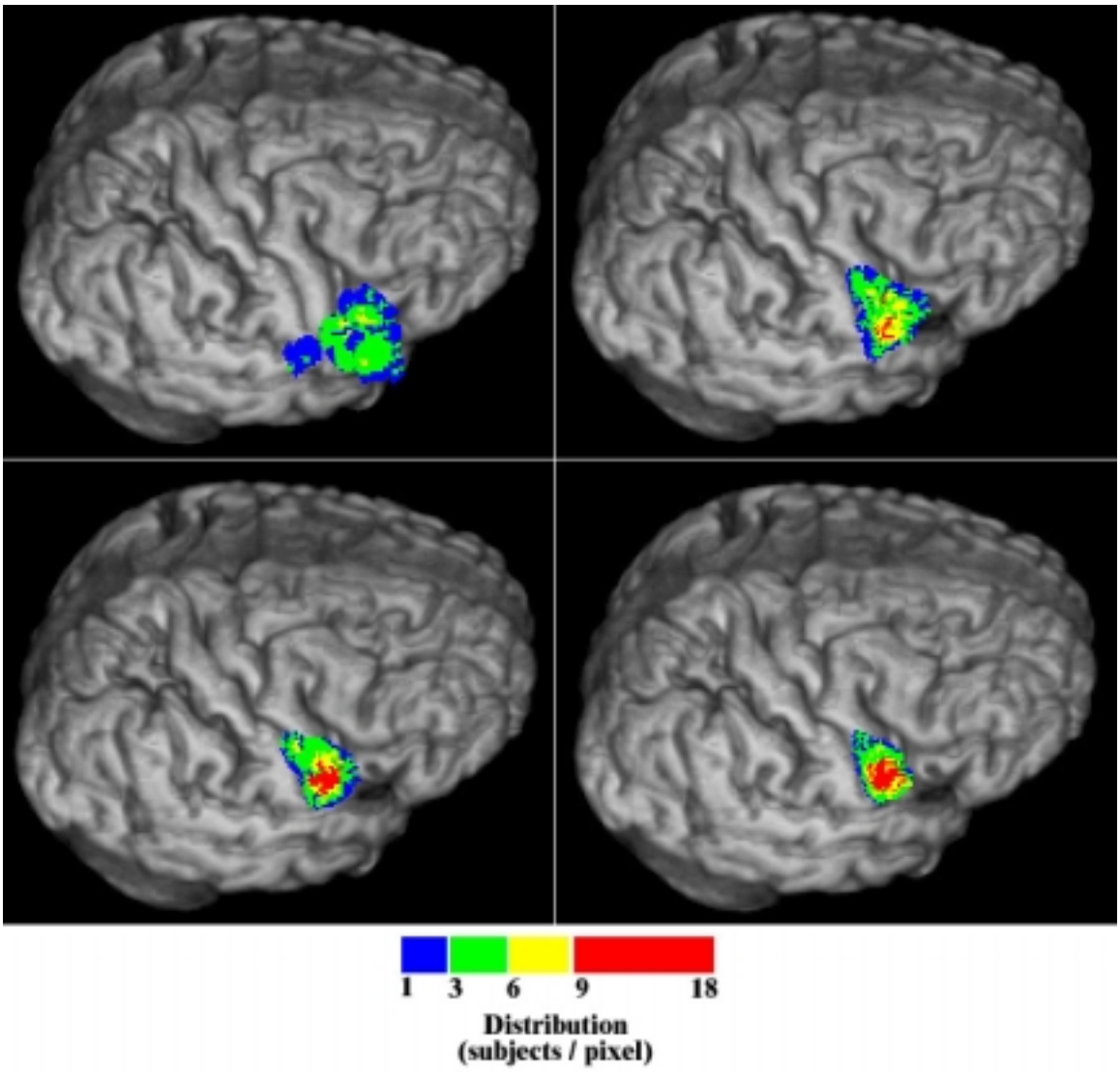

Figure 4.15: Projections onto the atlas volume of the regions shown in Figure 14 for the following registration methods: none (top-left), global (top-right), optical flow (bottom-left), and constrained optical flow (bottom-right). The projection of the functional regions for all 18 subjects are shown in each panel.

hemisphere of the atlas brain is shown in each panel. The projected points for all 18 subjects are overlaid onto the rendered image for each registration method: none (top-left), global (top-right), optical flow (bottom-left), and constrained optical flow (bottom-right). The constrained optical flow case contains a much tighter distribution of points than the other methods, and every region has been mapped to the lower portion of the motor gyrus on the atlas brain.

Discussion

In this study, a non-linear deformation field was computed in order to register 18 MR image volumes of six different subjects with a single MR atlas volume. This transformation was determined using an optical flow algorithm that was constrained according to the location of cortical sulci. A new method was developed for quickly identifying the location of the sulci on rendered images of the brain. Even though the user interaction required for this semi-automatic technique typically takes less than a minute per sulcus, future work involves fully automating this process.

The addition of sulcal constraints consistently provided a more accurate match of the desired cortical regions. There were cases, however, where the constraints provided little or no benefit (although the constrained case was never worse than the unconstrained case). This typically occurred when the cortical regions were closely aligned before deformation, and therefore were matched correctly using optical flow only. In a number of cases, however, the optical flow algorithm failed to properly match cortical regions, in some cases aligning a gyrus in a subject volume with an adjacent gyrus in the atlas volume (see Figure 4.9). In these cases the benefit of including cortical constraints is clear, especially when proper alignment of certain cortical regions is critical.

The addition of constraints from multiple sulci did not affect the registration near other constrained regions. For example, the lateral sulcus (the sulcus running approximately perpendicular to the inferior end of the central sulcus) was identified in a sample of the subject volumes (6) and used along with the central sulci information to constrain the deformation. The addition of this constraint had little or no effect on the matching of the central sulci and motor gyri, as compared to results obtained using only the central sulci as constraints.

In contrast to previous methods, a complete set of contours representing the entire cortical region is not required in order to determine the registration. In fact, using the methods described in this study, a transformation can be computed using a single contour for constraint. The remainder of the deformation will be determined by the optical flow algorithm. This is advantageous since only the sulci in the desired area of the brain need to be identified before registration. For example, during a typical neurosurgery only a small portion of the cortex is visible. It may be desirable during an image-guided surgery procedure to display functional information from an atlas database in the region of the exposed cortex. In this case, in order to

map functional information from the atlas to a specific patient, only the sulci in the exposed area of the brain need to be used for constraints.

As described previously, several techniques have been published for using cortical information to determine the registration between brain images of different subjects. Of these, the methods of Collins *et al* [28] and Hellier *et al* [29] are most similar to the work described in this study. Collins *et al* compute the image registration by estimating a piecewise constant affine transformation that maximizes the cross-correlation of the gradient. Hellier *et al* uses an optical flow technique for the registration process, which includes an additional regularization term that is not present in our method. The image volume is partitioned into cubes and a 12-parameter deformation field is computed for each cube, which also results in a piecewise affine transformation. In contrast, our method is fully free-form: a separate deformation vector is calculated for each voxel in the image.

Both Hellier *et al* and Collins *et al* use active ribbon methods to identify the cortical sulci. Although the active ribbon method gives a more complete description of the sulci, this added complexity was not required in our method. The emphasis of our registration was placed on the optical flow algorithm, with the cortical information used to prevent the transformation from aligning a particular sulcus of one subject to an adjacent sulcus in the other subject. Collins *et al* incorporate the cortical information into the deformation by computing a chamfer distance between selected sulci. Our approach is similar to that of Hellier *et al* in that the Euclidean distance between sulci is used to constrain the deformation. However, only a portion of the points representing each sulcus are used in our method, while Hellier *et al* explicitly match all sulci points.

The entire registration process, including the computation of the global transformation, takes approximately 5 minutes on a Microsoft Windows PC (1.0 GHz Pentium III processor with 1 GB of memory). In contrast, the registration technique of Hellier *et al* takes approximately 1.5 hours on a Sun Ultra Sparc 30 (300 MHz) workstation (although their image volumes have 200 slices instead of 124 slices) [30]. This rapid computation makes it feasible to execute during (or immediately before) surgery. During a surgery where image-guidance is used, the sulci of the exposed portion of the brain could be quickly identified using a tracked surgical probe. This information could be used to determine the transformation between the patient's image and a

functional brain atlas. Then information from the atlas could be mapped into the image-space of the patient and displayed along with the anatomic images during surgery.

Acknowledgements

The authors thank Dr. Mike Fitzpatrick for his helpful comments and suggestions.

References

[1] GR Cosgrove, BR Buchbinder, and H Jiang, "Functional magnetic resonance imaging for intracranial navigation," *Neurosurgery Clinics Of North America*, vol. 7, no. 2, pp. 313-322, 1996.

[2] JBA Maintz and MA Viergever, "A survey of medical image registration," *Medical Image Analysis*, vol. 2, no. 1, pp. 1-36, Apr, 1998.

[3] J Talairach and P Tournoux. *Co-planar stereotactic atlas of the human brain*, New York: Thieme Medical, 1988.

[4] SL Hartmann, MH Parks, PR Martin, and BM Dawant, "Automatic 3-D segmentation of the internal structures of the head in MR images using a combination of similarity and free form transformations: Part II, validation on severely atrophied brains," *IEEE Transactions on Medical Imaging*, vol. 18, no. 10, pp. 917-926, Oct, 1999.

[5] J-P Thirion, "Image matching as a diffusion process: an analogy with Maxwell's demons," *Medical Image Analysis*, vol. 2, no. 3, pp. 243-260, 1998.

[6] A Caunce and CJ Taylor, "Using local geometry to build 3D sulcal models," *Proceedings of Information Processing in Medical Imaging: IPMI '99*, vol. 1613, pp. 196-209, 1999.

[7] P Besl and N McKay, "A method for the registration of 3-D shapes," *IEEE Transactions on Pattern Analysis and Machine Intelligence*, vol. 14, no. 2, pp. 239-256, Feb, 1992.

[8] YR Ge, JM Fitzpatrick, BM Dawant, J Bao, RM Kessler, and RA Margolin, "Accurate localization of cortical convolutions in MR brain images," *IEEE Transactions on Medical Imaging*, vol. 15, no. 4, pp. 418-428, 1996.

[9] ME Rettmann, C Xu, DL Pham, and JL Prince, "Automated segmentation of sulcal regions," *Medical Image Computing and Computer-Assisted Intervention: MICCAI '99*, pp. 158-165, 1999.

[10] G Lohmann, "Extracting line representations of sulcal and gyral patterns in MR images of the human brain," *IEEE Transactions on Medical Imaging*, vol. 17, no. 6, pp. 1040-1048, Dec, 1998.

[11] G Le Goualher, C Barillot, and Y Bizais, "Modeling cortical sulci with active ribbons," *International Journal Of Pattern Recognition And Artificial Intelligence*, vol. 11, no. 8, pp. 1295-1315, 1997.

[12] M Kass, A Witkin, and D Terzopoulos, "Snakes: active contour models," *International Journal of Computer Vision*, vol. 1, no. 4, pp. 321-331, 1988.

[13] G Le Goualher, E Procyk, DL Collins, R Venugopal, C Barillot, and AC Evans, "Automated extraction and variability analysis of sulcal neuroanatomy," *IEEE Transactions on Medical Imaging*, vol. 18, no. 3, pp. 206-217, 1999.

[14] JP Thirion and A Gourdon, "The 3D marching lines algorithm," *Graphical Models and Image Processing*, vol. 58, no. 6, pp. 503-509, 1996.

[15] G Subsol, N Roberts, M Doran, J-P Thirion, and G Whitehouse, "Automatic analysis of cerebral atrophy," *Magnetic Resonance Imaging*, vol. 15, no. 8, pp. 917-927, 1997.

[16] G Subsol. Crest lines for curve-based warping. In: *Brain Warping*, ed. AW Toga. Academic Press, 1998. pp. 241-262.

[17] P Thompson and AW Toga, "A surface-based technique for warping three-dimensional images of the brain," *IEEE Transactions on Medical Imaging*, vol. 15, no. 4, pp. 402-417, 1996.

[18] C Davatzikos and RN Bryan, "Using a deformable surface model to obtain a shape representation of the cortex," *IEEE Transactions on Medical Imaging*, vol. 15, no. 6, pp. 785-795, 1996.

[19] M Vaillant and C Davatzikos, "Hierarchical matching of cortical features for deformable brain image registration," *Proceedings of Information Processing in Medical Imaging: IPMI '99*, vol. 1613, pp. 182-195, 1999.

[20] S Sandor and R Leahy, "Surface-based labeling of cortical anatomy using a deformable atlas," *IEEE Transactions on Medical Imaging*, vol. 16, no. 1, pp. 41-54, Feb, 1997.

[21] A Manceaux-Demiau, RN Bryan, and C Davatzikos, "A probabilistic ribbon model for shape analysis of the cerebral sulci: Application to the central sulcus," *Journal of Computer Assisted Tomography* , vol. 22, no. 6, pp. 962-971, 1998.

[22] XL Zeng, LH Staib, RT Schultz, and JS Duncan, "Segmentation and measurement of the cortex from 3-D MR images using coupled-surfaces propagation," *IEEE Transactions on Medical Imaging*, vol. 18, no. 10, pp. 927-937, 1999.

[23] BM Dawant, SL Hartmann, J-P Thirion, F Maes, D Vandermeulen, and P Demaerel, "Automatic 3D segmentation of internal structures of the head in MR images using a combination of similarity and free form transformations: Part I, methodology and validation on normal subjects," *IEEE Transactions on Medical Imaging*, vol. 18, no. 10, pp. 909-916, Oct, 1999.

[24] B Horn and B Schunck, "Determining optical flow," *Artificial Intelligence*, vol. 17, pp. 185-203, 1981.

[25] KS Arun, TS Huang, and SD Blostein, "Least-squares fitting of two 3-D point sets," *IEEE Transactions on Pattern Analysis and Machine Intelligence*, vol. 9, no. 5, pp. 698-700, Sep, 1987.

[26] R Sibson, "Studies in the robustness of multidimensional scaling: perturbation analysis of classical scaling," *Journal of the Royal Statistical Society*, vol. 41, no. 2, pp. 217-229, 1979.

[27] SL Hartmann and RL Galloway, Jr., "Depth-buffer targeting for spatially accurate 3-D visualization of medical images," *IEEE Transactions on Medical Imaging*, vol. 19, no. 10, pp. 1024-1031, Oct, 2000.

[28] DL Collins, G Le Goualher, and AC Evans, "Non-linear cerebral registration with sulcal constraints," *Medical Image Computing and Computer-Assisted Intervention: MICCAI '98*, vol. 1496, pp. 974-984, Oct, 1998.

[29] P Hellier and C Barillot, "Cooperation between local and global approaches to register brain images," *Proceedings of Information Processing in Medical Imaging: IPMI 2001*, vol. 2082, pp. 315-328, 2001.

[30] P Hellier, C Barillot, E Memin, and P Perez, "Hierarchical estimation of a dense deformation field for 3-D robust registration," *IEEE Transactions on Medical Imaging*, vol. 20, no. 5, pp. 388-402, May, 2001.

CHAPTER V

DEPTH BUFFER TARGETING FOR SPATIALLY ACCURATE 3-D VISUALIZATION OF MEDICAL IMAGES

Steven L. Hartmann and Robert L. Galloway, Jr.

Department of Biomedical Engineering

Vanderbilt University

Nashville, TN 37235

Portions of this manuscript have been published in:

IEEE Transactions on Medical Imaging
Vol. 19, No. 10, pp. 1024-1031, October 2000.

Abstract

During image-guided surgery (IGS), a surgeon uses data from medical images to help guide the surgical procedure. At Vanderbilt University, an IGS software system called Orion has been developed which is capable of displaying up to four 512 x 512 images and the current surgical position using an active optical tracking system. Orion is capable of displaying data from any tomographic image volume (MR, CT, PET) and from any NTSC video image.

An additional display module has been implemented to display three-dimensional information as well as the tomographic slices. Before the surgery a set of rendered images is created, each with a different angular view of the tomographic volume in order to surround the site of surgical interest. A unique "depth-buffer targeting" method was developed for determining the distance from the tip of the surgical probe to the object depicted in the rendered image. During the creation of each rendered image, a separate "depth-buffer" file is created that contains, for each pixel in the rendered image, the information necessary to determine the original 3-D tomogram location of each point of the rendered object. Using this information in addition to the location of a tracked surgical probe, it is possible to determine the distance between the probe and the object. A novel "depth-line indicator" method was used to convey this distance to the surgeon during surgery. The length of this line, which is shown directly on the rendered image, is proportional to the distance between the probe and the object.

Introduction

Medical images are used during interactive image-guided surgery (IIGS) to help guide the surgical procedure. Traditionally, these images have been stacked slice tomograms such as computed tomography (CT) and magnetic resonance (MR) volumes that are capable of showing high quality details of the human anatomy. Recently, three-dimensional (3-D) volume visualization techniques such as surface and volume rendering have been used to provide additional information during surgical planning, treatment, and guidance [1-3]. Examples of 3-D visualization include a volume rendering of the cortical surface of the brain, a surface rendering of a tumor, and a maximum intensity projection (MIP) of blood vessels acquired from an angiogram image volume. The rendering process creates a two-dimensional image from a 3-D volume. Hence, the third dimension (depth) is lost. This may not be important if the rendering is

used for qualitative information only. In order to use the rendered image for guidance during surgery, however, the depth dimension must be recovered.

The two most common methods used to provide depth information are motion parallax [4] and stereoscopic viewing [5]. With motion parallax, a selection of rendered images acquired on each side of the viewing angle are displayed in a sequence loop. This dithering about a center angle provides enough distinct angular cues to enable the surgeon to determine 3-D position. This method, however, requires an extended viewing period before the depth can be determined as the surgeon must observe several display cycles in order to understand the position relationships between objects in the renderings.

Additionally, the depth information is qualitative and requires visual interpretation. The rendering process leads to a problem known as surface normal uncertainty. Each rendered object can lie anywhere along a world line and the exact location of the object on this line cannot be resolved from the rendered image alone (Figure 5.1). The dithering process makes it possible to deduce if one object is in front of a second object, but the distance between a surgical probe and the desired object cannot be determined.

The second method used to recover depth information, stereoscopic viewing, creates two views of an object, each acquired at a slightly different angle in order to approximate the same geometry that would be obtained using binocular vision. The two images can be placed side by side and a person can view the third dimension by allowing their eyes to cross until the object comes into focus. This technique does not allow for quantitative interpretation of the image, and can be difficult to use during surgery since the surgeon must repeatedly adjust their focus each time they wish to view the image. This method can be improved by using a polarized viewing glass either placed in front of the monitor or worn directly by the operator. A shutter can be used to direct one of the stereo views to the appropriate eye. This way, each eye sees only the view corresponding to its geometry. With this method, it is possible to use triangulation to obtain quantitative spatial relationships between the surgical probe and the object [5]. This technique, however, requires additional hardware and a display capable of updating at twice the desired frame rate in order to sequence left and right views. In addition, two images must be created and displayed for each view. Non-stereo images such as tomographic slices may also be displayed on the same monitor, even though polarization is not necessary for these images. This can be done by refreshing the same image at each of the two stereo time frames, which can lead to an

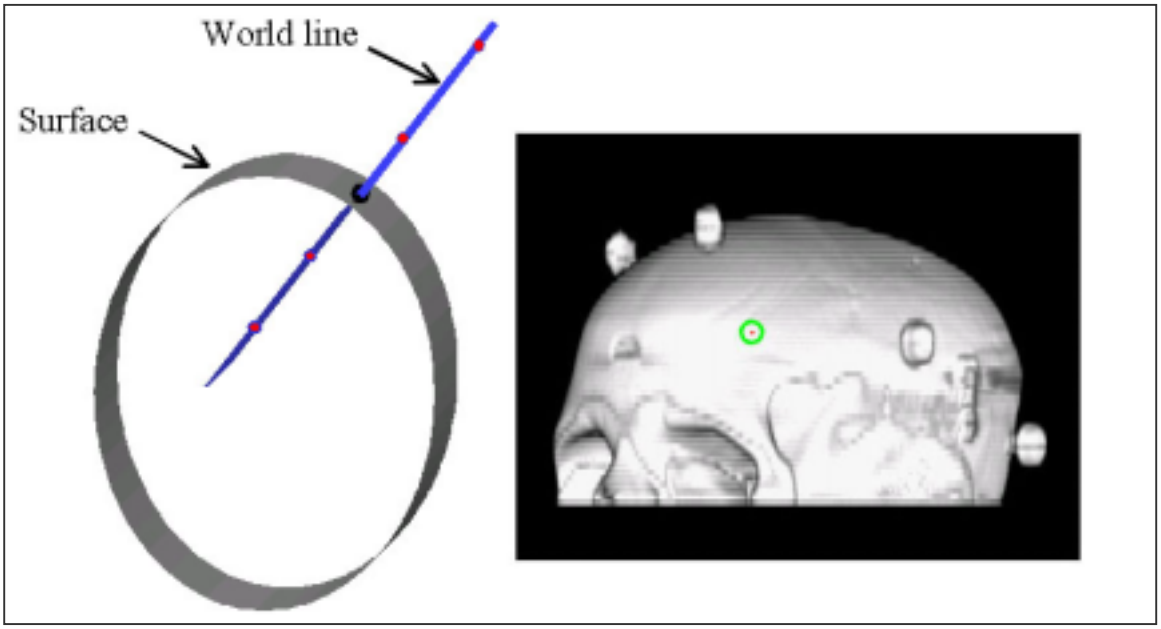

Figure 5.1: Surface normal uncertainty. The object identified on the rendered image can originate from any point along the projection ray (world line).

unpleasant flickering of the display. Additionally, the polarized glasses attenuate all light not in the polarization direction. This will darken the surgeon's view in the operating room, which either requires an increase in the operating room brightness or requires the surgeon work with less ambient light than desired. Finally, stereoscopic imaging will not work for those people with dominate-eye vision.

In this study a new method, called depth-buffer targeting, has been developed for quantitatively displaying 3-D rendered images. This technique requires no additional hardware, specialized equipment, or imaging methods. The depth information of a rendered image is determined by using a depth buffer (Z-buffer). This buffer is created at the same time as the rendering and contains, for each pixel in the rendered image, a corresponding value that represents the perpendicular distance between the object depicted in the pixel and a known geometry plane. This information can be used to determine the distance between a surgical probe and a physical object.

Methods

This section describes the techniques used to incorporate rendered images into an image-guided surgical software system. This requires several steps: creating a set of rendered images,

displaying the images along with the correct position of a surgical probe, and providing an indication of distance between the probe and the rendered object.

A. Creating the rendered image set

A rendered image set is created from a tomographic volume (either MR or CT) and includes multiple renderings, each from a different view, in order to obtain total coverage of the desired area. For example, projections can be obtained at 20º increments throughout a 360º revolution about the head. Rendered image sets were created using the volume rendering capabilities of IDL (Interactive Data Language, Research Systems Inc.). For a good discussion of volume-rendering methods see Jani and colleagues [6].

The renderings are computed ahead of time and not "on the fly" during surgery for two reasons. First, at the present time it is not possible on a standard computer to render the image and store the depth buffer fast enough to update in real time (greater than 30 Hz), considering that much of the computation cycle is spent determining the image-space position of the probe and displaying the image. Second, changing the view each time the probe is moved can cause confusion as the orientation of the image must continually be determined. If a known set of views is used, the picture changes less frequently while still providing sufficient coverage of the desired structure.

Each tomogram has an associated data file that contains parameters, such as pixel spacing and slice thickness, required to perform the renderings. The rendering program, created using IDL, reads information from this data file and loads the tomogram volume into memory. The rendered image is created by projecting a set of parallel rays perpendicular to the desired image plane, which maps positions from the 3-D volume onto a 2-D viewing plane. The projection rays have a set of properties that affect the quality and speed of the rendering. The first property, called the composite function, determines the value of a pixel on the viewing plane by analyzing the voxels intersected by each corresponding ray according to a specified function. For the study presented in this paper, the composite function is either alpha-blending or maximum intensity projection (MIP). In an alpha-blended image, each voxel occludes voxels behind it according to the opacity of the front voxel. Proper setting of the opacity table is necessary for producing quality renderings. In a maximum intensity projection, the value of each pixel on the viewing

plane is set to the brightest voxel, as determined by its opacity. An alpha blended image is useful when displaying surfaces; a MIP is useful for showing vasculature.

The second important property of a projection ray is the starting and stopping point, called the clipping planes. The clipping planes are set to only render the relevant part of the image volume. For this study, only the front half of the volume is rendered for each projection. This is done by first defining a center of rotation for the image volume, which can be the geometric center, the center of mass, or any other point in the volume. Then the rendered view is created by projecting parallel rays from outside the image volume to the perpendicular plane that intersects the center of rotation. Stopping the projections at the center plane prevents the display of objects furthest away from the viewer. This reduces confusion that may occur when multiple objects are rendered. For example, when displaying a MIP, it may not be desirable to display the posterior portion of the sagittal sinus when viewing the anterior portion of the image volume. The creation of surgically appropriate MIPs is explained by Palmisano and colleagues [7].

Additional ray properties are the step size and the interpolation method. The step size is the distance traveled along the ray between sample points and the interpolation method is used to determine the data value at each sample point. Each of these parameters result in a trade-off between rendering speed and quality. For this study, trilinear interpolation and a step size of one pixel were used in order to produce high quality renderings.

Each rendering takes approximately 20 seconds on a 500 MHz Pentium III computer. The entire set is stored consecutively as a one byte per pixel image file. A data file for the rendered image set is created which contains parameters necessary for display, such as number of renderings, viewing angle, and size of the images.

B. Displaying the rendered images

At Vanderbilt University, an image-guided surgery software system called Orion has been developed which is capable of displaying up to four 512 x 512 images. The system has been used to display tomographic image volumes such as CT and MR, and to indicate on these images the current image-space position of a surgical instrument or probe. This system has three key tasks: 1.) tracking a surgical probe using a 3-D spatial localizer, 2.) computing the transformation that maps the physical-space position of the probe to the image-space position of the image set, and 3.) displaying the current position of the probe on the correct tomogram slice using this

transformation. These requirements and how they were implemented for this study are described below.

1) Localization: The physical-space position of the probe is determined using an optically tracked position sensor (Optotrak 3020, Northern Digital, Inc, Waterloo, Ontario). The probe is cylindrical and contains 24 infrared light emitting diodes (IREDs) around the handle. The position sensor contains three linear CCD devices, each with 1024 elements, and is capable of accurate localization of any IRED in direct line of sight. If three or more of the IREDs can be localized with a high enough degree of certainty, the tip of the probe can be determined since the geometrical arrangement of the IREDs is known. It has been previously shown that the tip of the probe can be localized with an error of approximately 0.8 mm [8].

2) Registration: Registration between physical space and image space can be done in a number of ways, including point-based and surface-based techniques. For this study, a point-based registration method is used that matches the position of extrinsic fiducial markers attached to posts, which are implanted into the skull before the tomogram is obtained. The markers contain a fluid that is perceptible on both MR and CT images, and the center of each marker can be identified in image space using an automatic method [9]. The markers are removed from the posts before surgery and replaced with caps in which the tip of the surgical probe can be placed and used to identify the center of the marker in physical space (the imaging markers, caps, and posts can be seen in Figure 5.6). If the corresponding position of three or more fiducials in each space can be identified, then the transformation that maps physical space to image space can be determined using a closed-form solution [10].

3) Display: Once a rendered image set has been created, it can be displayed using the Orion software system. The Orion system consists of a main control program and several modules, which are implemented as independent run-time dynamic link libraries (DLL). All programs are written in C and compiled for the Windows NT operating system. The DLLs are responsible for the various tasks required during IIGS, such as registration and image display. Display of three-dimensional position can be updated at greater than 20 frames per second. Previously, Orion was capable of displaying data only from tomographic image volumes or from an NTSC video image. An additional display module has been designed to display three-dimensional information along with the tomographic images.

The main objectives of this new DLL are to display the appropriate rendered image from the set, identify the current probe position on the selected image, and provide an indication of distance between the probe and the physical point of the anatomy indicated on the rendering. The registration between physical space and the image space of the rendered set is done in two steps. The first step is to determine the mapping between physical space and image space of the original parent tomogram. As described previously, this is accomplished using implanted fiducial markers. Therefore, the same transformation used to register the tomogram is used. The second step is to determine the mapping between the tomographic volume and the individual rendering, which is straightforward since the viewing parameters used to create the rendered image are known.

The displayed image is chosen based on the view from the probe to the center of rotation for the particular rendered image volume. It is determined by comparing the current image-space position of the probe with the rotational information of the rendered image set. The rendering with a viewing angle closest to that of the probe is selected as the current image and displayed in the desired 512 x 512 window in Orion. The user also has the option of selecting any particular view and locking it in as the current view. Probe movement will not change which rendering is displayed when the current view has been locked.

A cursor is displayed on the rendered image to indicate current surgical position by projecting the probe position onto the plane of the displayed rendering. This calculation is straightforward since the projection angle from which the rendering was created and the probe's position in the original tomographic space are both known. The cursor is a circle whose size and color can be modified by the user. A circular cursor was chosen so the object of interest is not obscured, as would be the case if a cross-hair or arrow cursor was used. If a particular view has been locked in as the current view, the position of the cursor will still be updated with probe movement even though the displayed rendering will not change.

Finally, the distance between the probe and the anatomical point indicated by the cursor is determined using depth buffer information as described in the next section. This can provide the surgeon with vital information such as distance to blood vessels, tumors, or other critical structures. Figure 5.2 shows the Orion software, loaded with two image sets. The image on the left is a single slice of a CT volume and the image on the right is one view of the rendered image set. The current surgical position of the probe is shown on both images, indicated by the arrow

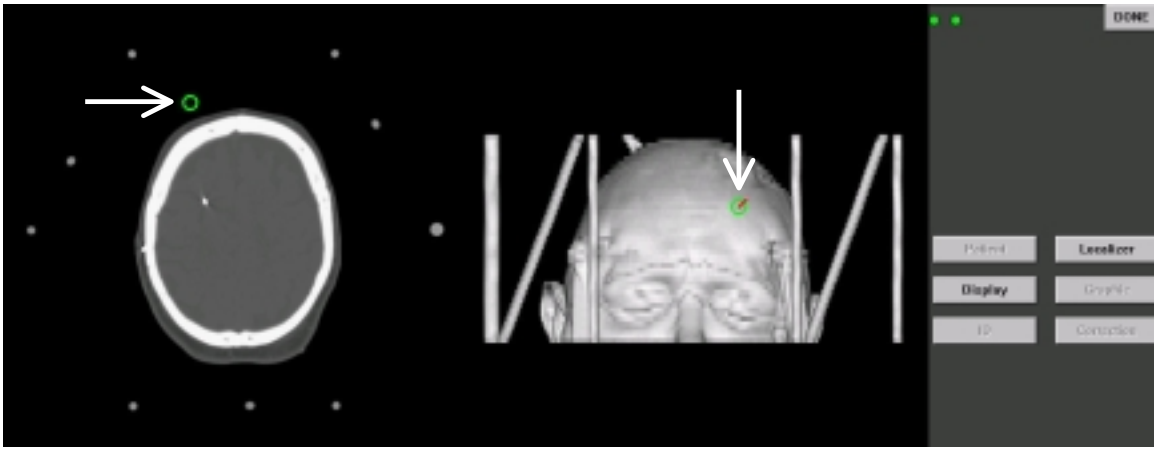

Figure 5.2: Sample screenshot of the Orion software system. On the left is one slice from a head CT image volume, while the right image is a volume rendering of the CT volume. The current surgical position of the probe is shown on each image by a circular cursor, indicated by the arrow.

(note that the arrow is not part of the Orion system). The bottom two display windows are empty and therefore not shown.

C. Depth-buffer targeting

The distance between the tip of the probe and the object indicated on the rendered image is determined by using the depth buffer information obtained for that particular rendering. For each pixel of a rendered image, a corresponding distance is stored in a separate depth buffer file of the same dimensions as the rendering. This depth value, in millimeters, is the perpendicular distance between the point on the rendered image and the center plane of rotation for the angular view used to create the rendering. The location of the rendered point (and therefore the depth value) depends on the composite function. For an alpha-blended image, the rendered location is generally the first sample along the projection ray whose opacity exceeds a minimum threshold. For MIPs, the rendered location is the brightest sample along the projection ray.

Figure 5.3 shows one projection ray for a particular rendering view. The rendered image is from a cross-section of a plastic skull phantom. Point B in the figure is the point where the ray first intersects the surface of the phantom; point A is the point where the ray intersects the center plane of rotation. In this case, the distance stored in the depth buffer file for that pixel is AB. Before storing the depth buffer file, each value is multiplied by 10, then rounded to the nearest integer and stored as a 2 byte-per-pixel and integer. This reduces the storage memory requirements by a factor of two, while still maintaining sub-millimetric precision of the depth

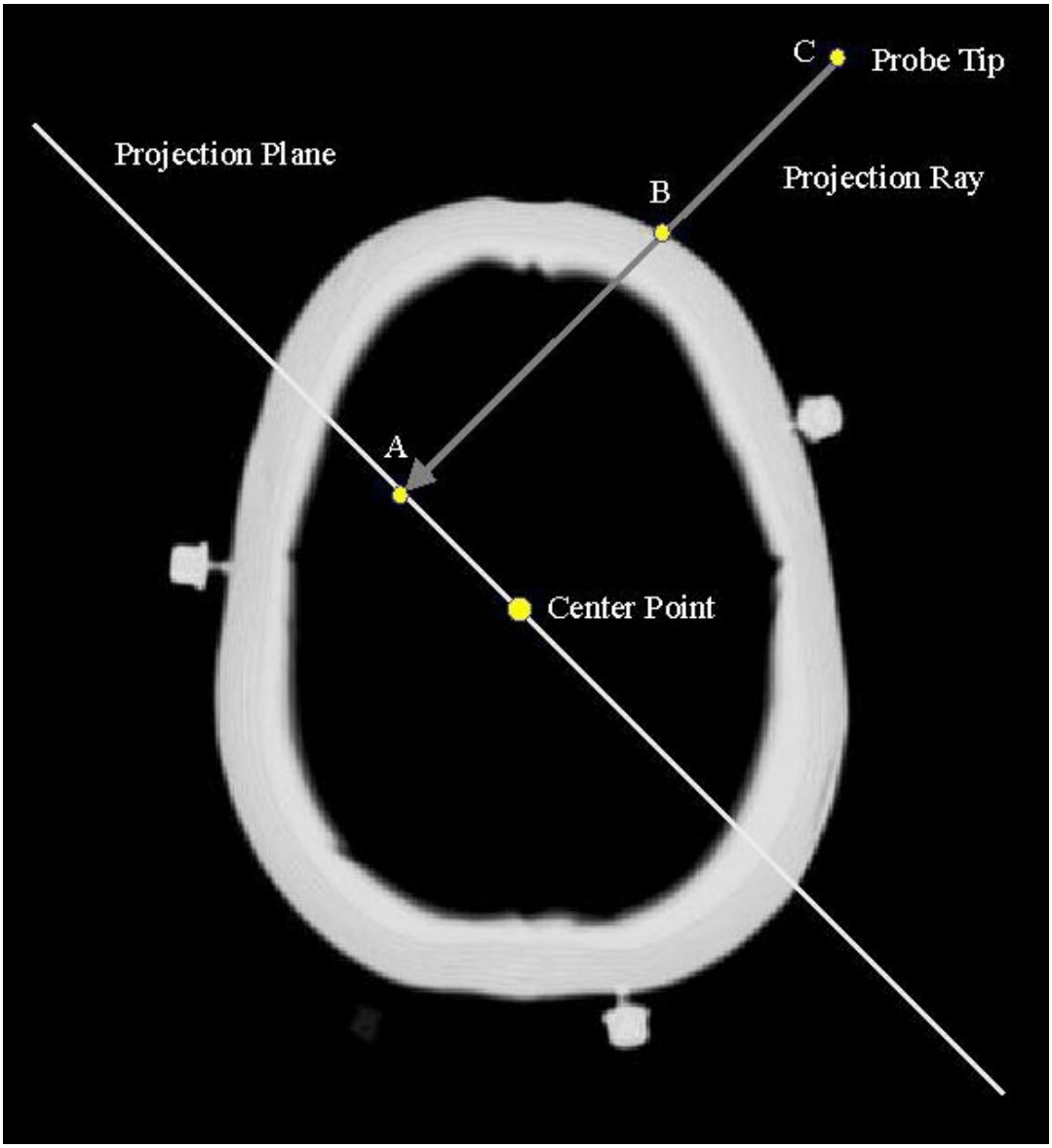

Figure 5.3: Example ray projection that shows for a given probe position the distance stored in the depth buffer file for a particular pixel.

buffer. As the probe tip is moved, the distance (in millimeters) between the probe and the center rotation plane for the rendered view currently displayed is determined. This is done by first mapping the probe's physical-space position to the image-space location in the original tomogram volume, and then using the angular geometry information used to create the current rendering to determine the distance. The desired depth, which is the distance between the probe and the object identified in the rendered image, is simply the difference between the probe-to-plane distance (AC in Figure 5.3) and the object-to-plane distance (AB in Figure 5.3).

Once the distance between the probe and the object is determined, a method must be chosen for conveying this information to the surgeon. A "depth-line indicator", extending from the cursor on the rendered image display, has been developed for this study. The length of the line increases as the distance between the probe and the object increases. If the object is positioned between the probe and the center plane, the line extends at a 45º angle from the cursor. Otherwise, the probe is considered inside the object, and the line extends at a 225º angle from the cursor. The length of the line can be defined to be a maximum at a certain probe-to-object distance (say 10 mm). A small ball is drawn at the end of the depth-line indicator if the distance exceeds this maximum value. The circular cursor is used to show additional depth cues. If the depth-line indicator does not extend outside the cursor, the distance is less than a set value (for example, 2 mm). Both of these threshold values can be adjusted by the user. The depth-line indicator can be seen in Figures 5.2, 5.4, 5.5, and 5.7.

This method of depth display allows the surgeon to quickly and easily determine the third dimension of the rendered image. The surgeon is not required to look in a separate location for the information or to read and interpret a number, but instead can obtain the depth with a quick glance.

Results

To test and evaluate the rendering display module, two experiments were performed. The first used existing tomographic images of two previous patients, and the results were purely qualitative to ensure the system was working properly. The second experiment used a CT scan of a skull phantom with attached fiducial markers, and quantitative as well as qualitative results were obtained.

A. Qualitative Results

Two different tomographic data sets were used: a spiral CT scan of the head from a patient wearing a stereotactic frame, and an MR angiogram (MRA) of a separate subject. In each case a rendered image set was created using IDL. Each set contained eight renderings, with the viewing angle equally spaced about a 360º revolution of the head. For the CT scan, the projection ray properties were set to provide a rendering of the surface. For the MRA, a MIP set was created in order to view the vasculature.

The original tomogram and the rendered set of one subject were both loaded into the Orion software system. Since the subjects were not available for this experiment nor were fiducial markers present during the original scans, the operating room environment was simulated by defining a 3-D space to represent the physical space of the subject. Physical-space to image-space registration was accomplished using corner points of the 3-D image space. Since the image dimensions are known, these points can also be identified in physical space, and therefore a transformation can be determined. Once registration is complete, the probe can be moved freely within the defined 3-D space, and the tomogram and rendered images are updated according to the probe's position.

Figure 5.4 shows Orion screenshots of the first subject for three different positions of the probe. The top three images are of the rendered image set; the bottom images are from the corresponding CT volume. In the left panel, the depth-line indicator shows that the probe is greater than 10 mm away from the portion of the skull depicted by the cursor. This can also be seen in the bottom CT image. The middle panel shows a situation where the probe is on the inside of the object, in this case between the N-bar of the frame and the skull, which can be seen in the corresponding CT image below the rendering. In the right panel, the probe has been placed at a point that would be touching the skull, as indicated by the depth-line on the rendered image and the cursor on the tomogram. The solid circles surrounding the tomographic slices are cross-sections of the N-bars from the stereotactic frame.

Figure 5.5 shows similar screenshots from the second subject. The three panels show MIP images on the top and the corresponding MRA slice on the bottom. In each case the length of the depth-line provides an indication of the distance from the probe to the identified vessel. Arrows have been used to identify the cursor on each image.

The results from these two subjects show that the software module for displaying rendered images as well as the depth-buffer targeting method work properly. At all times while the probe was tracked, the cursor position and depth-line indicator of the rendered image were determined to be in proper correspondence with the cursor position identified on the associated tomogram. The accuracy of the technique, however, cannot be determined using these subjects since the validation was by visual interpretation. Therefore, a second experiment was completed in order to provide quantitative error measurements.

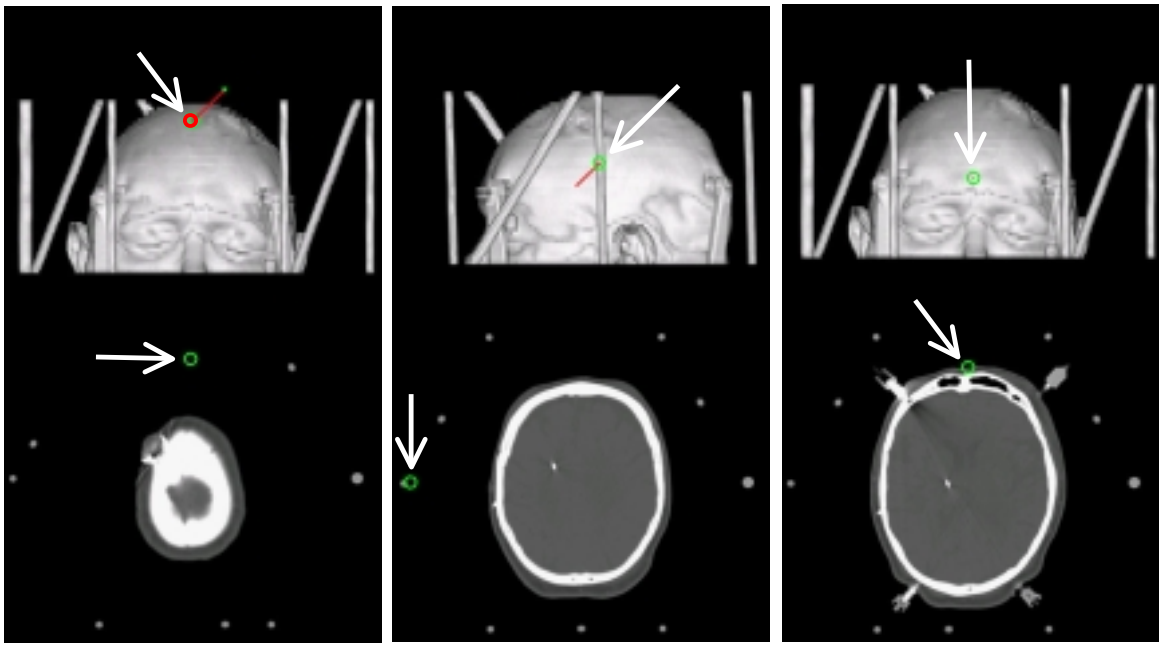

Figure 5.4: Orion screenshots for three different positions of the probe. The top row shows views from the rendered image set while the bottom row shows the corresponding position on the original CT volume. The three probe positions show when the probe is outside the object depicted on the rendering (left panel), inside the object (middle panel), and touching the object (right panel). The arrows in each image show the cursor representing probe position.

B. Quantitative Results

Determining the accuracy of the image-guided software system is a difficult and time consuming task. Yet, it is crucial to be able to assess the accuracy of any system that will be used to make critical decisions during a surgical procedure. There are many factors that contribute to the total error of the system such as localization of the probe, physical-space to image-space mapping due to errors in fiducial identification and registration, and errors in the imaging and rendering processes. For this study it was necessary to identify the total cumulative error associated with the depth-line indicator. In order to do this a CT scan of a plastic skull phantom was obtained. The phantom had 10 fiducial marker posts inserted at various locations around the skull. Figure 5.6 shows the phantom with attached markers. On the right side of the image is a post without any type of marker attached. The left-most post has an imaging marker attached and the middle post has a probe localization cap attached. During image acquisition, all 10 posts had imaging markers attached. The CT volume had dimensions of 512 x 512, with 51 slices. Pixel spacing was 0.4688 mm and slice thickness was 2.0 mm.

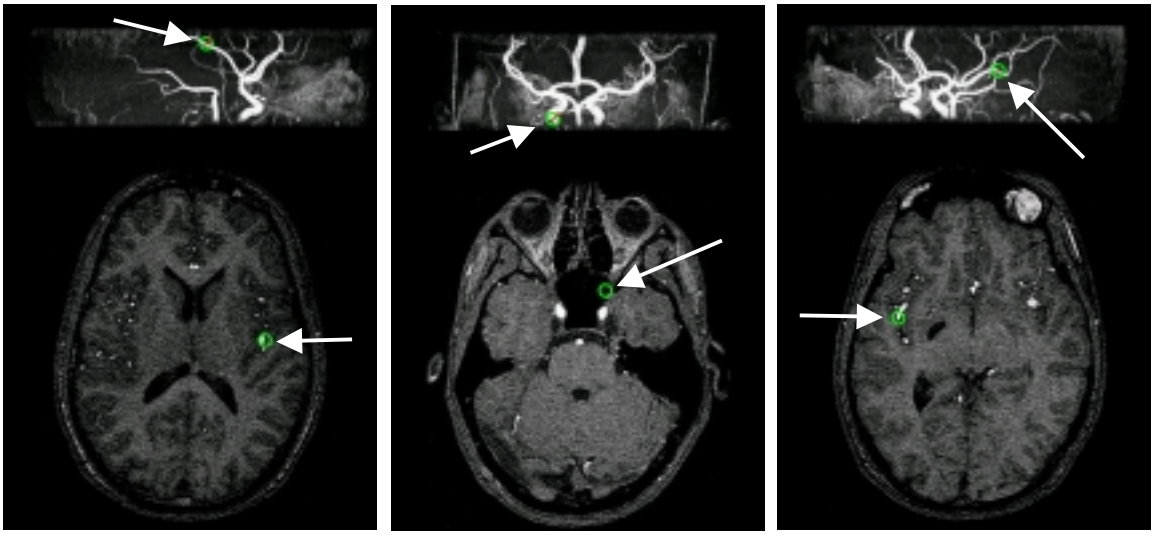

Figure 5.5: Orion screenshots for three different positions of the probe, similar to Figure 5.4. In this case, the rendered images (top row) are maximum intensity projections from an MR angiogram (bottom row). The arrows in each image show the cursor representing probe position.

Three rendered image sets and associated depth buffer files were created, each segmented using a different intensity cutoff threshold, from the CT volume. The projection ray properties were the same as those used for the patient CT volume in the qualitative study, which provided a rendering of the phantom's surface. For each set, eight renderings were acquired, equally spaced, about a 360º revolution of the CT volume. The phantom was secured to a table and the tomogram and rendered image set were loaded into the Orion software system. Physical-space to image-space registration was accomplished using 4 of the 10 available markers. Figure 5.7 shows a sample screen shot of Orion when the probe has been placed on the surface of the phantom. The cursor position on both the tomogram and rendering correspond to the same anatomical position and the depth-line indicator reveals a distance of zero between the probe and the surface, as expected.

To measure the error of the system, the probe was touched to the surface of the phantom and the value of the depth indicator at that position was recorded. This value provides a direct error measurement since when the probe is touching the surface the depth indicator should be equal to zero. For this study, the error between actual probe position and the surface position indicated by the cursor was not determined. In each case, however, the cursor position on the rendered image was visually verified to correspond with the surface point touched by the probe.

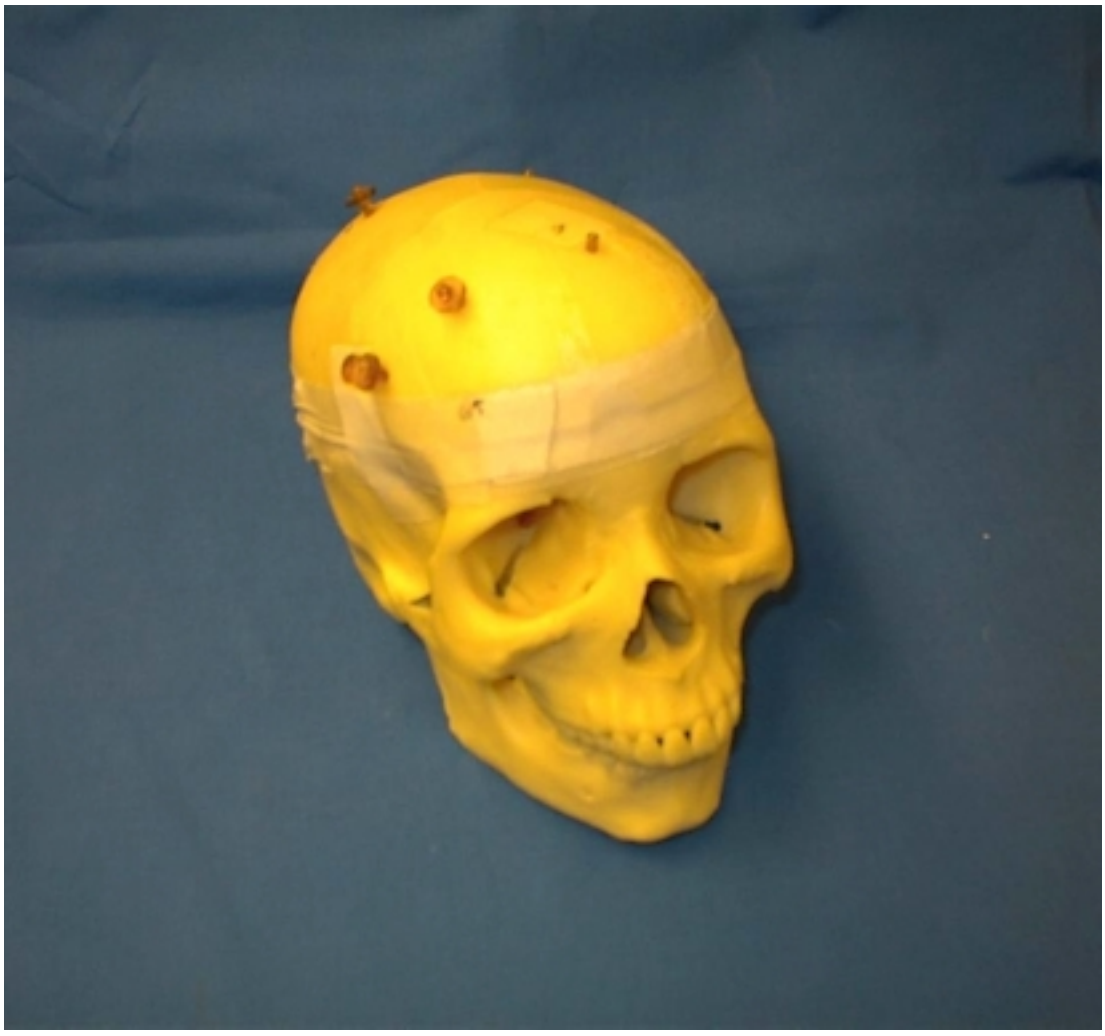

Figure 5.6: Skull phantom showing an imaging marker, localizing cap, and screw-in post.

Error measurements were taken at 10 different locations on the phantom: one each in the area of the 6 markers not used in the registration and four additional measurements taken around the eye and nose areas. The registration process and point collection was repeated three times for a particular set of registration markers. Then, a different set of markers were used for the registration and three additional sets of measurements were taken. For each of the three rendered image sets (one for each threshold value) a total of three different marker configurations were used, which resulted in nine separate sets of measurements (ten error values per set). For each set of measurements, a registration error was calculated which provides an indication of the quality of the mapping between physical-space and image-space. This error, called the fiducial

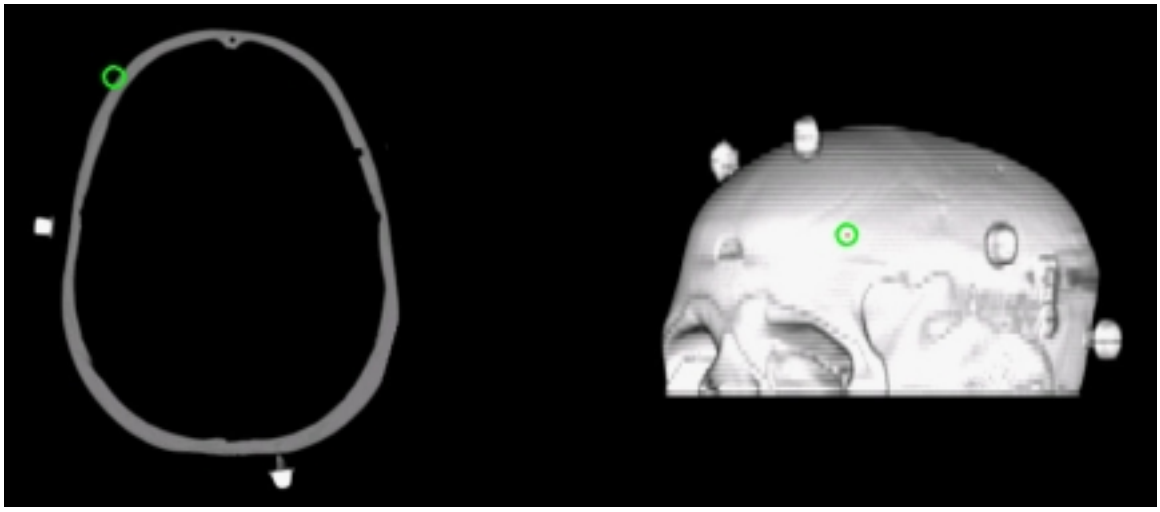

Figure 5.7: Orion screenshot using the skull phantom as the subject. The left image shows the CT image, while right image shows one view of the rendered image set. The probe was placed on the surface of the phantom, which is depicted by the cursor position on both images.

registration error (FRE), is the root-mean-square of the distances between the image-space coordinates of the markers and their transformed physical-space location.

Threshold values were chosen to cover the range of intensity values that, when used as the cutoff threshold, produced quality rendered images. The intensity histogram for the phantom CT volume is shown in Figure 5.8. The first peak at approximately 210 corresponds to the background (air) and the second peak at approximately 1410 corresponds to the plastic of the phantom. There is also a small peak from the fluid in the imaging markers at 3300 that is not shown in the histogram. For this study, threshold values were chosen at 300, 800, and 1200. All intensity values of the tomogram that were below the threshold were set equal to zero before the rendering process.

The results from these 27 trials are listed in Table 5.1. For each trial, the FRE and the average depth error are listed. The overall average depth error (in mm) for each intensity threshold was 1.26 (+/- 0.54), 0.75 (+/- 0.41), and 0.41 (+/- 0.20) for the threshold values of 300, 800, and 1200 respectively.

These results indicate that accurate depth measurements can be determined and used to display current surgical position on rendered images The depth-buffer technique for displaying rendered images does not require any additional hardware from that already used by the Orion system. Additionally, this method provides near real-time display update and does not require large amounts of memory to operate. When all four Orion display windows are loaded, each

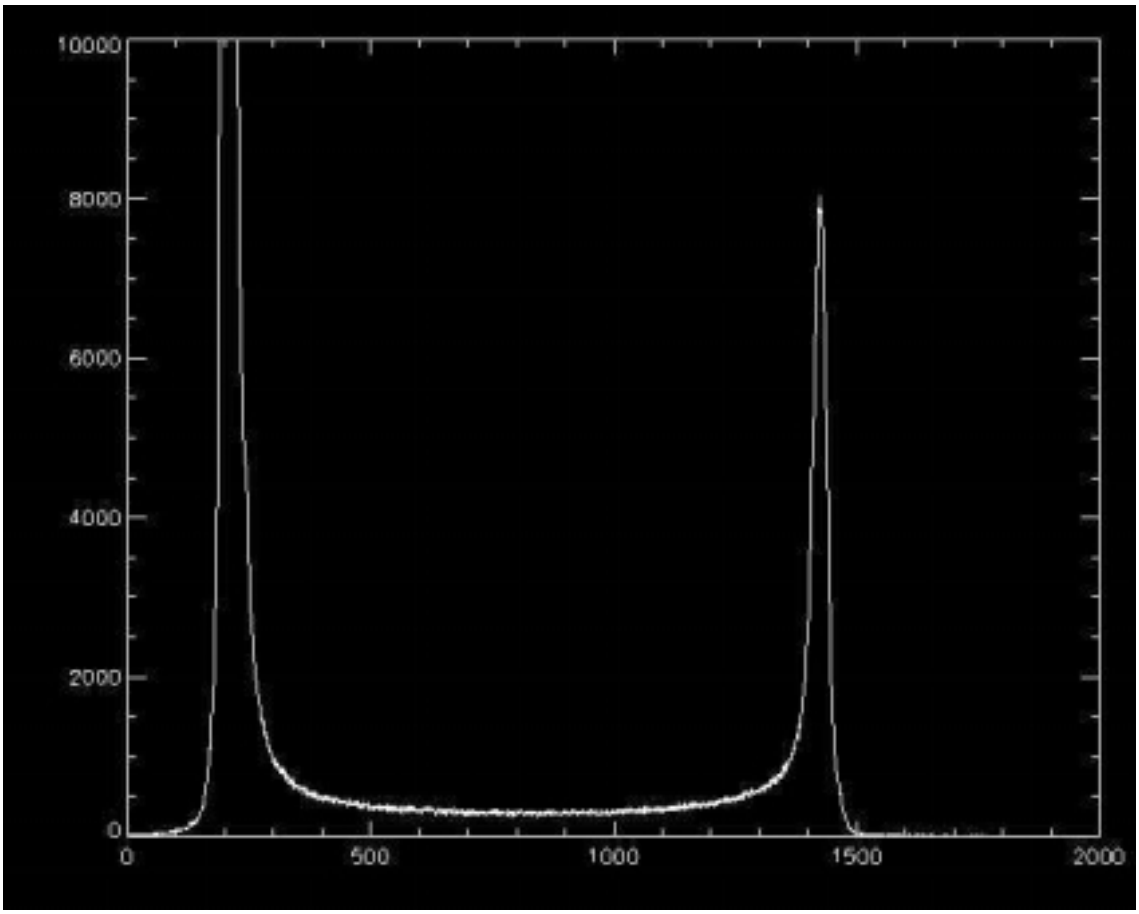

Figure 5.8: Intensity histogram from the CT volume of the skull phantom.

image can be refreshed at greater than 20 frames per second using a 400 MHz Pentium III processor with 128 Mb of memory. When fewer than four display windows are used, the refresh rate is greater than 30 Hz.

Discussion

The additional display module created for the Orion image-guided software system allows for displaying rendered images in addition to tomographic data. With this implementation the surgeon now has access to complementary information to help guide surgical procedures. The rendered image set and associated depth-line indicator provide a three-dimensional perspective that cannot be easily obtained from the 2-D tomographic slices. The interface is fast and intuitive, providing additional beneficial information during surgery.

Table 5.1: Fiducial registration and mean depth error measurements for each of the 27 trials.

Threshold	Error (mm)	Marker Combination #1			Marker Combination #2			Marker Combination #3		
300	FRE	1.17	0.92	0.92	1.34	1.11	1.18	0.90	1.40	0.94
	Depth	1.01	1.27	1.09	1.13	1.20	1.24	1.58	1.59	1.18
800	FRE	1.17	0.80	0.58	1.58	1.66	1.30	1.09	1.31	1.05
	Depth	0.68	0.76	0.51	0.76	0.62	0.65	0.85	1.05	0.84
1200	FRE	0.47	0.50	0.98	1.68	1.62	1.57	1.49	1.09	1.11
	Depth	0.43	0.26	0.34	0.35	0.38	0.50	0.48	0.48	0.45

An important step in creating the rendered image set is the segmentation of the original tomogram. In our experiments we had an ideal scenario and used a simple threshold segmentation. As shown in Table 5.1, the rendered set with a threshold of 1200 produced much lower error values than the set created using a threshold of 300. The fact that the threshold choice made a significant difference in the case of a plastic phantom shows how sensitive error is to the segmentation. The segmentation threshold for the skull phantom used in this study may appear obvious by looking at the intensity histogram shown in Figure 5.8. In a more complicated tomogram, however, a simple threshold may not be appropriate for the segmentation, especially if the desired structure to be rendered does not have well-defined intensity characteristics. Particularly with MR images, inhomogeneity artifacts make it unlikely that a single threshold will produce quality results, and a more complex segmentation method, such as an atlas-based technique [11], will be required.

A good measure for determining the appropriateness of the threshold is to view the depth-buffer file for inconsistencies. Figure 5.9 shows three depth-buffer images after the phantom was rendered using different threshold choices. The depth-buffer image on the top was created using a cutoff threshold of 200. This threshold was too low, and much of the background (air) was rendered which covered up the actual surface of the phantom. In this case the rendered image appeared similar to that shown in Figure 5.7 and therefore did not provide any clues to indicate the depth-buffer values would be inappropriate. The depth-buffer image in the middle was created after using a threshold of 1450, which was too large and therefore much of the surface was eliminated before the rendering. The image on the bottom was created after using a threshold of 1200, and shows one view of the depth-buffer image that produced the lowest error in this study.

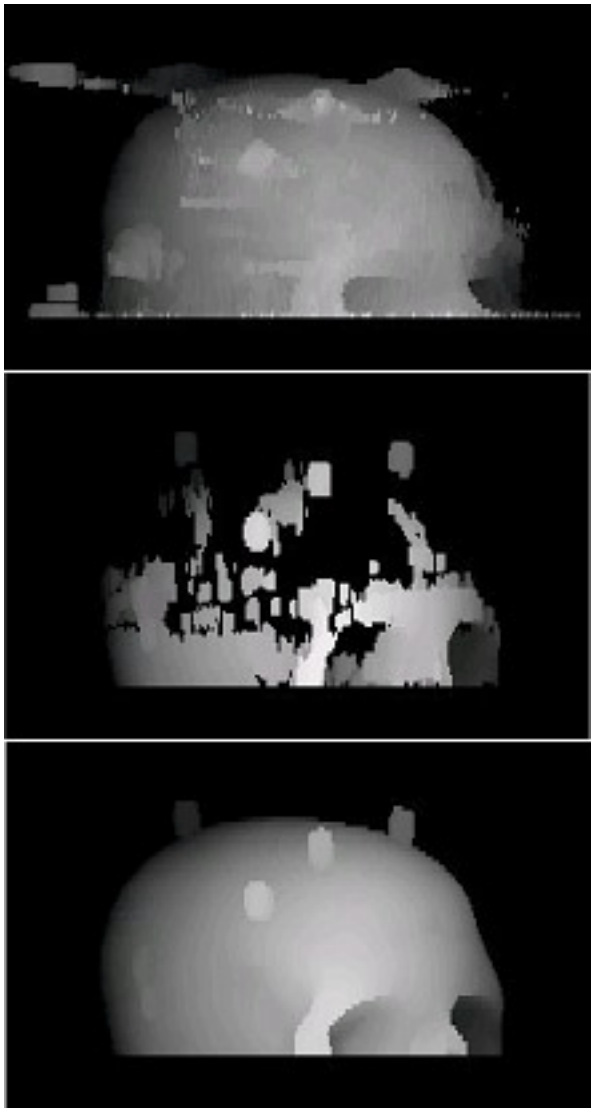

Figure 5.9: Depth-buffer images for three different renderings of the skull phantom. The images were created after applying thresholds of 200 (top panel), 1450 (middle panel), and 1200 (bottom panel).

It is important to note that only one object per world line can be depicted using the z-buffer value. For example, in the case of a MIP, if a single world line intersects multiple vessels a decision must be made as to which vessel is represented by the depth indication. Although the results presented in this study indicate this technique works effectively, additional studies should be performed. As mentioned, the quantitative results measured the error only in the depth direction. The error in placing the cursor over the correct pixel in the rendered image was not measured in this study. It could be assumed, however, that if there were significant error in cursor placement then there would also be significant error in the depth indication since a depth-

buffer value from a different location would have been used. This was not the case. Also, the cursor placement was visually verified to match that of the probe's position on the phantom as well as the cursor placement on the associated tomogram. The only error measurements collected were when the probe was actually touching the surface and the depth was expected to be zero. Accuracy at other distances was not tested, although qualitative results using a ruler to place the probe a given distance from the surface indicate accuracy similar to that reported for the zero depth case. Finally, although this method is also useful for displaying a set of MIPs, error measurements were taken only from a surface projection. An additional phantom is necessary and should have simulated vessels with probe access in order to touch specific points along the vessels. An appropriate phantom would also allow testing on an MRI volume to complement the CT studies.

The depth-buffer method described in this study enables a rendered image set to be registered with physical-space and image-space. This provides opportunity for further IIGS applications. For example, functional information from a pre-operative fMRI study could be mapped and displayed on a rendered cortical surface during surgery. This information would complement the anatomical information from a tomogram volume and inform the surgeon of critical areas that should be avoided, such as speech and motor locations. An electrical stimulator could be tracked in the same manner as the localizing probe and functional data acquired during the surgery could be displayed in the same way. Both of these methods would provide the surgeon with additional information that could benefit and improve surgical procedures.

Acknowledgements

The authors wish to thank Andy Bass, Jim Stefansic, and David Cash for their assistance with this project.

References

[1] TM Peters, B Davey, P Munger, RM Comeau, AC Evans, and A Olivier, "Three-dimensional multimodal image-guidance for neurosurgery," *IEEE Transactions on Medical Imaging*, vol. 15, no. 2, pp. 121-128, 1996.

[2] S Nakajima, H Atsumi, AH Bhalerao, FA Jolesz, R Kikinis, T Yoshimine, TM Moriarty, and PE Stieg, "Computer-assisted surgical planning for cerebrovascular neurosurgery," *Neurosurgery*, vol. 41, no. 2, pp. 403-410, Aug, 1997.

[3] P St-Jean, AF Sadikot, DL Collins, D Clonda, R Karsai, AC Evans, and TM Peters, "Automated atlas integration and interactive three-dimensional visualization tools for planning and guidance in functional neurosurgery," *IEEE Transactions on Medical Imaging*, vol. 17, no. 5, pp. 672-680, Oct, 1998.

[4] RL Galloway, WA Bass, JD Stefansic, and RJ Maciunas, "Incorporation of vascular information into interactive, image-guided surgery," *SPIE Medical Imaging*, vol. 2707, pp. 168-179, 1996.

[5] TM Peters, CJ Henri, P Munger, AM Takahashi, AC Evans, B Davey, and A Olivier, "Integration of stereoscopic DSA and 3D MRI for image-guided neurosurgery," *Computerized Medical Imaging and Graphics*, vol. 18, no. 4, pp. 289-299, 1994.

[6] AB Jani, CA Pelizzari, GTY Chen, and RP Grzeszczuk, "Accuracy of object depiction and opacity transfer function optimization in CT volume-rendered images," *Journal of Computer Assisted Tomography* , vol. 22, no. 3, pp. 459-470, 1998.

[7] MG Palmisano, RL Galloway, and RJ Maciunas, "Modified maximum intensity projections for surgical guidance," *SPIE Medical Imaging*, vol. 3031, pp. 643-650, 1997.

[8] RL Galloway, RJ Maciunas, WA Bass, and WJ Carpini, "Optical localization for interactive, image-guided neurosurgery," *SPIE Medical Imaging*, vol. 2164, pp. 137-145, 1994.

[9] MY Wang, CR Maurer, JM Fitzpatrick, and RJ Maciunas, "An automatic technique for finding and localizing externally attached markers in CT and MR volume images of the head," *IEEE Transactions on Biomedical Engineering*, vol. 43, no. 6, pp. 627-637, Jun, 1996.

[10] B Horn, "Closed-form solution of absolute orientation using unit quaternions," *Journal of the Optical Society of America*, vol. 4, pp. 629-642, 1987.

[11] SL Hartmann, MH Parks, PR Martin, and BM Dawant, "Automatic 3D segmentation of the internal structures of the head in MR images using a combination of similarity and free form transformations: Part II, validation on severely atrophied brains," *IEEE Transactions on Medical Imaging*, vol. 18, no. 10, pp. 917-926, Oct, 1999.

CHAPTER VI

IDENTIFICATION AND DISPLAY OF CORTICAL BRAIN FUNCTION DURING IMAGE-GUIDED NEUROSURGERY

Steven L. Hartmann[1], Peter E. Konrad[1,2], Robert J. Weil[2], and Robert L. Galloway, Jr.[1,2]

[1]Department of Biomedical Engineering
[2]Department of Neurological Surgery

Vanderbilt University

Nashville, TN 37235

Portions of this manuscript have been submitted for publication in:

Medical Physics, March 2002.

Abstract

During a typical image-guided neurosurgery procedure, the surgeon uses anatomical information from tomographic image sets to help guide the surgery. These images provide high-level details of the patient's anatomy. The images do not, however, provide the surgeon with information regarding brain function. The identification of cortical function in addition to the display of tomographic images during surgery would allow the surgeon to visualize critical areas of the anatomy. This would be beneficial during surgical planning and procedures by identifying eloquent cortical regions (such as speech, sensory, and motor areas) that should be avoided.

This study describes the design and implementation of a system for recording and displaying cortical brain function during image-guided surgery. Brain function is determined using an optically tracked cortical stimulator. The image-space location of each stimulation event is recorded, and the user has the ability to label this location according to function type. Functional data can be displayed on both tomographic and rendered images. Tracking accuracy of the cortical stimulator has been determined by comparing its position to that of a tracked surgical probe with known localizing accuracy. This system was tested and evaluated during three neurosurgery procedures. Functional information acquired during these procedures was mapped to a common reference frame in order to determine the potential of using this system to create a functional atlas of the brain.

Introduction

The primary objective of a typical neurosurgery is to localize and remove a cerebral lesion without causing neurological deficit. The risk involved with these procedures increases when the lesion or the surgical path to the lesion is adjacent to functionally important brain regions, since damage to functional regions is often irreversible [1]. Image-guided technology has increased the accuracy of localizing targets but has not, for the most part, included the identification of functionally important areas of the cortex. The ability to localize critical cortical regions and their corresponding function would aid in surgical planning by determining the safest and most appropriate trajectory. Intraoperatively, the functional information would complement the anatomical information already utilized during image-guided procedures.

Cortical brain function can be mapped directly during surgery using a cortical stimulator. This device is typically portable and battery-operated, and is utilized by stimulating the cortex

with a small amount of electric current and observing the response. The function type is traditionally identified by attaching a label directly to the surface of the brain [2]. This approach can be problematic as multiple labels can clutter the operating area. Additionally, if the label falls off or is removed, the functional information from that site is generally lost and the mapping must be repeated.

To help alleviate these problems, a system has been developed to record the location of each cortical stimulation and overlay this functional information onto pre-operative images of the patient. With this approach, attaching labels directly to the cortex is not required. Instead, functional areas of the cortex will be identified on tomographic and rendered images displayed during image-guided neurosurgery procedures. The type of brain function, as determined by the response to the cortical stimulation, is represented distinctly on the images. The user is able to turn on or off these "digital labels", and the location of the stimulation can be stored for future reference or for inclusion in an atlas database.

Methods

This section describes the techniques used to identify and display the location of functional brain regions during interactive, image-guided neurosurgery. Several steps are required for this purpose: displaying pre-operative tomogram and rendered images using an image-guided surgery system, identifying the position of each cortical stimulation and classifying the location according to function type, and overlaying this information onto the tomographic and rendered images.

A. Tomogram and rendered image display

At Vanderbilt University, an image-guided surgery software system called Orion has been developed which is capable of displaying tomographic and rendered image volumes, and to indicate on these images the current image-space position of a surgical instrument or probe. This system has three key tasks: 1.) tracking a surgical probe using a 3-D spatial localizer, 2.) computing the transformation that maps the physical-space position of the probe to the image-space position of the image set, and 3.) displaying the current position of the probe on the correct tomogram slice or rendered image. These requirements and how they were implemented for this

study are described below. A detailed explanation of the Orion system is presented elsewhere [3].

1) Localization: A localizing system is used to determine the physical-space position of a probe or other surgical instrument. The Orion system is compatible with three different localizing systems: the Optotrak 3020 and Polaris position sensors from Northern Digital, Inc. (Waterloo, Ontario) and the Fastrak system from Polhemus, Inc. (Colchester, VT). The two Northern Digital systems are optical localizers while the Fastrak is a magnetic localizing system. The Optotrak 3020 was used for localization in this study. A typical probe used with this system is cylindrical and contains 24 infrared light emitting diodes (IREDs) around the handle (the localizing probe can be seen in Figure 6.5). The Optotrak position sensor contains three linear CCDs, each with 1024 elements, and is capable of accurate localization of any IRED in direct line of sight. If three or more of the IREDs can be localized with a high enough degree of certainty, the tip of the probe can be determined since the geometrical arrangement of the IREDs is known. It has been previously determined that the tip of the probe can be localized using the Optotrak camera with an error of approximately 0.8 mm [4].

2) Registration: Registration between physical space and image space can be done in a number of ways, including point-based and surface-based techniques. For this study, a point-based registration method was used that matches the position of extrinsic fiducial markers. Two different types of markers were used in this study – those that are implanted directly into the skull and those that are attached to the surface of the head using an adhesive. The implanted markers are more accurate and therefore the adhesive markers are used only where it is not feasible to attach posts directly to the skull. Both types of markers are perceptible on MR and CT images, and the center of each marker can be identified in image space using either an automatic (implanted markers) or semi-automatic (adhesive markers) method. The image-space position of the implanted fiducial markers have been identified using the technique of Wang *et al* [5]. During surgery, the tracked probe is used to identify the physical-space position of the center of the marker. If the corresponding position of three or more fiducials in each space can be identified, then the transformation that maps physical space to image space can be determined using a closed-form solution [6]. Although the registration can be mathematically determined using only three markers, typically at least four markers are used in order to increase the registration accuracy.

3) Display: The Orion system consists of a main control program and several modules, which are implemented as independent run-time dynamic link libraries (DLLs). All programs are written in C and compiled for the Windows NT/2000 operating systems. The DLLs are responsible for the various tasks required during image-guided surgery such as localization, registration, and image display.

There are two different types of display DLLs used in this study – one for the display of tomogram images and one for the display of rendered images. The display DLL uses the transformation that registers physical space to image space to determine which image from a tomogram or rendered set that should be displayed. For tomographic images, the slice closest to the image-space position of the stimulator is displayed in one of four Orion display windows. A circular cursor corresponding to the location of the probe's tip is drawn on the slice image. A slightly different process is required for the display of rendered images. A rendered image set is created before the surgery from a tomographic volume (either MR or CT) which includes multiple renderings, each from a different view, in order to obtain total coverage of the desired area. For this study the rendered set is created from an MR volume of the head in order to view the cortical surface. Initial segmentation of the brain envelop is required before rendering and is accomplished using an atlas-based method [7]. The displayed image is chosen based on the angular view from the probe to the center of rotation for the particular rendered image set, and is determined by comparing the current image-space position of the probe with the rotational information used to create the rendered set. The rendering with a viewing angle closest to that of the probe is selected as the current image and displayed in the desired Orion display window. In order to display the current position of the probe on the rendered image, a circular cursor is drawn at the location determined by projecting the stimulator's position onto the plane of the rendering. The distance between the tip of the stimulator and the anatomical point indicated by the cursor is conveyed using a "depth-line indicator". A complete discussion of this technique is described elsewhere [8].

Example screenshots from Orion are shown in Figure 6.1. Each of the three panels represents a different position of a tracked localizing probe. The top image in each panel shows a cortical surface rendering, while a single slice from the original MR image is shown in the bottom of the panel. In the left panel, the probe is placed at a position just outside of the skull's surface. The projection of this point onto the rendered image is indicated by a circular cursor.

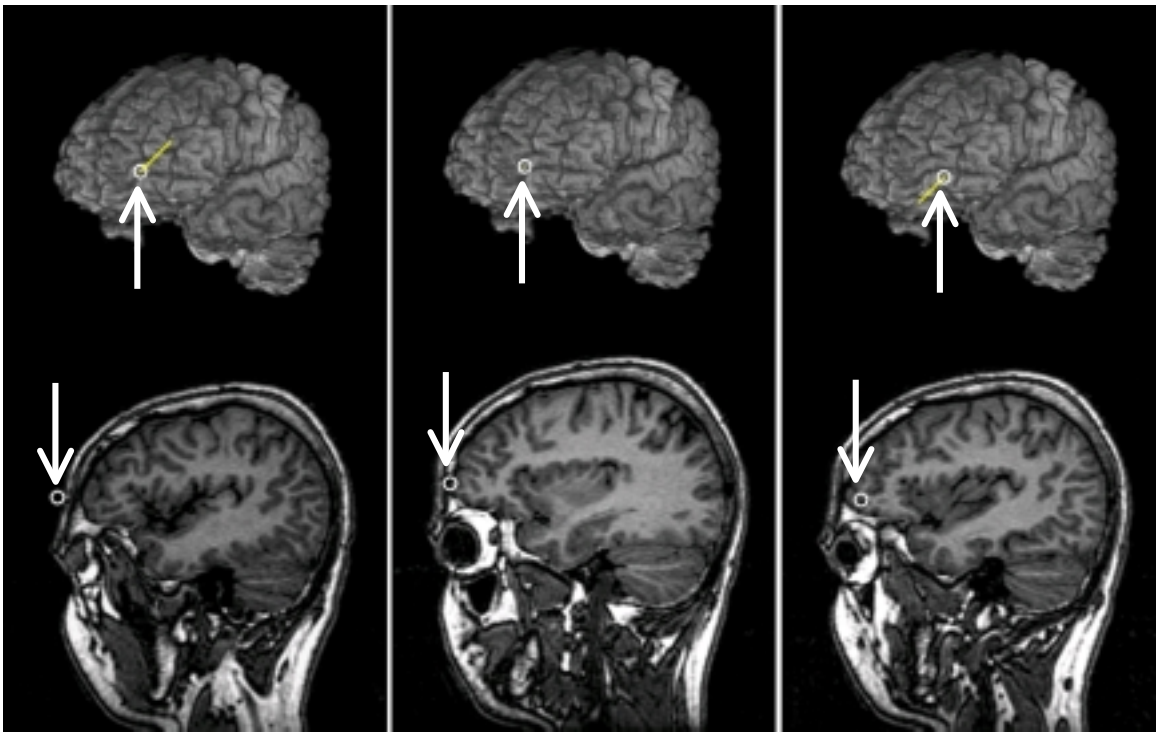

Figure 6.1: Example screenshots from the Orion image-guided surgery system. Each column represents a different position of the tracked localizing probe. The position of the probe is indicated on a rendered image on the top and on the corresponding slice of the original MR volume on the bottom. The arrows pointing to the cursor locations are not part of the Orion display.

The solid line extending from the cursor (the depth-line indicator) represents the distance between the stimulator's tip and the cortical surface point identified by the cursor. The line is drawn at a 45º angle from the cursor to indicate that the probe is outside of the object, as can be seen in the MR slice below the rendering. The middle panel represents a case when the probe is touching the cortical surface. In this case, no depth-line is drawn. In the right panel, the probe is placed at a position inside the cortical surface, as can be seen in the MR slice. In this case, the depth-line is drawn at a 225º angle from the cursor. The arrows have been added to the figure and are not part of the original display in Orion.

The display of three-dimensional position on four separate tomogram or rendered image sets can be updated at greater than 30 frames per second using the Orion system.

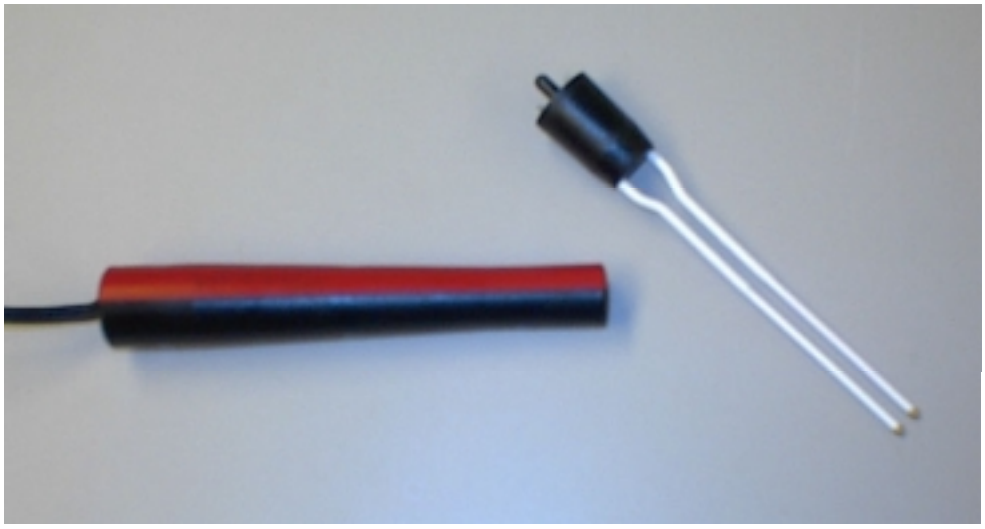

Figure 6.2: The cortical stimulator used to determine brain function. The electrode probe on the right attaches directly to the base unit on the left.

B. Cortical stimulator localization and calibration

The cortical stimulator (Nicolet Biomedical, Madison WI) used for this study is shown in Figure 6.2. This stimulator consists of two parts: a base unit and an attachable electrode probe. A device was designed to track the stimulator using the Optotrak localizing system in order to determine the physical-space position of the stimulator. A standard Optotrak probe is securely attached directly to the base unit of the stimulator. The electrodes of the stimulator are flexible and since the device is assumed to be rigid, any bending will reduce the localization accuracy. To help minimize this error, a rigid sheath has been designed to fit over the electrode probe, exposing only the tips of each electrode. This helps stabilize the entire device without severely limiting its usability. The partially assembled tracked stimulator device can be seen in Figure 6.3. The localization probe shown in the bottom of the figure can be attached directly to the base unit (the assembled tracked stimulator can be seen in the right-hand panel of Figure 6.7).

Since the geometrical arrangement of the IREDs and the dimensions of the stimulator are known, the physical-space location of the stimulator's tip can be determined after a calibration process. Typically, a tracked instrument is calibrated by recording the position of all IREDs in view of the camera for a period of time (60-90 seconds) as the instrument is rotated about a common pivot point. This process determines the position of the instrument's rotation point (usually corresponding to the tip of the device) in relation to the arrangement of the IREDs, and only needs to be repeated if the geometry of the device changes. It is the physical-space location

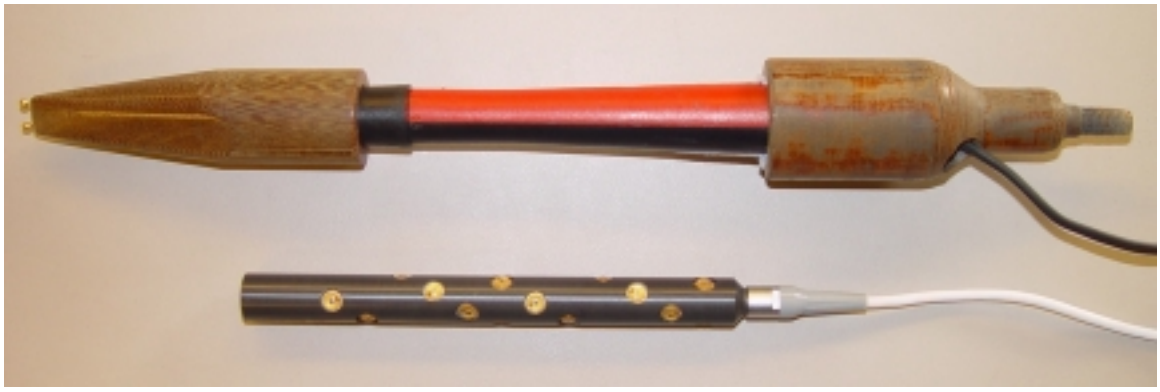

Figure 6.3: The cortical stimulator as used with the Orion image-guided surgery system. The electrode tips are stabilized with a rigid sheath. The localizing probe shown in the bottom of the figure securely attaches to the right-hand side of the stimulator.

of this pivot point that is typically tracked during image-guided surgery. This calibration process, however, is not ideal for calibrating the cortical stimulator since the device must be taken apart before surgery in order to be sterilized. The stimulator is reassembled in the operating room immediately before surgery and must be calibrated before use. The time-consuming process of rotating the stimulator about a pivot point is not feasible in the operating room, especially considering that if the device comes apart or shifts in any way the calibration process must be repeated.

A new calibration process, therefore, has been developed for this purpose. A sterilized calibration block that contains three evenly spaced divots is mounted securely during surgery. The tip of a localizing probe is then touched to the center divot and the physical-space location of this point is recorded, as shown in the left-hand panel of Figure 6.4. Then the electrodes of the stimulator are placed in the outside two divots and this location is also recorded, as shown in the right-hand panel of the figure. The IRED configuration of the tracked stimulator has previously been determined but the offset to the tip is unknown. Using the rotation and translation parameters of the stimulator's recorded position and the position of the center divot, this offset can be determined and stored so that all future localization updates return the physical-space location of the stimulator's tip. The tip is defined to be the mid-point between the stimulator's two electrodes (this is the purpose of the three divots on the calibration block). This calibration process needs to be repeated if the geometry of the device has changed. However, if the calibration block has not moved, the center divot does not need to be relocated. This technique provides a simple and fast method for calibrating the tracked stimulator. The disadvantage of this

Figure 6.4: The process used to calibrate the tracked cortical stimulator. A standard localizing probe is placed in the center divot of the calibration block and its position is recorded (left). The tips of the stimulator are then placed in the outside divots in order to calibrate the device.

method from the original method is that it must be done at the start every surgery. However, since the geometry of the stimulator may change depending on how it is assembled, calibration is required at the start of surgery regardless, and this method is faster and more practical than the original method.

C. Identification and display of functional brain information

An additional Orion module has been created for managing all data associated with the tracked stimulator. This DLL has two main functions: (1) record the image-space location and corresponding function type of each cortical stimulation, and (2) pass this information to the appropriate display DLL in order to identify the recorded functional information on the tomographic and rendered images displayed during surgery.

1) Recording the location of each stimulation: When the cortical stimulator is used to apply electrical current to the cortex of the brain, a user can simultaneously capture its location into the Orion system by clicking on a button with the mouse (the dialog box for controlling this task can be seen in Figure 6.9). This requires some coordination between the user and the surgeon, but since the stimulator can be set to make an audible noise during activity, capturing a stimulation event is fairly intuitive. This physical-space position is converted to its corresponding image-space position using the transformation determined by the fiducial marker mapping. The image-space coordinate is stored and the surgeon is free to move the cortical stimulator while determining the response to the stimulus. The surgeon can then determine whether or not to accept this point based on the presence and quality of the observed response. If the surgeon decides not to include this point, no action is required. The next stimulation will overwrite the stored position and the previous point will not be included. This process continues until a point is accepted and classified according to function type. The operator selects this type from a menu, and then both the image-space location of the stimulation and the function type are stored in a database for that patient. For this study function type is classified into one of three categories: motor, sensory, or speech. A second method of storing points, the "record on capture" method, can also be used. In this case it is not necessary to capture and record in two separate steps. Instead, each captured point is automatically recorded and classified according to the function type currently selected. This is useful in cases where a functional area has been determined (such as the motor cortex) and it is desired to record many locations as quickly as possible. Once a stimulation event is recorded, its location is passed to the Orion DLLs responsible for displaying tomographic and rendered images. The display DLLs will overlay the functional information onto the appropriate images, as described in the next section. The stimulator DLL stores the location of all points mapped during the surgery (and their corresponding function type), and this information can be saved to a file for future use. Previously saved points can be loaded from a file by the stimulator DLL. The stimulator DLL also has the capability of deleting the most recently acquired stimulation point or deleting all previously recorded points.

2*) Displaying functional information:* As the tracked stimulator is moved during surgery, the appropriate tomogram slice or rendered image is displayed and the stimulator's position is represented on that image by a circular cursor, as described previously. The display DLLs

receive notification from the main Orion module whenever a stimulation event has been recorded. When this occurs, the display DLL retrieves the image-space location and function type of the stimulation event in order to overlay this information onto the appropriate image. Functional regions are overlaid onto the tomographic and rendered images using a different color for each particular function type. Each data point is drawn as a solid circle using Window's Graphics Device Interface (GDI). Since each stimulation point represents function from a 3-D region and not a 2-D area, the location corresponding to the function is drawn on multiple tomogram slices. The function point can be considered as a sphere of desired radius. A circle with this radius is drawn on the slice corresponding to the center of the stimulation, while smaller circles are drawn on slices adjacent to the center point.

For rendered images, a single circle of desired radius is sufficient to indicate function since the rendering is already a 3-D projection. The same function point, however, may appear on multiple renderings from the set since this point may be visible from different viewing angles. Since it is possible to record a stimulation event at a location that is not shown on any of the rendered images (such as an internal cortical location), it is necessary to determine whether or not to include a particular event on the currently displayed rendering. This can be accomplished using the depth-buffer targeting method reported previously [8]. Using this technique, it is possible to determine the distance between the location of the stimulation and its projection onto the rendered image. A sensitivity threshold is set such that if the distance between the stimulation and the cortical surface shown on the rendered image is greater than the threshold, the function for that location will not be displayed.

The speed at which the Orion system is capable of updating the display of images is crucial. Any delay between the actual and displayed position of the surgical probe is at least inconvenient and potentially critical if surgical decisions are made based on outdated display information. To improve the efficiency of the display, functional locations are computed and stored at the time of the stimulation. For each tomogram slice and rendered image, a data structure is created that stores the information required to draw the functional data on that particular image. This information is calculated only once – at the time of the stimulation event. The type of cortical function identified and the pixel coordinates of the function's location are stored for both tomographic and rendered images. The data structure associated with a tomogram image also stores a scaling factor used to determine the size of the circle drawn for that particular

function. Since function is represented as a sphere, a single event can appear on multiple tomogram slices, as previously described. Additional data structures for adjacent slices are created at the time of the event and contain the same information as the central slice, differing only by the scaling factor used to draw the circle. Although these additional data structures are somewhat redundant, this strategy allows the display to be updated at a faster rate. The data structure for a rendered image also stores the distance (in millimeters) between the location of the stimulation and the rendered object. This distance is used, along with a threshold selected by the user, to determine if the function should be displayed. At the time of each stimulation event, a data structure is created for each rendering in which the object appears. Since any physical-space location can be projected to a point on any rendered image view, inclusion of the event for a particular rendering is determined by the distance to the object. If the stimulation event occurs at distance from the rendered object greater than a certain limit (the maximum sensitivity threshold), a data structure for the event is not created and the function will not be displayed on that particular rendering.

Finally, the user can select whether or not any functional information should be displayed at all by simply checking or clearing a selection box in an options dialog window. This can be done for each of the four Orion display windows.

Results

The ability to accurately localize the tracked cortical stimulator was determined by comparing its position to a tracked surgical probe with known localization accuracy. The entire surgical guidance system was then evaluated during three human neurosurgery procedures. Finally, the functional data acquired during these procedures was mapped to a common reference volume in order to determine the feasibility of using this system to create a functional brain atlas.

A. Localization accuracy of the tracked cortical stimulator

The cortical stimulator body was securely attached to the IRED probe and the sheath was placed over the electrodes, as shown in Figure 6.3. The entire device was then calibrated using the technique described in the previous section. In order to measure the accuracy of Orion's ability to localize the stimulator, the physical-space coordinate (as determined by the Optotrak) was recorded when the stimulator's tip was touching a known location.

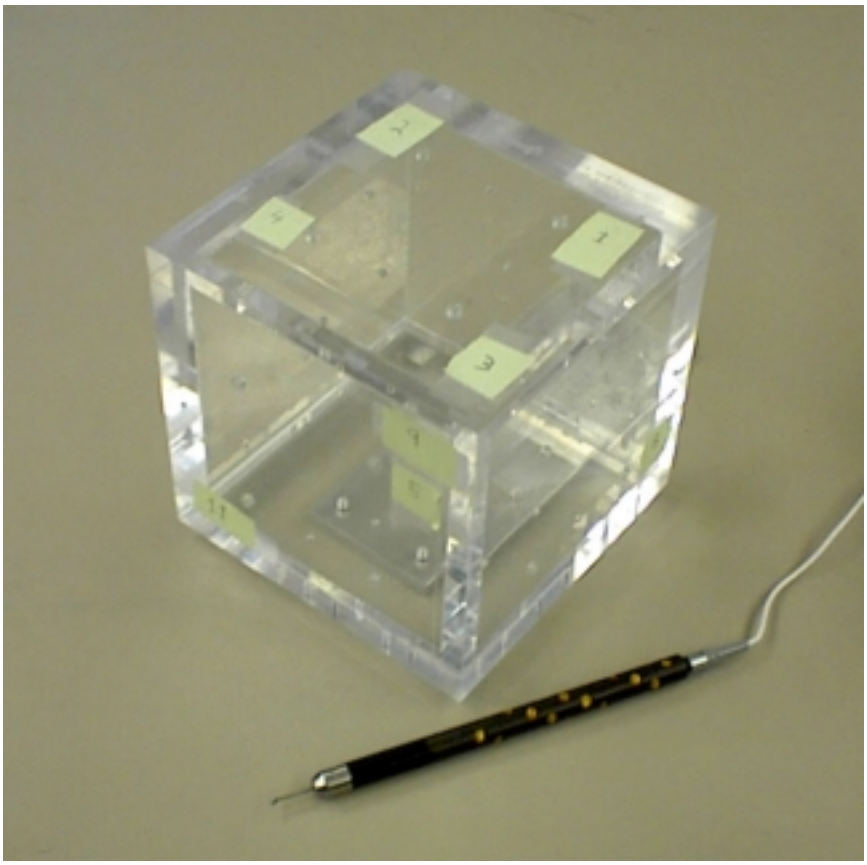

Figure 6.5: Plastic phantom and surgical probe used to determine the accuracy of localizing the position of the tracked cortical stimulator.

A plastic phantom of known dimensions, shown in Figure 6.5, was used for accuracy testing. First, the tip of the tracked stimulator was placed in twelve separate divots drilled into the sides of the cube (four divots on three different sides) and the physical-space coordinate was recorded for each position. Then the tip of a surgical probe with known localization accuracy was placed in each of the twelve divots and the physical-space coordinates were again recorded. For determining localization accuracy, the tip of the stimulator was selected as one of the two electrode tips instead of the mid-point between the electrodes.

This process was repeated four additional times, with the phantom repositioned to a different location for each set of measurements. Table 6.1 lists the error results for each of these five studies. These error values represent the root-mean-square distance (in mm) between the location of the stimulator and the location of the surgical probe. The average error for all 60 measurements was 1.85 +/- 0.15 mm.

Table 6.1: Localization accuracy for identifying the position of the tracked cortical stimulator. The error results (in mm) are determined by comparing the location of the tracked stimulator with the location of a surgical probe with known localization accuracy.

Trial	1	2	3	4	5
Error (mm)	1.89	2.05	1.68	1.73	1.92

B. Evaluation during neurosurgery

Before the image-guided surgery system was used during surgery, all methods were documented and approved by the Institutional Review Board (IRB) of the Vanderbilt University Medical Center (IRB number: 010270, Expiration date: May 25, 2002). Informed consent was obtained from all patients prior to the procedure, and their confidentiality has been protected. Patient identification was removed from all medical images and photographs used in this study.

1) Image data: For each case, an axial Magnetic Resonance (MR) image volume of the head was obtained the day before the surgery. A set of 7-9 adhesive skin markers were attached to the patient's head before the scan and used as fiducial markers for calculating the physical-space to image-space transformation (the skin markers can be seen in Figure 6.6). The axial MR volume was reformatted to create both coronal and sagittal orientations. The image-space location of the skin markers was identified and stored in a data file. A volume-rendered image set consisting of 16 separate cortical surface renderings, each with a different viewing angle, was created from the sagittal MR volume of the head. Prior to creating the rendered images, the brain was segmented from the MR volume using an automatic method [7].

2) Surgery protocol: Immediately before the surgery, the three tomogram volumes (each with a different orientation) and the rendered image set were loaded into the Orion software system. Once the patient was positioned in the operating room, the physical-space location of the skin markers were recorded using a tracked surgical probe, as shown in Figure 6.6, and the registration between image space and physical space was calculated. The fiducial registration error (FRE), defined as the root-mean-square (rms) difference between corresponding fiducial markers after registration, was calculated to be 1.8, 2.8, and 3.2 mm for each of the three cases. These values were considered well within the acceptable range considering the potential for movement of the adhesive skin markers.

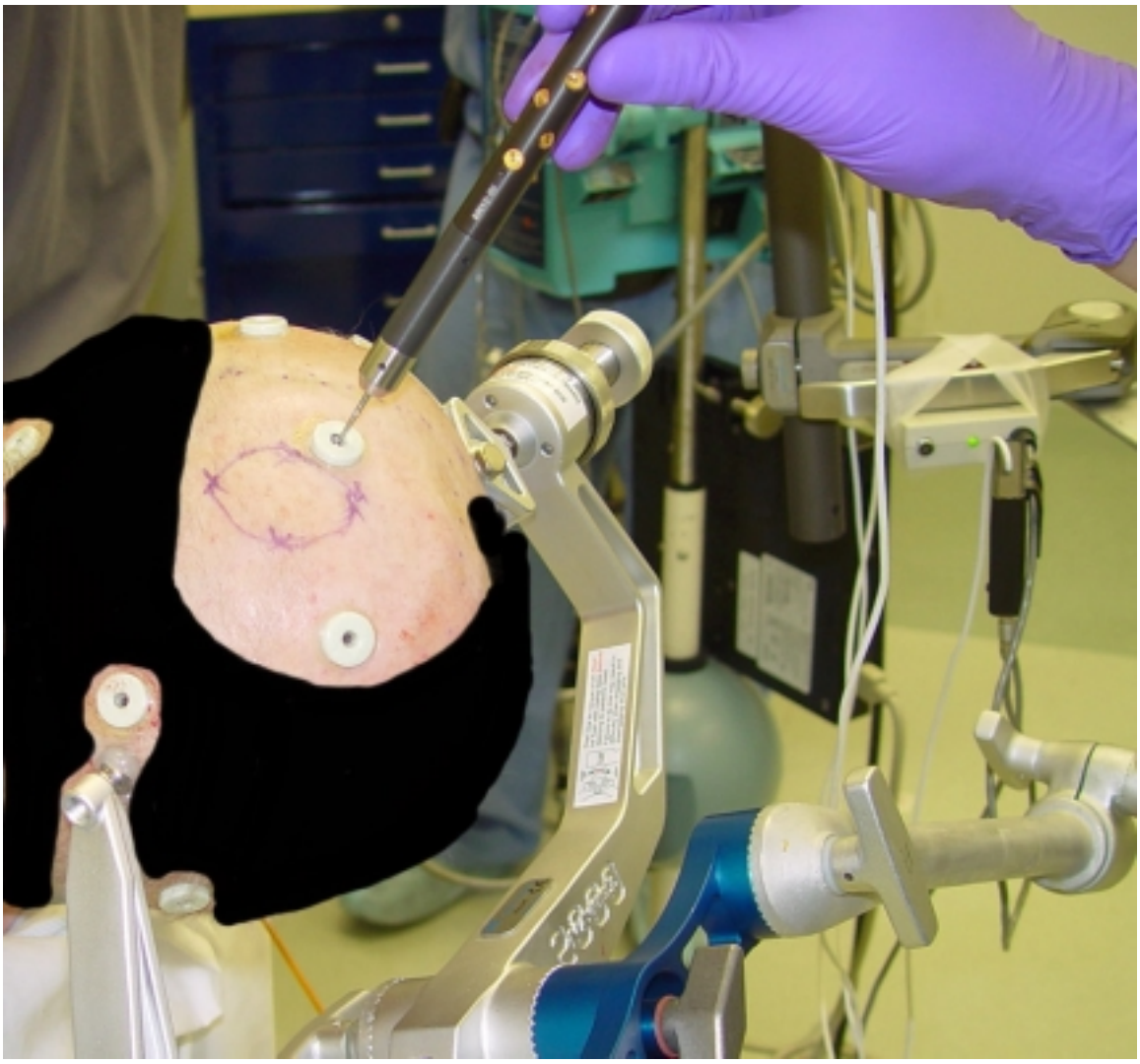

Figure 6.6: The process used to identify the physical-space position of the adhesive skin markers. The tip of a localizing probe is placed in the center of the marker and its location is recorded. This information is used to determine a physical-space to image-space transformation.

The probe was moved to different locations on the patient's head in order to visually verify the registration accuracy. Once a sterile environment was established in the operating room, the probe used for identifying the fiducial markers was replaced with two sterilized devices: a second localization probe and the tracked cortical stimulator. The sterilized calibration plate was mounted and the tracked stimulator was calibrated using the procedure explained in the previous section. This two-step process is shown in Figure 6.7 for one of the surgery cases. Once the calibration was complete, either of the tracked devices could be used to update current position on the tomographic and rendered images. Typically the surgical probe was used to

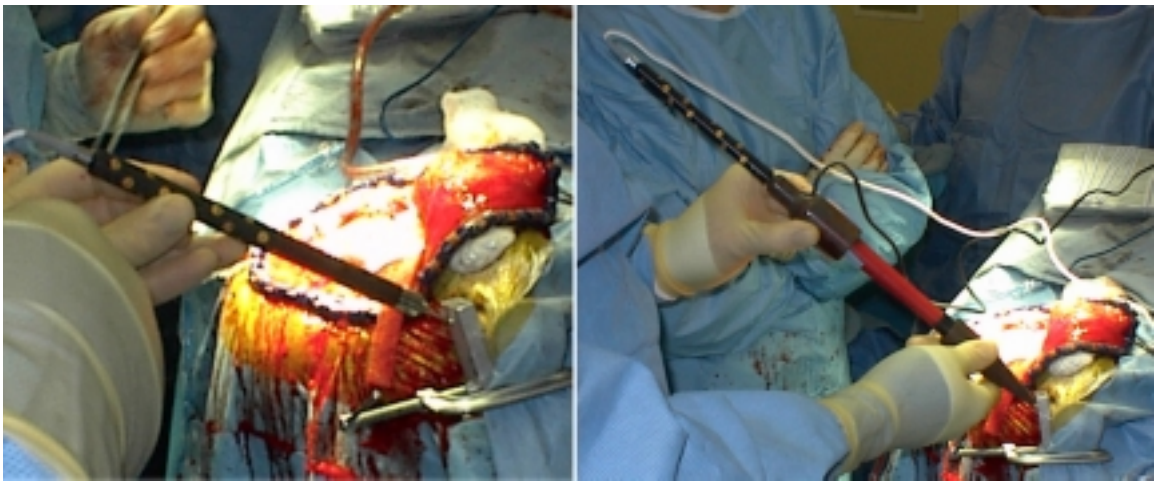

Figure 6.7: Calibration process of the cortical stimulator during surgery. All equipment, including the calibration block and clamp, has been sterilized.

provide image guidance since it is smaller, lighter, and more accurate than the tracked stimulator, although the stimulator can also be used for guidance with comparable accuracy. Cortical function was mapped during each procedure using the tracked stimulator. Figure 6.8 shows the stimulator being used to map function during one of the surgery cases. If a response was observed to the stimulus, it was recorded and classified according to type (motor, sensory, or speech for this study). This information was entered into the Orion system using the options dialog box shown in the lower-right corner of Figure 6.9. Each recorded point was overlaid onto the displayed tomographic and rendered images, as explained in the previous section.

3) Surgery results: A screen capture from the Orion image-guided surgery system, acquired during one of the three neurosurgery procedures used in this study, is shown in Figure 6.9. During this case (tumor removal from the left hemisphere), three different function events were recorded: two events corresponding to the motor function of the right hand, and one event corresponding to the sensory function of the right hand. Each of these events can be seen in the rendering of the cortical surface of the left hemisphere, shown in the bottom-right Orion window. The top two solid circles denote the motor events, while the bottom circle denotes the sensory event. The circular cursor surrounding the upper motor event represents the position of the tracked stimulator. The motor events and the cursor can also be seen in the three tomogram orientations. For this particular location of the stimulator, the sensory event can only be seen on the coronal tomogram slice (upper-right of the figure). The smaller solid circles displayed on the tomogram slices indicate an event centered on an adjacent slice. A second view of this surgery,

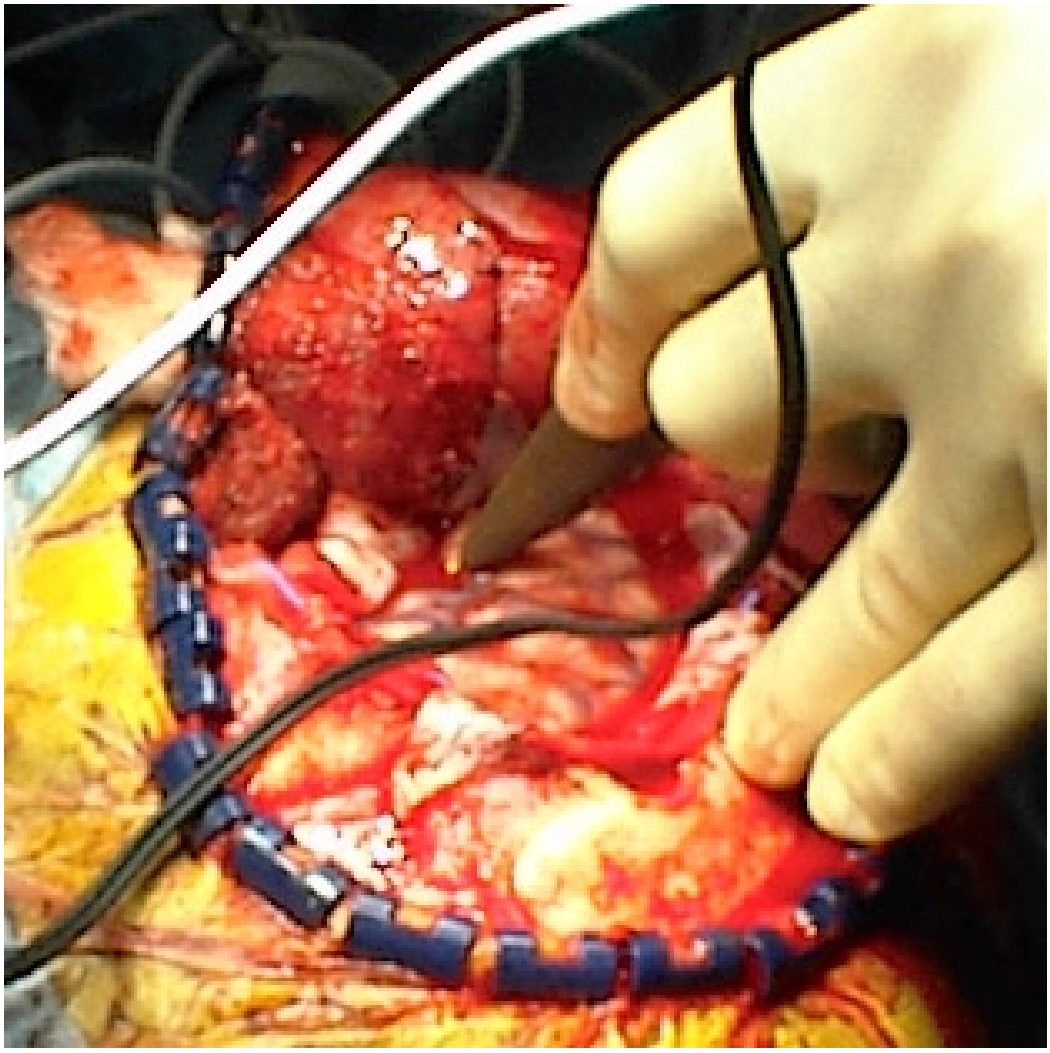

Figure 6.8: Actual use of the tracked cortical stimulator during neurosurgery. The location of the stimulation on the cortical surface is recorded by the Orion image-guided surgery system.

corresponding to a different location of the stimulator, is shown in Figure 6.10 (only the images are shown here). For this location, the sensory event can be seen in the axial (top-left) and sagittal (bottom-left) tomogram slices. The stimulator has been placed directly on the surface of the tumor, which is visible in all right side four images.

The second surgery case was also for removal of a tumor from the left hemisphere. A screen capture taken during this case in shown in Figure 6.11. Six total events were recorded: three corresponding to regions responsible for speech (the three left-most circles shown on the sagittal MR slice and on the rendering of the cortex), and three events corresponding to the facial motor region for the of the face (the three right-most circles in the same images). The three

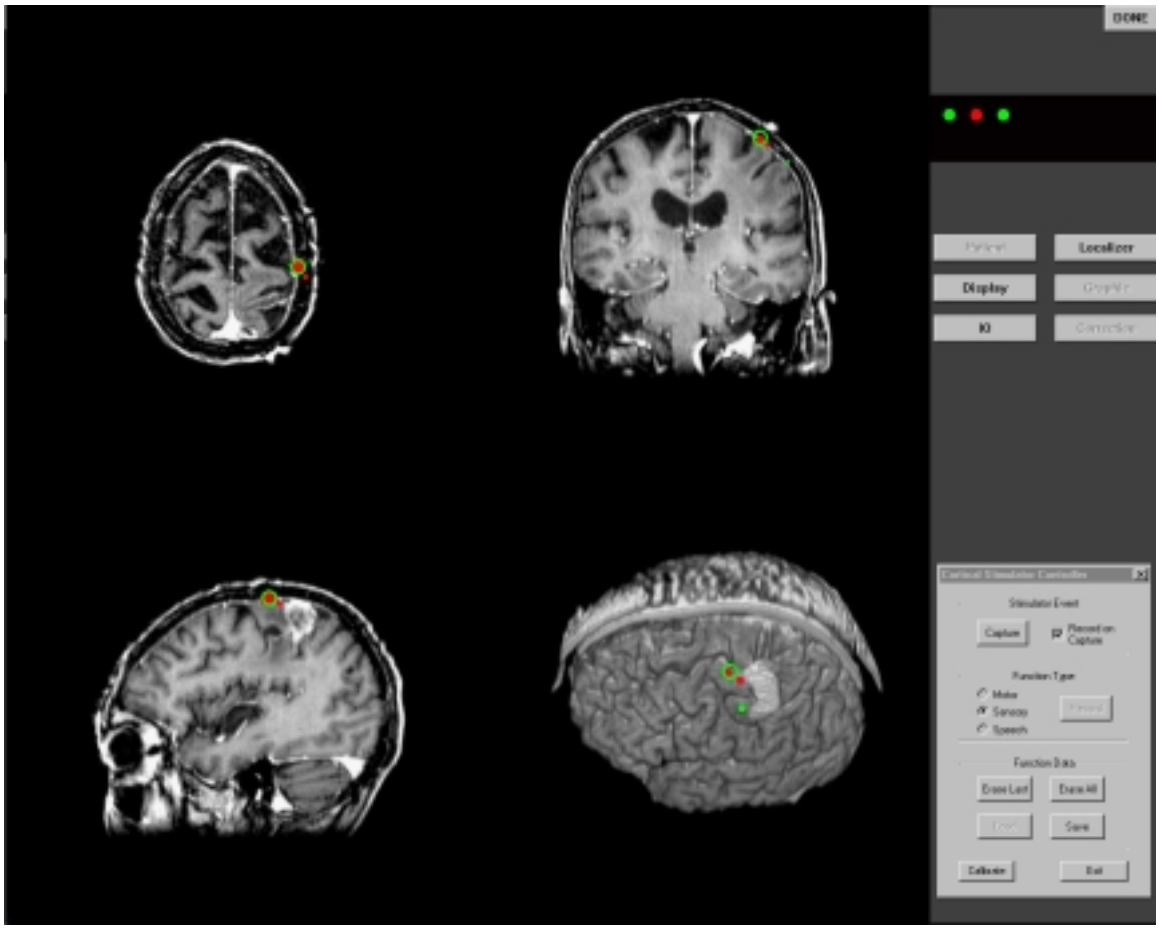

Figure 6.9: A screenshot from the Orion system during an actual neurosurgery procedure. Three different tomogram orientations (axial, coronal, and sagittal) and a rendering of the cortical surface are displayed. The dialog box used to record and identify stimulated locations is shown in the bottom-right of the figure.

motor events can also be seen in the coronal MR slice (upper-right). No events are located on the axial slice shown for this location of the stimulator.

The third surgery case was performed in order to remove a tumor located in the right hemisphere. Three events, all corresponding to the facial motor region of the left side of the face, were recorded. A screen capture taken during this surgery is shown in the Figure 6.12.

During the first two cases, labels were attached directly to the cortex for each stimulated location where function was observed. This allowed for a direct comparison between the standard method (attached labels) and the computerized method presented in this study. Figure 6.13 shows a side-by-side comparison (the first case is shown in the top row). The left panel shows the location of each recorded event on the cortical rendering, while the right panel shows a photograph of the cortex with attached labels. The photographs have been rotated to

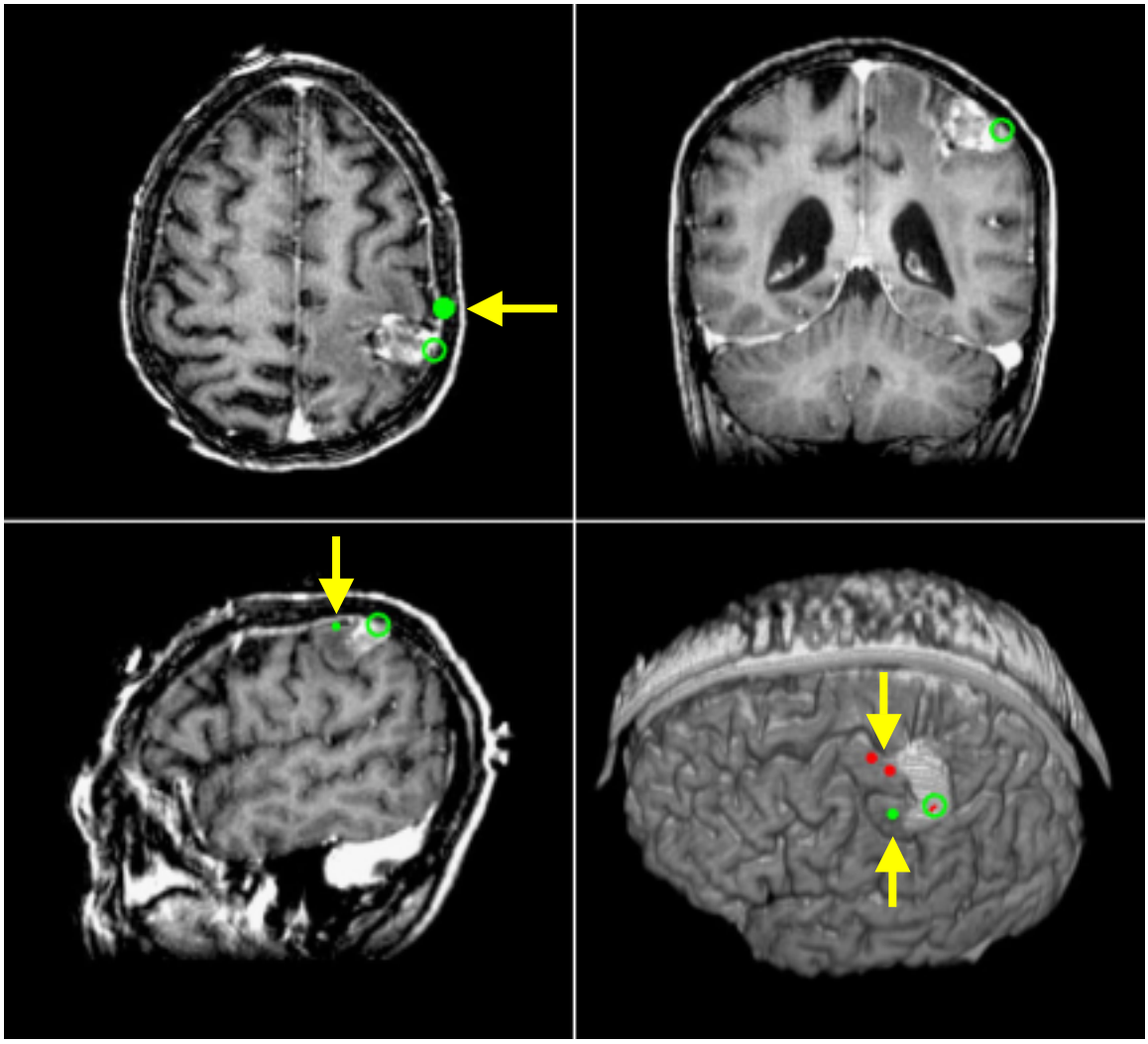

Figure 6.10: A second screenshot from the same surgery shown in Figure 6.9. Two motor events (upper solid circles displayed on the rendered image) and one sensory event have been recorded. The sensory event also appears in the axial (upper-left image) and sagittal (lower-left image) MR slices. None of the events appear on the particular coronal slice displayed for this location of the stimulator (upper-right image). Arrows point to the function points recorded using the Orion system.

approximate the same orientation as the rendered images. Arrows are included in the top row to indicate the location of the three labels. A localizing probe is touching one of the speech labels in the bottom photograph. In each case the digital labels displayed on the rendered images appear to be in the same location as the physical labels attached to the cortex.

The location of the events on the images and the ability to distinguish between event type using different colors are more apparent on a high-resolution color monitor than on the figures shown here.

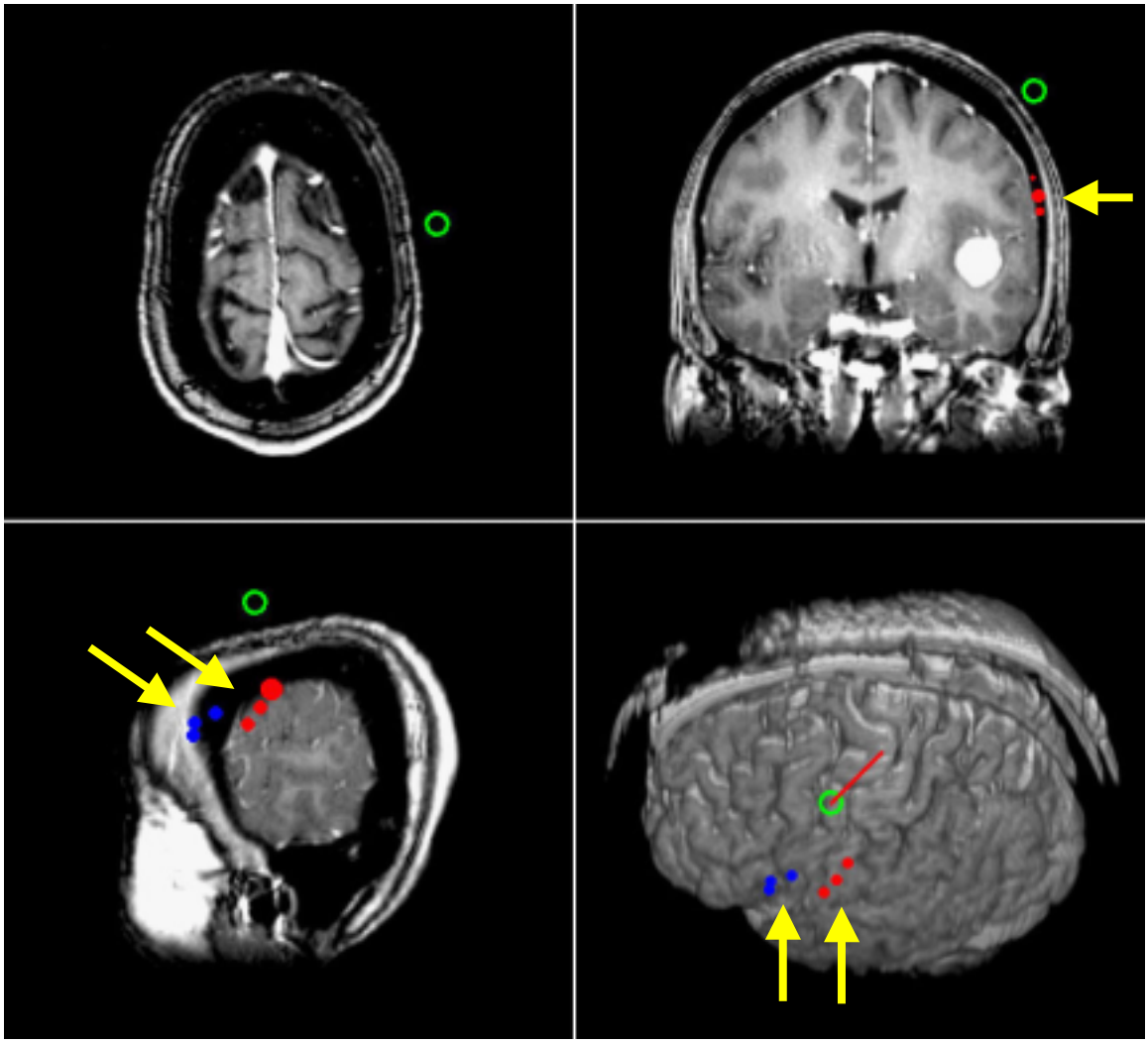

Figure 6.11: An Orion screenshot from the second surgery used in this study. Three speech events and three facial motor events have been recorded. The facial motor locations are the three right-most solid circles displayed on the sagittal MR slice (lower-left image) and on the rendered image (bottom-right), and the three solid circles shown on the coronal slice (upper-right image). None of the events appear on the particular axial slice displayed (upper-left image).

C. Functional brain atlas creation

Statistical information on the location of brain function, obtained from multiple patients, may provide additional perspective or guidance that cannot be obtained from the particular patient's functional map alone. An average brain map can be created by registering each patient's tomogram to a standard reference frame. Once this transformation is determined, the location of functional data can be mapped to the same reference space. A number of atlas-based registration techniques have been developed for the purpose of inter-subject registration (see [9]

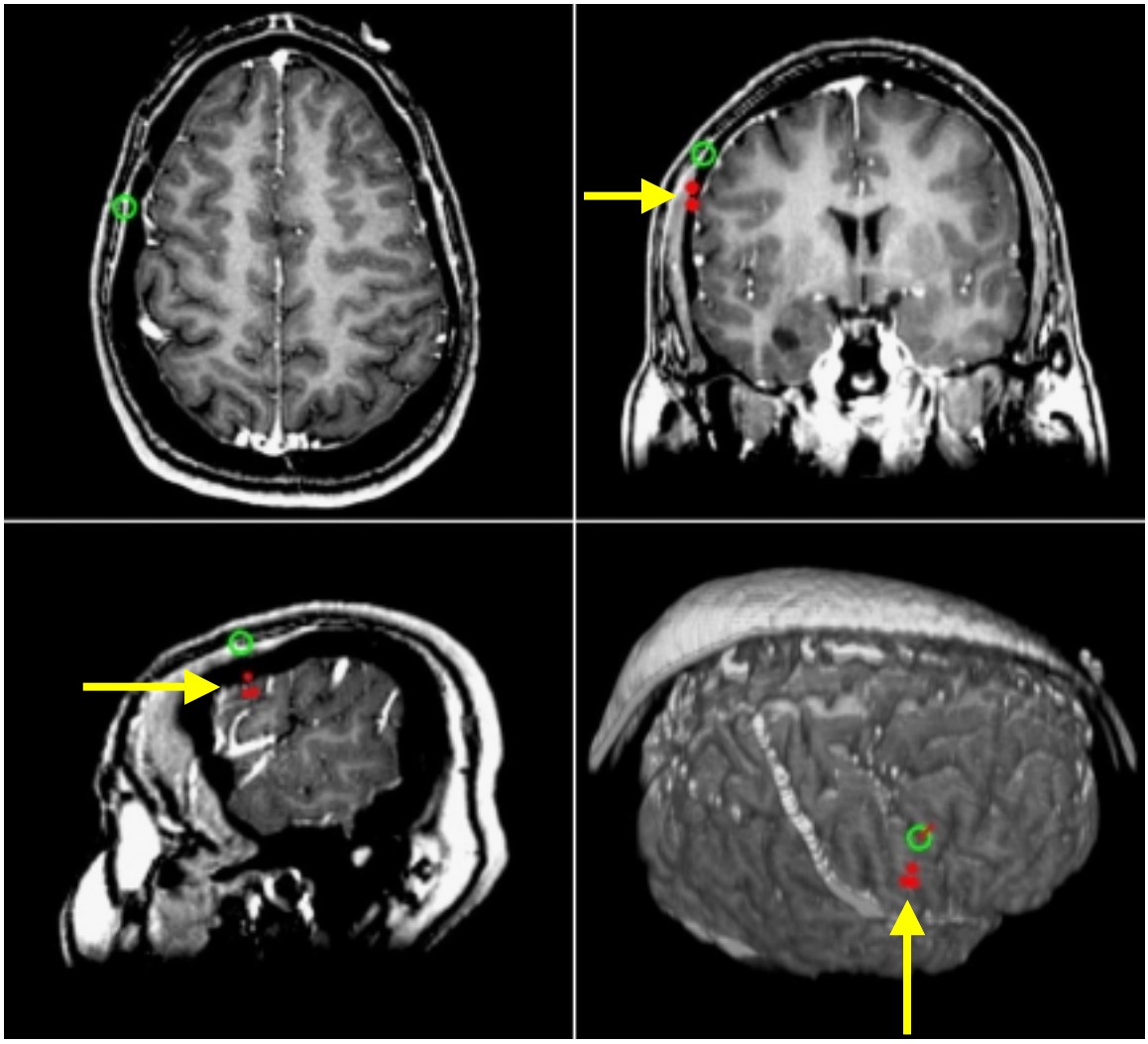

Figure 6.12: An Orion screenshot form the third surgery used in this study. Three facial motor events have been recorded.

for a detailed review). Computerized anatomical atlases, such as the Talairach atlas [10], have been used to map cortical regions identified on a reference brain to the desired brain volume using atlas-based registration techniques. Most of these techniques use linear proportional scaling, which does not account for the large cortical variations between the atlas and the individual subject volumes, and therefore result in poorly matched cortical regions.

For this study, a brain volume from a fourth subject was used as the reference volume. This MR volume was acquired with the same imaging parameters as the three patient volumes. An optical-flow based registration method was used to determine the transformation between the reference volume and each of the three patient volumes. This non-linear registration algorithm

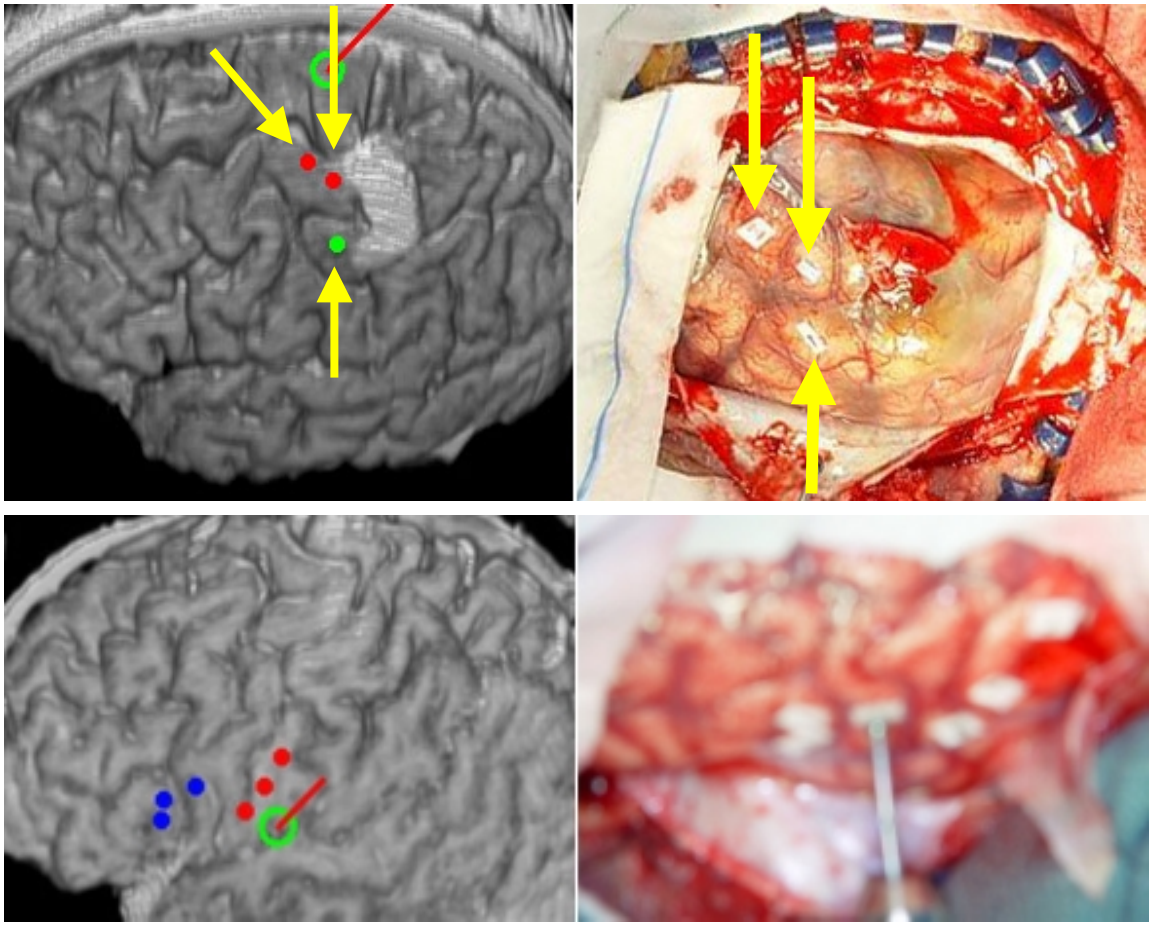

Figure 6.13: Comparison between stimulation events identified and displayed by the Orion system and labels attached directly to the surface of the brain. Results for two of the three surgery cases are shown (labels were not attached to the cortex during the third case).

does not use any structural information from the image to determine the registration, but instead computes a 3-D deformation field (i.e. a displacement for each voxel in the image) using the intensity characteristics of each image volume. It has been shown previously that this method is capable of accurately matching major brain structures (cerebrum and cerebellum) between MR image volumes of different subjects [7]. In order to accurately map the cortical regions between an atlas volume and a patient volume, this method has been improved by using the location of major sulci to constrain the deformation field [11].

This modified registration algorithm was used to determine the transformation between the atlas volume and each of the three patient volumes. The transformation was then used to map the location of each of the stimulation events recorded during surgery into the coordinate system of the atlas volume. These 3-D image-space coordinates were then projected onto volume

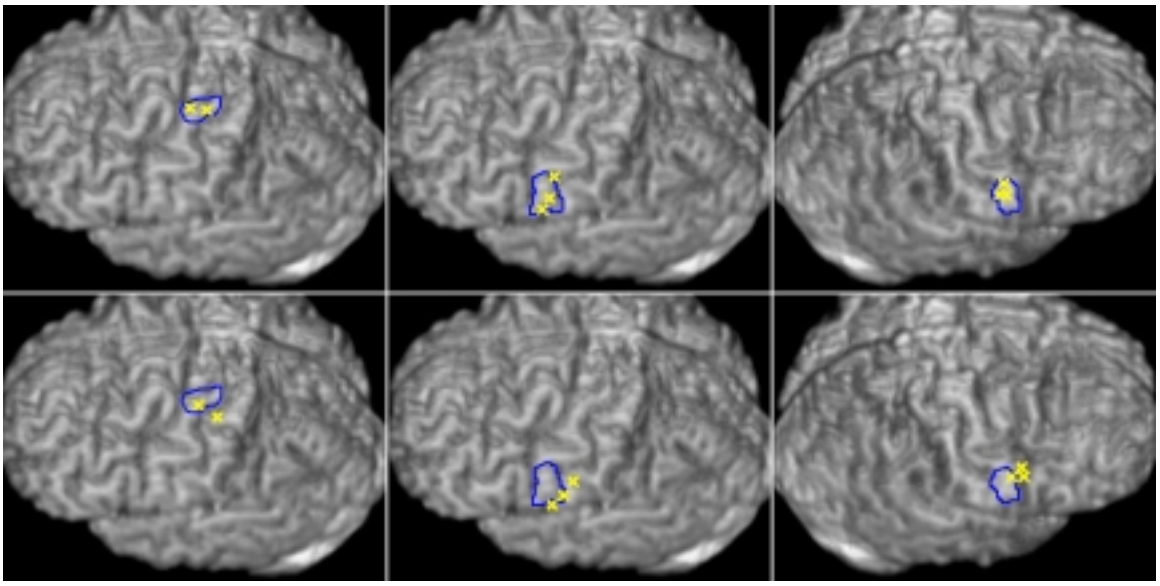

Figure 6.14: Initial results for creating a functional brain atlas. Each motor event for the three subjects have been mapped to their corresponding location on a reference brain volume (top row). The mapping was computed using a non-linear optical flow deformation algorithm. The approximate region for the particular motor function has been outlined for each case (right hand motor, right facial motor, and left facial motor for each column, respectively). For comparison, the location of each point after mapping using a global transform is shown in the bottom row.

rendered images of the atlas brain, as shown in the top row of Figure 6.14. Each column in the figure shows the results for one of the three patients. For this figure, only the events corresponding to motor function are shown. The approximate location for the particular motor function is outlined on each rendered image. The location of these points on the original patient images can be seen in Figures 6.10 - 6.12. For the first case (left-hand column) there are two points corresponding to the motor function of the right hand. The second (middle column) and third (right-hand column) cases each contain three points corresponding to the facial motor region (one case per hemisphere). Using the optical flow registration technique, seven of the eight points were mapped to locations within the defined region, while one point (second case, shown in the middle column) was mapped to a location just on the border of the region.

For comparison, a global registration method was also used to map these same motor points onto the atlas volume (bottom row). The global transformation included three rotation parameters, three translation parameters, and a single isotropic scaling factor, as described in [7]. This type of transformation is similar (although not identical) to that typically used for mapping with the Talairach atlas. For each of the three subjects, the global registration alone was not

sufficient to accurately map the function points onto the correct anatomical region of the atlas volume. In fact, only two of the eight points were mapped to locations within the outlined regions (with an additional point mapped onto a border of the region). Since most of the poorly registered points have been mapped onto an adjacent gyrus or sulcal region, even redefining the approximated functional areas would not improve the results in this case.

Discussion

The additional display module created for the Orion software system enables the surgeon to identify, record, and display functional regions of the cortex during image-guided neurosurgery. This new system can be used to help eliminate the potentially error prone process of attaching labels directly to a patient's cortex. Using this system, the surgeon is able to view critical functional information as well as the traditional anatomical information displayed during image-guided procedures.

The tracking accuracy of the cortical stimulator, while not as accurate as the surgical probe, is well within the acceptable range for its application. Function defined using the stimulator does not produce a single point, but a region surrounding the electrodes (the two electrode tips are approximately 6 mm apart). Although it is important to reduce sources of error wherever possible, the accuracy needed to effectively define the location of function is not as critical as typical neurosurgery applications, where sub-millimeter accuracy is often required.

There are many factors that contribute to the total error of this system, including system specific factors such as marker identification and image registration. Additional factors not directly associated with the system, such as geometrical distortion of the preoperative images and the shifting or sagging of the brain between imaging and surgery also reduce the overall accuracy of the system. Reducing the error contribution from external factors such these, although important, were not the focus of this study and were not pursued. Any future work that improves or corrects errors caused by these factors could be used directly to improve the overall accuracy of the image-guided surgery system described in this research.

The tracked stimulator used in this study consisted of a tracking system designed to fit around an existing cortical stimulator. Future improvements include designing a new stimulator specifically for image-guided surgery. This device will be smaller, lighter, and easier to use than

the prototype used in this study. The new design will also make it possible to automatically signal the Orion system when a stimulation has occurred.

The ability to record and save the functional information identified during surgery may prove useful in other applications. As discussed previously, a database of cortical function could be created from multiple patients. This could then be used during additional procedures by mapping the database onto the tomogram images of the current patient. This would allow functional information from a population of patients to be displayed along with any function acquired from the specific patient. The database could then be updated by including new information obtained during each additional surgery. As the number of surgery cases in the database increase, the categories used to classify the function type may also expand. For this study, only three major categories were used (speech, motor, and sensory). These may be further divided into several sub-categories (such as classifying motor function according to the specific anatomical location or separating speech function into Broca and Wernicke areas) as the amount of data groes.

Traditionally, information obtained using a cortical stimulator is used during the surgery but is then lost since the data is not saved. Using the tracked stimulator system described in this study, valuable information regarding the location of brain function that was previously available only to the surgeon could now be used by others for additional research purposes. For example, this data could help researchers investigate the ability of the brain to re-map function from one area of the brain to another under certain conditions such as epilepsy or the presence of a tumor.

Acknowledgments

The authors thank Dr. John Song for his valuable assistance during surgery and Phil Davis for his help constructing the tracked cortical stimulator.

References

[1] GR Cosgrove, BR Buchbinder, and H Jiang, "Functional magnetic resonance imaging for intracranial navigation," *Neurosurgery Clinics Of North America*, vol. 7, no. 2, pp. 313-322, 1996.

[2] RL Galloway, MS Berger, WA Bass, and RJ Maciunas. Registered intraoperative information: electrophysiology, ultrasound, and endoscopy. In: *Interactive Image-Guided*

Neurosurgery, ed. RJ Maciunas. Park Ridge, IL: American Association of Neurological Surgeons, 1993. pp. 247-258.

[3] JD Stefansic, WA Bass, SL Hartmann, RA Beasley, TK Sinha, DM Cash, AJ Herline, and RL Galloway, "Design and implementation of a PC-based image-guided surgical system," *Computer Methods and Programs in Biomedicine*, In press, Aug, 2001.

[4] RL Galloway, RJ Maciunas, WA Bass, and WJ Carpini, "Optical localization for interactive, image-guided neurosurgery," *SPIE Medical Imaging*, vol. 2164, pp. 137-145, 1994.

[5] MY Wang, CR Maurer, JM Fitzpatrick, and RJ Maciunas, "An automatic technique for finding and localizing externally attached markers in CT and MR volume images of the head," *IEEE Transactions on Biomedical Engineering*, vol. 43, no. 6, pp. 627-637, Jun, 1996.

[6] B Horn, "Closed-form solution of absolute orientation using unit quaternions," *Journal of the Optical Society of America*, vol. 4, pp. 629-642, 1987.

[7] SL Hartmann, MH Parks, PR Martin, and BM Dawant, "Automatic 3-D segmentation of the internal structures of the head in MR images using a combination of similarity and free form transformations: Part II, validation on severely atrophied brains," *IEEE Transactions on Medical Imaging*, vol. 18, no. 10, pp. 917-926, Oct, 1999.

[8] SL Hartmann and RL Galloway, Jr., "Depth-buffer targeting for spatially accurate 3-D visualization of medical images," *IEEE Transactions on Medical Imaging*, vol. 19, no. 10, pp. 1024-1031, Oct, 2000.

[9] JBA Maintz and MA Viergever, "A survey of medical image registration," *Medical Image Analysis*, vol. 2, no. 1, pp. 1-36, Apr, 1998.

[10] J Talairach and P Tournoux. *Co-planar stereotactic atlas of the human brain*, New York: Thieme Medical, 1988.

[11] SL Hartmann, RL Galloway, and BM Dawant, "Optical flow based brain registration with sulcal constraints for improved cortical alignment," *IEEE Transactions on Medical Imaging*, In review, Jan, 2002.

CHAPTER VII

SUMMARY

The objective of this research was to design and develop a system capable of displaying cortical brain function during interactive, image-guided neurosurgery. Brain function was determined using a cortical stimulator, classified according to function type, and displayed along with pre-operative tomographic and rendered images of the brain. In addition to displaying brain function acquired from the patient undergoing surgery, a probabilistic map of functional information acquired from a database or previous patients may also be displayed. This information is stored in an atlas coordinate system and can be mapped to the patient's coordinate system for display during surgery.

In order to accomplish these objectives, three main research components were required. First, a non-linear inter-subject registration method was developed in order to map functional data to and from the atlas database. An optical-flow based registration method was used for this purpose. This algorithm does not use any structural information from the image to determine the registration, but instead computes a 3-D deformation field (i.e. a displacement for each voxel in the image) using the intensity characteristics of each image volume. In order to provide a highly accurate match between the cortical regions of two image volumes, the deformation field was constrained according to the location of major sulci in the brain. A novel semi-automatic process for identifying the location of these sulci was developed for this purpose. The total deformation field was used to map functional data acquired during surgery to the atlas coordinate system in order to update the population database. Before each additional surgery, the same technique can be used to map information from the atlas database onto the current patient's tomogram and rendered images.

The second main component of this research was to design and develop an image-guided surgery system in order to display the current position of a surgical probe on tomogram and rendered images. Separate software modules were developed for the display of tomogram and rendered images. For displaying rendered images, a novel method for indicating depth (the distance between the surgical probe and the rendered object) was developed. Software modules were also developed to communicate with three different spatial localizers (two optical and one

magnetic). Each of these localizers is capable of determine the physical-space position of a tracked instrument. The most accurate of these devices, the Optotrak 3020 (Northern Digital, Inc.), was used for spatial localization during surgery.

The third main component of this research was to enhance the image-guided surgery system in order to identify and display the location of cortical brain function. An optically-tracked cortical stimulator was designed for this purpose. A spatial localizer was used to identify the position of each cortical stimulation during surgery. A software module was developed for recording, classifying, and saving the location of stimulated cortical regions. The display of functional information was integrated with the image display by overlaying data onto the tomogram and rendered images. Using this system, the surgeon is able to view critical functional information as well as the traditional anatomical information displayed during image-guided procedures.

Once all three of the main components of this research were completed, the entire system was tested and evaluated during three human neurosurgery procedures. Functional information corresponding to speech, motor, and sensory regions was identified and displayed during surgery. This data was then mapped to a common reference database in order to evaluate the feasibility of using this system to create a functional atlas of the human brain.

Future Work

There are several areas of research where this work can be continued or improved. In order to use the current version of the image-guided surgery system, the patient's tomogram images must be formatted before surgery to be compatible with the Orion system. This is done off-line (i.e. not part of the Orion system), typically the day before the surgery. Several programs were used for the different tasks required: converting the DICOM images to the Orion format, reformatting the original tomogram into different orientations, segmenting the brain from the tomogram volumes, and creating the rendered image set from the segmented volume. All of these tasks could be built into a single Orion module, which could be executed before each surgery. The fiducial markers are identified using a separate visualization package developed specifically for this research, and a data file containing their image-space location is created. The Orion system reads this data file and uses the information to determine the registration. This entire process could also be accomplished within the new Orion module. Finally, this module

could be used to map the functional information from the atlas database onto the images of the patient. As with the preparation of the images, this could also be accomplished immediately before the surgery.

The reference database of brain function was created using a single subject for the atlas volume. This may introduce biasing errors if the shapes and sizes of its features are not representative of the population. It may be beneficial to create the reference volume from an average of multiple subjects, or possibly create more than one reference volume and use the most appropriate atlas depending on the size and shape of the current patient's volume. This is an area of research that could be pursued as the number of cases in the database increases.

The inter-subject registration method will be used to register the atlas volume with a volume of a neurosurgery patient. Additional registration difficulties not encountered in the evaluation process may arise since the registration algorithm was primarily tested using tomogram volumes from normal subjects and alcoholic patients. None of these images contained space-occupying tumors which may be present in neurosurgery patients. Even though this registration method was used for three neurosurgery cases where tumors were present, the intensity characteristics of some tumors may produce undesired results using intensity-based matching algorithms. Tumors may also drastically alter the morphology of the brain, which can cause further problems using atlas-based techniques. An approach similar to that proposed by Dawant and Hartmann *et al* [1,2] could be used to overcome the problems associated with the registration of images containing space-occupying tumors. This technique involves several steps. First, the atlas volume is registered to the patient volume using the optical flow method. The standard deviation of the Gaussian smoothing filter is set to a high value so the deformation is less elastic. This prevents undesired deformation around areas of high morphological difference. At this point the two images are in approximate correspondence, with the regions that have been altered by the presence of the tumor still misaligned. The deformed atlas is then "seeded" with a small structure centered approximately on the centroid of the tumor. Finally, the optical flow deformation algorithm is applied again to the seeded deformed atlas, this time with a lower standard deviation for the smoothing kernel which allows for a more elastic deformation. In this step, the seeded tumor is grown until it reaches the size of the actual tumor and surrounding tissues in the atlas are displaced and deformed. Initial results using this method should be further

pursued in order to determine the possibility of using this technique within the image-guided surgery system.

The tracked stimulator used in this study consisted of a tracking system designed to fit around an existing cortical stimulator. Future improvements include the design of a new stimulator specifically for image-guided surgery. This device will be smaller, lighter, and easier to use than the prototype used in this study. The new design will also make it possible to automatically signal the Orion system when a stimulation has occurred.

The ability to record and save the functional information identified during surgery may prove useful in other applications. As discussed previously, a database of cortical function could be created from multiple patients. This could then be used during additional procedures by mapping the database onto the tomogram images of the current patient. This would allow functional information from a population of patients to be displayed along with any function acquired from the specific patient. The database could then be updated by including new information obtained during each additional surgery. As the number of surgery cases in the database increase, the categories used to classify the function type may also expand. For this study, only three major categories were used (speech, motor, and sensory). As the amount of data increases, these categories may be further divided into several sub-categories, such as classifying motor function according to the specific anatomical location or separating speech function into Broca and Wernicke areas.

There are many factors that contribute to the total error of this system, including system specific factors such as marker identification and image registration. Additional factors not directly associated with the system, such as geometrical distortion of the preoperative images [3] and the shifting or sagging of the brain between imaging and surgery [4,5], also reduce the overall accuracy of the system. Reducing the error contribution from external factors such these, although important, were not the focus of this research and were not pursued. Any future work that improves or corrects errors caused by these factors could be used directly to improve the overall accuracy of the image-guided surgery system described in this research.

Research Considerations

Before beginning this research, two major factors were considered: how to protect the health and confidentiality of any human subjects used in this research and what, if any, contributions this research would make on society. These factors are described below:

1) Protection of Research Subjects: Since human subjects were used in this research, all techniques were documented and approved by the Institutional Review Board (IRB) of the Vanderbilt University Medical Center Center (IRB number: 010270, Expiration date: May 25, 2002). Informed consent was obtained from all patients prior to the procedure, and their confidentiality has been protected. Patient identification was removed from all medical images and photography used in this research. Storage of all patient documents and data pertaining to this research has been completed in accordance with IRB regulations.

2) Societal Implication: This project has made a significant contribution to the biomedical engineering science by combining principles from several research areas to solve a clinical problem. The incorporation of functional brain information into interactive image-guided neurosurgery may improve the existing techniques currently used during these procedures. Functional information acquired during surgery is typically lost since the data is not saved. Using the system described in this study, valuable information regarding the location of brain function that was previously available only to the surgeon may prove valuable in other research areas.

References

[1] BM Dawant, SL Hartmann, and S Gadamsetty, "Brain atlas deformation in the presence of large space-occupying tumors," *Medical Image Computing and Computer-Assisted Intervention: MICCAI '99*, vol. 1679, pp. 589-596, Sep 19, 1999.

[2] BM Dawant, SL Hartmann, S Pan, and Gadamsetty S., "Brain atlas deformation in the presence of small and large space-occupying tumors," *Computer Aided Surgery*, In press, Nov, 2001.

[3] RJ Maciunas, JM Fitzpatrick, S Gadamsetty, and CR Maurer, Jr., "A universal method for geometric correction of magnetic resonance images for stereotactic neurosurgery," *Stereotact.Funct.Neurosurg.*, vol. 66, no. 1-3, pp. 137-140, 1996.

[4] CR Maurer, Jr., DL Hill, AJ Martin, H Liu, M McCue, D Rueckert, D Lloret, WA Hall, RE Maxwell, DJ Hawkes, and CL Truwit, "Investigation of intraoperative brain deformation using a 1.5-T interventional MR system: preliminary results," *IEEE Transactions on Medical Imaging*, vol. 17, no. 5, pp. 817-825, Oct, 1998.

[5] DL Hill, CR Maurer, Jr., RJ Maciunas, JA Barwise, JM Fitzpatrick, and MY Wang, "Measurement of intraoperative brain surface deformation under a craniotomy," *Neurosurgery*, vol. 43, no. 3, pp. 514-526, Sep, 1998.

BIBLIOGRAPHY

Andreasen NC, Rajarethinam R, Cizadlo T, Arndt S, Swayze VW, II, Flashman LA, O'Leary DS, Ehrhardt JC, and Yuh WTC, "Automatic atlas-based volume estimation of human brain regions from MR images," *Journal of Computer Assisted Tomography*, vol. 20, no. 1, pp. 98-106, 1996.

Arun KS, Huang TS, and Blostein SD, "Least-squares fitting of two 3-D point sets," *IEEE Transactions on Pattern Analysis and Machine Intelligence*, vol. 9, no. 5, pp. 698-700, Sep, 1987.

Bajcsy R and Kovacic S, "Multiresolution elastic matching," *Computer Vision, Graphics, and Image Processing*, vol. 46, pp. 1-21, 1989.

Besl P and McKay N, "A method for the registration of 3-D shapes," *IEEE Transactions on Pattern Analysis and Machine Intelligence*, vol. 14, no. 2, pp. 239-256, Feb, 1992.

Bezdek JC, Hall LO, and Clarke LP, "Review of MR image segmentation techniques using pattern recognition," *Medical Physics*, vol. 20, no. 4, pp. 1033-1048, 1993.

Bookstein FL, "Principal warps: thin-plate splines and the decomposition of deformations," *IEEE Transactions on Pattern Analysis and Machine Intelligence*, vol. 11, no. 6, pp. 567-585, 1989.

Bro-Nielsen M and Gramkow C, "Fast fluid registration of medical images," *Visualization In Biomedical Computing*, vol. 1131, pp. 267-276, Sep, 1995.

Broit C, Optimal registration of deformed images. *Doctoral dissertation*, University of Pennsylvania, 1981.

Burr DJ, "A dynamic model for image registration," *Computer Graphics and Image Processing*, vol. 15, pp. 102-112, 1981.

Burr DJ, "Elastic matching of line drawings," *IEEE Transactions on Pattern Analysis and Machine Intelligence*, vol. 3, no. 6, pp. 708-713, 1981.

Caunce A and Taylor CJ, "Using local geometry to build 3D sulcal models," *Proceedings of Information Processing in Medical Imaging: IPMI '99*, vol. 1613, pp. 196-209, 1999.

Chen M, Kanade T, Pomerleau D, and Rowley HA, "Anomaly detection through registration," *Pattern Recognition*, vol. 32, no. 1, pp. 113-128, 1999.

Chen M, Kanade T, Pomerleau D, and Schneider J, "3-D deformable registration of medical images using a statistical atlas," *Medical Image Computing and Computer-Assisted Intervention: MICCAI '99*, pp. 621-630, 1999.

Christensen GE, Joshi SC, and Miller MI, "Individual anatomical atlases of the head," *Visualization In Biomedical Computing* , vol. 1131, pp. 343-348, Sep, 1996.

Christensen GE, Rabbit RD, Miller MI, Joshi SC, Grenander U, Coogan TA, and Van Essen DC, "Topological properties of smooth anatomic maps," *Information Processing In Medical Imaging*, pp. 101-112, 1995.

Cohen LD and Cohen I, "Deformable models for 3-D medical images using finite elements and balloons," *IEEE Computer Society Conference on Computer Vision and Pattern Recognition*, pp. 592-598, 1992.

Collignon A, Maes F, Delaere D, Vandermeulen D, Suetens P, and Marchal G, "Automated multimodality image registration using information theory," *Proceedings of Information Processing in Medical Imaging: IPMI '95*, pp. 263-274, 1995.

Collins DL, Holmes CJ, Peters TM, and Evans AC, "Automatic 3-D model-based neuroanatomical segmentation," *Human Brain Mapping*, vol. 3, no. 3, pp. 190-208, 1995.

Collins DL, Le Goualher G, and Evans AC, "Non-linear cerebral registration with sulcal constraints," *Medical Image Computing and Computer-Assisted Intervention: MICCAI '98*, vol. 1496, pp. 974-984, Oct, 1998.

Collins DL, Le Goualher G, Venugopal R, Caramanos A, Evans AC, and Barillot C, "Cortical constraints for non-linear cortical registration," *Visualization In Biomedical Computing*, vol. 1131, pp. 307-316, Sep, 1996.

Collins DL, Neelin P, Peters TM, and Evans AC, "Automatic 3D intersubject registration of MR volumetric data in standardized Talairach space," *Journal of Computer Assisted Tomography*, vol. 18, no. 2, pp. 192-205, 1994.

Cosgrove GR, Buchbinder BR, and Jiang H, "Functional magnetic resonance imaging for intracranial navigation," *Neurosurgery Clinics Of North America*, vol. 7, no. 2, pp. 313-322, 1996.

Dann R, Hoford J, Kovacic S, Reivich M, and Bajcsy R, "Evaluation of elastic matching system for anatomic (CT, MR) and functional (PET) cerebral images," *Journal of Computer Assisted Tomography*, vol. 13, no. 4, pp. 603-611, 1989.

Davatzikos C, "Spatial Normalization of 3D brain images using deformable models," *Journal of Computer Assisted Tomography*, vol. 20, no. 4, pp. 656-665, 1996.

Davatzikos C and Bryan RN, "Using a deformable surface model to obtain a shape representation of the cortex," *IEEE Transactions on Medical Imaging*, vol. 15, no. 6, pp. 785-795, 1996.

Davatzikos C and Prince JL, "An active contour model for mapping the cortex," *IEEE Transactions on Medical Imaging*, vol. 14, no. 1, pp. 65-80, Mar, 1995.

Davatzikos C, Prince JL, and Bryan RN, "Image registration based on boundary mapping," *IEEE Transactions on Medical Imaging* , vol. 15, no. 1, pp. 112-115, Feb, 1996.

Dawant BM, Hartmann SL, and Gadamsetty S, "Brain atlas deformation in the presence of large space-occupying tumors," *Medical Image Computing and Computer-Assisted Intervention: MICCAI '99*, vol. 1679, pp. 589-596, Sep 19, 1999.

Dawant BM, Hartmann SL, Pan S, and Gadamsetty S., "Brain atlas deformation in the presence of small and large space-occupying tumors," *Computer Aided Surgery*, In press, Nov, 2001.

Dawant BM, Hartmann SL, Thirion J-P, Maes F, Vandermeulen D, and Demaerel P, "Automatic 3D segmentation of internal structures of the head in MR images using a combination of similarity and free form transformations: Part I, methodology and validation on normal subjects," *IEEE Transactions on Medical Imaging*, vol. 18, no. 10, pp. 909-916, Oct, 1999.

Evans AC, Dai W, Collins DL, Neelin P, and Marrett S, "Warping of a computerized 3-D atlas to match brain image volumes for quantitative neuroanatomical and functional analysis," *SPIE Medical Imaging*, vol. 1445, pp. 236-246, 1991.

Fitzpatrick JM, Hill DLG, and Maurer CR, Image Registration. In: *Handbook of Medical Imaging, Volume 2: Medical Image Processing and Analysis*, eds. M Sonka and JM Fitzpatrick. Bellingham WA: SPIE Press, 2000.

Gaens T, Maes F, Vandermeulen D, and Suetens P, "Non-rigid multimodal image registration using mutual information," *Medical Image Computing and Computer-Assisted Intervention: MICCAI '98*, vol. 1496, pp. 1099-1106, Oct 1, 1998.

Galloway RL, Bass WA, Stefansic JD, and Maciunas RJ, "Incorporation of vascular information into interactive, image-guided surgery," *SPIE Medical Imaging*, vol. 2707, pp. 168-179, 1996.

Galloway RL, Berger MS, Bass WA, and Maciunas RJ. Registered intraoperative information: electrophysiology, ultrasound, and endoscopy. In: *Interactive Image-Guided Neurosurgery*, ed. RJ Maciunas. Park Ridge, IL: American Association of Neurological Surgeons, 1993.pp. 247-258.

Galloway RL, Maciunas RJ, Bass WA, and Carpini WJ, "Optical localization for interactive, image-guided neurosurgery," *SPIE Medical Imaging*, vol. 2164, pp. 137-145, 1994.

Ge YR, Fitzpatrick JM, Dawant BM, Bao J, Kessler RM, and Margolin RA, "Accurate localization of cortical convolutions in MR brain images," *IEEE Transactions on Medical Imaging*, vol. 15, no. 4, pp. 418-428, 1996.

Gee JC, Reivich M, and Bajcsy R, "Elastically deforming 3D atlas to match anatomical brain images," *Journal of Computer Assisted Tomography*, vol. 17, no. 2, pp. 225-236, 1993.

Gee JC, Reivich M, Bilaniuk L, Hackney D, Zimmerman R, Kovacic S, and Bajcsy R, "Evaluation of multiresolution elastic matching using MRI data," *Proceedings of SPIE: Medical Imaging*, vol. 1445, pp. 226-234, 1991.

Goshtasby A, "Registration of images with geometric distortions," *IEEE Transactions on Geoscience and Remote Sensing*, vol. 26, no. 1, pp. 60-64, 1988.

Hajnal JV, Hill DLG, and Hawkes DJ, *Medical Image Registration*. CRC Press, 2001.

Hartmann SL, Galloway RL, and Dawant BM, "Optical flow based brain registration with sulcal constraints for improved cortical alignment," *IEEE Transactions on Medical Imaging*, In review, Jan, 2002.

Hartmann SL and Galloway RL, Jr., "Depth-buffer targeting for spatially accurate 3-D visualization of medical images," *IEEE Transactions on Medical Imaging*, vol. 19, no. 10, pp. 1024-1031, Oct, 2000.

Hartmann SL, Parks MH, Martin PR, and Dawant BM, "Automatic 3-D segmentation of the internal structures of the head in MR images using a combination of similarity and free form transformations: Part II, validation on severely atrophied brains," *IEEE Transactions on Medical Imaging*, vol. 18, no. 10, pp. 917-926, Oct, 1999.

Hellier P and Barillot C, "Cooperation between local and global approaches to register brain images," *Proceedings of Information Processing in Medical Imaging: IPMI 2001*, vol. 2082, pp. 315-328, 2001.

Hellier P, Barillot C, Memin E, and Perez P, "Hierarchical estimation of a dense deformation field for 3-D robust registration," *IEEE Transactions on Medical Imaging*, vol. 20, no. 5, pp. 388-402, May, 2001.

Hill DL, Maurer CR, Jr., Maciunas RJ, Barwise JA, Fitzpatrick JM, and Wang MY, "Measurement of intraoperative brain surface deformation under a craniotomy," *Neurosurgery*, vol. 43, no. 3, pp. 514-526, Sep, 1998.

Horn B, "Closed-form solution of absolute orientation using unit quaternions," *Journal of the Optical Society of America*, vol. 4, pp. 629-642, 1987.

Horn B and Schunck B, "Determining optical flow," *Artificial Intelligence*, vol. 17, pp. 185-203, 1981.

Jani AB, Pelizzari CA, Chen GTY, and Grzeszczuk RP, "Accuracy of object depiction and opacity transfer function optimization in CT volume-rendered images," *Journal of Computer Assisted Tomography*, vol. 22, no. 3, pp. 459-470, 1998.

Kamber M, Shinghal R, Collins DL, Francis G, and Evans AC, "Model-based 3D segmentation of multiple sclerosis lesions from magnetic resonance brain images," *IEEE Transactions on Medical Imaging*, vol. 14, no. 3, pp. 442-453, 1994.

Kass M, Witkin A, and Terzopoulos D, "Snakes: active contour models," *International Journal of Computer Vision*, vol. 1, no. 4, pp. 321-331, 1988.

Le Goualher G, Barillot C, and Bizais Y, "Modeling cortical sulci with active ribbons," *International Journal Of Pattern Recognition And Artificial Intelligence*, vol. 11, no. 8, pp. 1295-1315, 1997.

Le Goualher G, Procyk E, Collins DL, Venugopal R, Barillot C, and Evans AC, "Automated extraction and variability analysis of sulcal neuroanatomy," *IEEE Transactions on Medical Imaging*, vol. 18, no. 3, pp. 206-217, 1999.

Lohmann G, "Extracting line representations of sulcal and gyral patterns in MR images of the human brain," *IEEE Transactions on Medical Imaging*, vol. 17, no. 6, pp. 1040-1048, Dec, 1998.

Maciunas RJ, Fitzpatrick JM, Gadamsetty S, and Maurer CR, Jr., "A universal method for geometric correction of magnetic resonance images for stereotactic neurosurgery," *Stereotact.Funct.Neurosurg.*, vol. 66, no. 1-3, pp. 137-140, 1996.

Maes F, Collignon A, Vandermeulen D, Marchal G, and Suetens P, "Multimodality image registration by maximization of mutual information," *IEEE Transactions on Medical Imaging*, vol. 16, no. 2, pp. 187-198, 1997.

Maintz JBA and Viergever MA, "A survey of medical image registration," *Medical Image Analysis*, vol. 2, no. 1, pp. 1-36, Apr, 1998.

Manceaux-Demiau A, Bryan RN, and Davatzikos C, "A probabilistic ribbon model for shape analysis of the cerebral sulci: Application to the central sulcus," *Journal of Computer Assisted Tomography*, vol. 22, no. 6, pp. 962-971, 1998.

Maurer CR and Fitzpatrick JM. A review of medical image registration. In: *Interactive Image-Guided Neurosurgery*, ed. RJ Maciunas. Park Ridge, IL: American Association of Neurological Surgeons, 1993.pp. 17-44.

Maurer CR, Jr., Hill DL, Martin AJ, Liu H, McCue M, Rueckert D, Lloret D, Hall WA, Maxwell RE, Hawkes DJ, and Truwit CL, "Investigation of intraoperative brain deformation using a 1.5-T interventional MR system: preliminary results," *IEEE Transactions on Medical Imaging*, vol. 17, no. 5, pp. 817-825, Oct, 1998.

Moshfeghi M, Ranganath S, and Nawyn K, "Three-dimensional elastic matching of volumes," *IEEE Transactions on Image Processing*, vol. 3, no. 2, pp. 128-138, 1994.

Nakajima S, Atsumi H, Bhalerao AH, Jolesz FA, Kikinis R, Yoshimine T, Moriarty TM, and Stieg PE, "Computer-assisted surgical planning for cerebrovascular neurosurgery," *Neurosurgery*, vol. 41, no. 2, pp. 403-410, Aug, 1997.

Palmisano MG, Galloway RL, and Maciunas RJ, "Modified maximum intensity projections for surgical guidance," *SPIE Medical Imaging*, vol. 3031, pp. 643-650, 1997.

Peters TM, Davey B, Munger P, Comeau RM, Evans AC, and Olivier A, "Three-dimensional multimodal image-guidance for neurosurgery," *IEEE Transactions on Medical Imaging*, vol. 15, no. 2, pp. 121-128, 1996.

Peters TM, Henri CJ, Munger P, Takahashi AM, Evans AC, Davey B, and Olivier A, "Integration of stereoscopic DSA and 3D MRI for image-guided neurosurgery," *Computerized Medical Imaging and Graphics*, vol. 18, no. 4, pp. 289-299, 1994.

Pfefferbaum A, Sullivan EV, Mathalon DH, Shear PK, Rosenbloom MJ, and Lim KO, "Longitudinal changes in magnetic resonance imaging brain volumes in abstinent and relapsed alcoholics," *Alcoholism: clinical and experimental research*, vol. 19, no. 5, pp. 1177-1191, 1995.

Rettmann ME, Xu C, Pham DL, and Prince JL, "Automated segmentation of sulcal regions," *Medical Image Computing and Computer-Assisted Intervention: MICCAI '99*, pp. 158-165, 1999.

Rohr K, Stiehl HS, Sprengel R, Beil W, Buzug TM, Weese J, and Kuhn MH, "Point-based elastic registration of medical image data using approximating thin-plate splines," *Visualization In Biomedical Computing*, vol. 1131, pp. 297-306, Sep, 1996.

Sandor S and Leahy R, "Surface-based labeling of cortical anatomy using a deformable atlas," *IEEE Transactions on Medical Imaging*, vol. 16, no. 1, pp. 41-54, Feb, 1997.

Sibson R, "Studies in the robustness of multidimensional scaling: perturbation analysis of classical scaling," *Journal of the Royal Statistical Society*, vol. 41, no. 2, pp. 217-229, 1979.

Sokolnikoff IS. *Mathematical theory of elasticity*, New York: 1956.

St-Jean P, Sadikot AF, Collins DL, Clonda D, Karsai R, Evans AC, and Peters TM, "Automated atlas integration and interactive three-dimensional visualization tools for planning and guidance in functional neurosurgery," *IEEE Transactions on Medical Imaging*, vol. 17, no. 5, pp. 672-680, Oct, 1998.

Stefansic JD, Bass WA, Hartmann SL, Beasley RA, Sinha TK, Cash DM, Herline AJ, and Galloway RL, "Design and implementation of a PC-based image-guided surgical system," *Computer Methods and Programs in Biomedicine*, In press, Aug, 2001.

Subsol G. Crest lines for curve-based warping. In: *Brain Warping*, ed. AW Toga. Academic Press, 1998.pp. 241-262.

Subsol G, Roberts N, Doran M, Thirion J-P, and Whitehouse G, "Automatic analysis of cerebral atrophy," *Magnetic Resonance Imaging*, vol. 15, no. 8, pp. 917-927, 1997.

Talairach J and Tournoux P. *Co-planar stereotactic atlas of the human brain*, New York: Thieme Medical, 1988.

Thirion J-P, Fast non-rigid matching of medical images. INRIA technical report, nr. 2547, pp. 1-37, May, 1995.

Thirion J-P, "Image matching as a diffusion process: an analogy with Maxwell's demons," *Medical Image Analysis*, vol. 2, no. 3, pp. 243-260, 1998.

Thirion JP and Gourdon A, "The 3D marching lines algorithm," *Graphical Models and Image Processing*, vol. 58, no. 6, pp. 503-509, 1996.

Thompson P and Toga AW, "A surface-based technique for warping three-dimensional images of the brain," *IEEE Transactions on Medical Imaging*, vol. 15, no. 4, pp. 402-417, 1996.

Vaillant M and Davatzikos C, "Hierarchical matching of cortical features for deformable brain image registration," *Proceedings of Information Processing in Medical Imaging: IPMI '99*, vol. 1613, pp. 182-195, 1999.

Wada JA, Clarke R, and Hamm A, "Cerebral hemispheric asymmetry in humans: cortical speech zones in 100 adult and 100 infant brains," *Archives of Neurology*, vol. 32, pp. 239-246, 1975.

Wang MY, Maurer CR, Fitzpatrick JM, and Maciunas RJ, "An automatic technique for finding and localizing externally attached markers in CT and MR volume images of the head," *IEEE Transactions on Biomedical Engineering*, vol. 43, no. 6, pp. 627-637, Jun, 1996.

Wang YM and Staib LH, "Elastic model based non-rigid registration incorporating statistical shape information," *Medical Image Computing and Computer-Assisted Intervention: MICCAI '98*, vol. 1496, pp. 1162-1173, 1998.

Wells III WM, Viola P, Atsumi H, Nakajima S, and Kikinis R, "Multi-modal volume registration by maximization of mutual information," *Medical Image Analysis*, vol. 1, pp. 35-51, 1996.

West JB, Fitzpatrick JM, Wang MY, Dawant BM, Maurer CR, Kessler RM, Maciunas RJ, Barillot C, Lemoine D, Collignon A, Maes F, Suetens P, Vandermeulen D, vandenElsen PA, Napel S, Sumanaweera TS, Harkness B, Hemler PF, Hill DLG, Hawkes DJ, Studholme C, Maintz JBA, Viergever MA, Malandain G, Pennec X, Noz ME, Maguire GQ, Pollack M, Pelizzari CA, Robb RA, Hanson D, and Woods RP, "Comparison and evaluation of

retrospective intermodality image registration techniques," *Journal of Computer Assisted Tomography*, vol. 21, no. 4, pp. 554-566, 1997.

Zachmann H., Interpretation of cranial MR images using a digital atlas of the human head. eds. H. H. Lemke, C. C. Rhodes, C. C. Jaffe, and R. Felix. pp. 283-288, 1991. *Proceedings Computer Assisted Radiology*. Springer-Verlag. Berlin.

Zeng XL, Staib LH, Schultz RT, and Duncan JS, "Segmentation and measurement of the cortex from 3-D MR images using coupled-surfaces propagation," *IEEE Transactions on Medical Imaging*, vol. 18, no. 10, pp. 927-937, 1999.

Zijdenbos AP, Dawant BM, and Margolin R, "Morphometric analysis of white matter lesions in MR images: method and validation," *IEEE Transactions on Medical Imaging*, vol. 13, no. 4, pp. 716-724, 1994.